NAVAL POSTGRADUATE SCHOOL

MONTEREY, CALIFORNIA

THESIS

DESIGN, MODELING AND PERFORMANCE OF A SPLIT PATH JP-10/AIR PULSE DETONATION ENGINE

by

Patrick D. Hutcheson

December 2006

Thesis Advisor:	Christopher M. Brophy
Second Reader:	Garth V. Hobson

Approved for public release; distribution is unlimited

THIS PAGE INTENTIONALLY LEFT BLANK

REPORT DOCUMENTATION PAGE			Form Approved OMB No. 0704-0188
Public reporting burden for this collection of information is estimated to average 1 hour per response, including the time for reviewing instruction, searching existing data sources, gathering and maintaining the data needed, and completing and reviewing the collection of information. Send comments regarding this burden estimate or any other aspect of this collection of information, including suggestions for reducing this burden, to Washington headquarters Services, Directorate for Information Operations and Reports, 1215 Jefferson Davis Highway, Suite 1204, Arlington, VA 22202-4302, and to the Office of Management and Budget, Paperwork Reduction Project (0704-0188) Washington DC 20503.			
1. AGENCY USE ONLY ***(Leave blank)***	**2. REPORT DATE** December 2006	**3. REPORT TYPE AND DATES COVERED** Masters and Engineers Thesis	
4. TITLE AND SUBTITLE: Design, Modeling and Performance of a Split Path JP-10/Air Pulse Detonation Engine			**5. FUNDING NUMBERS** N0001406WR20161
6. AUTHOR(S) Patrick D. Hutcheson			
7. PERFORMING ORGANIZATION NAME(S) AND ADDRESS(ES) Naval Postgraduate School Monterey, CA 93943-5000			**8. PERFORMING ORGANIZATION REPORT NUMBER**
9. SPONSORING /MONITORING AGENCY NAME(S) AND ADDRESS(ES) Office of Naval Research (ONR) Ballstone Tower One 800 N. Quincy St. Arlington, VA 22217-5660			**10. SPONSORING/MONITORING AGENCY REPORT NUMBER** N/A
11. SUPPLEMENTARY NOTES The views expressed in this thesis are those of the author and do not reflect the official policy or position of the Department of Defense or the U.S. Government.			
12a. DISTRIBUTION / AVAILABILITY STATEMENT Approved for public release; distribution is unlimited			**12b. DISTRIBUTION CODE**
13. ABSTRACT (maximum 200 words) The initiation of a detonation in Pulse Detonation Engines (PDE) has been identified as one of the critical and enabling technologies for PDEs. In particular, the initiation of practical fuel-air mixtures containing liquid droplets without supplementary oxygen or other high loss mechanisms is a capability that could enable the PDE to exceed the performance of ramjets and expendable turbo-machinery based systems. Although past engine designs have relied upon a sensitive fuel/oxygen initiator unit or unrealistic gaseous fuels such as ethylene and propane, a PDE was designed and partially tested that has eliminated the requirement for supplementary oxygen as well as enabling the use of a JP-10, high-density liquid fuel. Air flow through segments of this PDE was simulated using Computational Fluid Dynamics and experimentally evaluated in the laboratory at simulated flight conditions, including supersonic cruising conditions. The spiral lined initiator demonstrated a lower total pressure loss when compared to the geometry with rings, and thus was the preferred initiator configuration. Experimental values for the turbulence were found to be significantly lower than the computed values at similar conditions when using the k-ε model. Finally, successful ignitions of the JP-10/Air initiator at frequencies of up to 20 Hz were experimentally demonstrated.			
14. SUBJECT TERMS Pulse Detonation Engines, PDE, PDE Ignition, Transient Plasma Ignition, TPI, Refresh Mach Number, Split Path, JP-10			**15. NUMBER OF PAGES** 117
			16. PRICE CODE
17. SECURITY CLASSIFICATION OF REPORT Unclassified	**18. SECURITY CLASSIFICATION OF THIS PAGE** Unclassified	**19. SECURITY CLASSIFICATION OF ABSTRACT** Unclassified	**20. LIMITATION OF ABSTRACT** UL

NSN 7540-01-280-5500 Standard Form 298 (Rev. 2-89)
Prescribed by ANSI Std. 239-18

THIS PAGE INTENTIONALLY LEFT BLANK

Approved for public release; distribution is unlimited

DESIGN, MODELING AND PERFORMANCE OF A SPLIT PATH JP-10/AIR PULSE DETONATION ENGINE

Patrick D. Hutcheson
Captain, Canadian Air Force
B.Eng., Royal Military College of Canada, 2001

Submitted in partial fulfillment of the
requirements for the degrees of

MASTER OF SCIENCE IN MECHANICAL ENGINEERING
AND
MECHANICAL ENGINEER

from the

NAVAL POSTGRADUATE SCHOOL
December 2006

Author: Patrick D. Hutcheson

Approved by: Christopher M. Brophy
Thesis Advisor

Garth Hobson
Second Reader

Anthony J. Healey
Chairman, Department of Mechanical & Astronautical Engineering

THIS PAGE INTENTIONALLY LEFT BLANK

ABSTRACT

The initiation of a detonation in Pulse Detonation Engines (PDE) has been identified as one of the critical and enabling technologies for PDEs. In particular, the initiation of practical fuel-air mixtures containing liquid droplets without supplementary oxygen or other high loss mechanisms is a capability that could enable the PDE to exceed the performance of ramjets and expendable turbo-machinery based systems. Although past engine designs have relied upon a sensitive fuel/oxygen initiator unit or unrealistic gaseous fuels such as ethylene and propane, a PDE was designed and partially tested that has eliminated the requirement for supplementary oxygen as well as enabling the use of a JP-10, high-density liquid fuel. Air flow through segments of this PDE was simulated using Computational Fluid Dynamics and experimentally evaluated in the laboratory at simulated flight conditions, including supersonic cruising conditions. The spiral lined initiator demonstrated a lower total pressure loss when compared to the geometry with rings, and thus was the preferred initiator configuration. Experimental values for the turbulence were found to be significantly lower than the computed values at similar conditions when using the k-ε model. Finally, successful ignitions of the JP-10/Air initiator at frequencies of up to 20 Hz were experimentally demonstrated.

THIS PAGE INTENTIONALLY LEFT BLANK

TABLE OF CONTENTS

I. INTRODUCTION....1

II. BACKGROUND....5
- A. DETONATION THERMODYNAMICS....5
- B. DETONATION INITIATION....7
- C. PDE THERMODYNAMIC CYCLE....13
- D. PERFORMANCE CONSIDERATIONS....19

III. DESIGN & MODELING....23

VI. EXPERIMENTAL SETUP....35
- A. PDE....35
- B. VITIATOR....36
- C. TEST CELL AND PDE CONTROL....37
- D. DATA ACQUISITION....39

VII. RESULTS....41
- A. CFD....41
- B. EXPERIMENTAL....45

VIII. SUMMARY AND CONCLUSIONS....49

IX. FUTURE WORK....51

APPENDIX A: CFD SETTINGS....53

APPENDIX B: CFD RESULTS....57

APPENDIX C: WIRING TABLES....59

APPENDIX D: TEST CELL #2 SOP....63

APPENDIX E: ENGINEERING DRAWINGS....67

LIST OF REFERENCES....97

INITIAL DISTRIBUTION LIST....99

THIS PAGE INTENTIONALLY LEFT BLANK

LIST OF FIGURES

Figure 1. Performance Comparison of High-Speed Propulsion Technologies 1
Figure 2. Schematic Diagram of a Stationary 1-D Combustion Wave (Deflagration or Detonation) 5
Figure 3. Hugonoit curve on *P*-versus-$1/\rho$ plane 6
Figure 4. Streak Schlieren Photograph of the Development of Detonation 8
Figure 5. Streak Schlieren Photograph of the Onset of Retonation 9
Figure 6. Flash Schlieren Photograph of the Onset of Retonation 9
Figure 7. Flash Schlieren Photograph of Transverse Waves Set up at the Onset of Retonation 10
Figure 8. Variation of physical properties through a ZND detonation wave 11
Figure 9. Smoked-foil record and schematic diagram of symmetric planar interaction 12
Figure 10. Schematic Diagram Showing the Shock-wave Pattern and Triple Point in a Two-dimensional Supersonic Flow Passing Through a Convergent Ramp Section 12
Figure 11. Comparison of Propulsion Technologies Using Combustion Simulation 14
Figure 12. Schematic of a Generic PDE and Appropriate Stages 15
Figure 13. Schematic of a Generic Ramjet and Appropriate Stages 15
Figure 14. Temperature-Entropy Diagram for a Generic PDE at M=4 16
Figure 15. Temperature-Entropy Diagram for a Generic Ramjet at M=4 16
Figure 16. P-V Diagram for a Generic PDE at M=4 17
Figure 17. P-V Diagram for a Generic Ramjet at M=4 18
Figure 18. New PDE Initiator Design With Combustor Section View 23
Figure 19. Corona from TPI 23
Figure 20. Voltage and Current from TPI 24
Figure 21. TPI Holder Screw Cap Failure 25
Figure 22. TPI Electrode Holder and Insulator Design Installed in Ignition Section 25
Figure 23. New PDE Initiator Design Architecture 26
Figure 24. Flow Conditioning Screens 26
Figure 25. Fuel Injector Flow Rate at Varying Fuel Pressure 28
Figure 26. PDE Initiator Section View 28
Figure 27. New PDE Design Cycle Steps 30
Figure 28. Grid Model of Initiator with Ring Turbulence Generators 31
Figure 29. Model of Initiator with Ramp Turbulence Generators 32
Figure 30. Grid Model of Initiator with No Turbulence Generators 32
Figure 31. Grid Model of PDE with No Turbulence Generators 34
Figure 32. PDE Initiator Experimental Set-up 35
Figure 33. H_2/O_2 Vitiator 36
Figure 34. Facility Control Schematic 38
Figure 35. Test Cell #2 Graphics-User Interface 39
Figure 36. Kistler High Speed Pressure Transducers 40

Figure 37. CFD Results for Flow Field Turbulence Comparison at $M_{refresh}$ = 0.25 42
Figure 38. Exit Centerline CFD Results for Turbulence Generated by Obstacles 42
Figure 39. CFD Results for Pressure Drop Over Obstacles 43
Figure 40. CFD Results for Pressure Drop Over Obstacles Versus Mass Flow Rate 44
Figure 41. CFD Results for Shock Propagation from Initiator 45
Figure 42. CFD Results for Pressure Shock Propagation to Combustor 45
Figure 43. Exit Centerline Laboratory Result for Turbulence Induced by Rings 46
Figure 44. Laboratory Result for Pressure Drop over Obstacles 47
Figure 45. Thrust Stand Load Cell Wiring Diagram 60
Figure 46. PDE Engine Adapter 67
Figure 47. TPI Holder 68
Figure 48. TPI Holder Extension Assembly 69
Figure 49. TPI Holder Extension Assembly 70
Figure 50. TPI Holder (version 2) 71
Figure 51. TPI Holder Extension Flange 72
Figure 52. New TPI Assembly 73
Figure 53. Macor Insulator 74
Figure 54. Nylon\Teflon Insulator 75
Figure 55. New TPI Metal Holder 76
Figure 56. Metal Insert 77
Figure 57. Metal Cap 78
Figure 58. New PDE Design Entire Assembly 79
Figure 59. Pickoff Assembly 80
Figure 60. Pickoff 81
Figure 61. TPI Holder Extension Flange 81
Figure 62. Pickoff Flange 82
Figure 63. Igniter Assembly 83
Figure 64. Igniter Section 84
Figure 65. Igniter Section flange 85
Figure 66. Igniter to Initiator Flange 86
Figure 67. Ringholder Assembly 87
Figure 68. Ringholder Flange 88
Figure 69. Ringholder 89
Figure 70. Ring 90
Figure 71. Initiator Assembly 91
Figure 72. Initiator Flange 92
Figure 73. Initiator Tube 93
Figure 74. Initiator Tube Version 2 for Pressure Transducers 94
Figure 75. Pressure Transducer Mounting Block 95

LIST OF TABLES

Table 1. Qualitative Differences between Detonation and Deflagration 5
Table 2. Flow properties for a PDE at M=4 at stages 1,3,6 &7 18
Table 3. Flow properties for a Ramjet at M=4 at stages 1,2,6 &7 19
Table 4. Cycle comparison for PDE and ramjet engines at M=4 19
Table 5. Centerline Velocity and Turbulence Effects from Flow Conditioning Screens 26
Table 6. Fuel Injector Characterization for Varying Fuel Pressure 27
Table 7. CFD-ACE Solver Setting for All Initiator Pre-detonation Simulations 53
Table 8. CFD-ACE Solver Setting for Designed Initiator Post-detonation Simulations 54
Table 9. CFD-FASTRAN Solver Settings for Designed Initiator During Detonation Simulations 55
Table 10. CFD Results for Initiator with Rings 57
Table 11. CFD Results for Clean Initiator 57
Table 12. CFD Results for Initiator with Ramps 57
Table 13. CFD Results for Initiator with Rings Post-detonation Conditions 58
Table 14. Electrical Relay Assignments 59
Table 15. Data Acquisition Assignments 59
Table 16. High Speed Data Wiring 60
Table 17. Thrust Stand Load Cell Data Acquisition Assignments 61

THIS PAGE INTENTIONALLY LEFT BLANK

NOMENCLATURE

CCET	-	Compressible Chemical Equilibrium and Transport
Cequel	-	Chemical Equilibrium in Excel
CFD	-	Computational Fluid Dynamics
CFDRC	-	Computational Fluid Dynamics Research Corporation
DDT	-	Deflagration to Detonation Transition
NPS	-	Naval Postgraduate School
ONR	-	Office of Naval Research
PDE	-	Pulse Detonation Engine
TPI	-	Transient Plasma Ignition
USC	-	University of Southern California
ZND	-	Zeldovich–Neumann–Döring
A	-	amperage
A	-	Area
c	-	speed of sound
C_P	-	constant pressure coefficient of specific heat
f	-	fuel to air ratio
g	-	gravitational constant
I_{sp}	-	specific impulse
l	-	length
m	-	meter
mm	-	millimeter
M	-	Mach number
$M_{refresh}$	-	refresh Mach number
$\dot{m}_f$	-	mass flow rate of fuel
$\dot{m}_a$	-	mass flow rate of air
$\dot{m}_{tot}$	-	total mass flow rate
mJ	-	milli-Joules
P	-	pressure
q	-	specific heat
T	-	temperature
s	-	entropy
t	-	time
TI	-	Turbulence Intensity
u	-	velocity
U	-	velocity
V	-	voltage
v	-	specific volume
$\bar{V}$	-	bulk velocity
w	-	specific work
ϕ	-	equivalence ratio
γ	-	specific heat ratio
λ	-	wave length
ρ	-	density

THIS PAGE INTENTIONALLY LEFT BLANK

ACKNOWLEDGMENTS

The author wishes to recognize and express his appreciation and admiration to Professors Chris Brophy and Jose Sinibaldi for their enthusiasm, expertise, and patient assistance throughout this thesis work. Thanks also go to Mr. George Hageman for his technical expertise and hours of work dedicated to this endeavor. The efforts and support of our colleagues at the University of Southern California (USC) and Stanford University as well as our research sponsors at the Office of Naval Research (ONR) are acknowledged and truly appreciated.

The author also thanks his wife, Keri, and son, Payden, for their understanding and patience during the many late hours and weekends spent working on this research. The Canadian Air Force is also appreciated for providing the funding for the author and sponsoring the authors time at the Naval Postgraduate School.

THIS PAGE INTENTIONALLY LEFT BLANK

I. INTRODUCTION

Pulse Detonation Engines (PDEs) have received renewed interest over the past 10 years due to advances made in the technology and study of PDEs. Detonations have been actively studied for more than a century; however, most of the studies have included non-propulsion applications for detonations. One of the key problems of using detonations for the application of propulsion is the detonation initiation process. The PDE uses repetitive detonations as a method of producing thrust, an idea first explored by German scientist H. Hoffman in the late 1930's [1]. The PDE is predicted to be capable of producing practical thrust levels with a specific impulse equal to or in excess of those seen in both gas turbine engines and ramjet engines when operating in a particular range of Mach numbers. Figure 1 depicts various engine concepts and their respective specific impulse over their practical flight Mach number range [2].

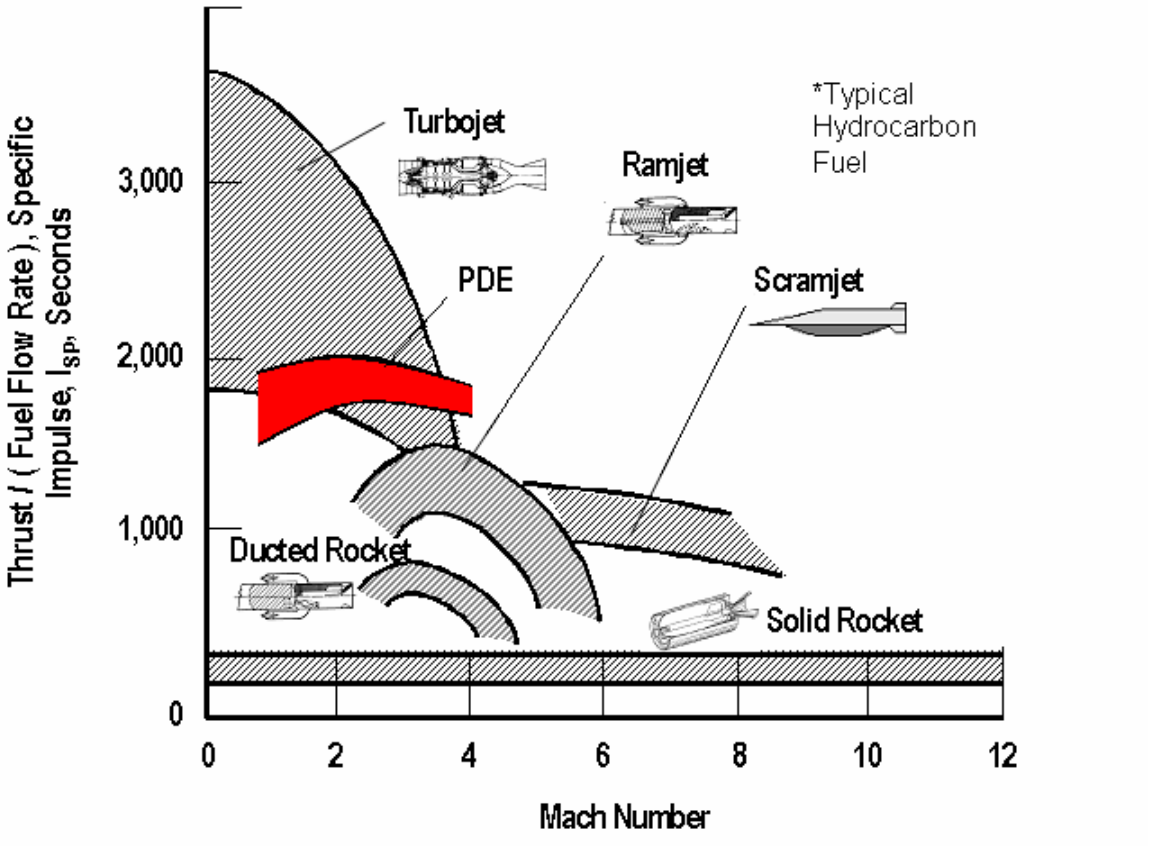

Figure 1. Performance Comparison of High-Speed Propulsion Technologies

Although turbojets demonstrate superior performance at subsonic and low supersonic Mach numbers, their performance decreases rapidly as Mach number increases. As Mach number approaches approximately four, a turbojet's performance is diminished not only by thermodynamic limits but also by structural limitations of the internal machinery and combustor casing. Ramjet and scramjet engines are able to produce thrust with a comparable specific impulse at these higher Mach Numbers but lack the capability to operate at lower Mach numbers due to the fact that they have no mechanical compression and rely solely on the inlet diffuser which requires high Mach number. Due to this operating limitation, these engines must be boosted to a transitional flight speed by either a rocket or another engine adding complexity, cost, and weight.

Conventional fighter aircraft have been limited to flight Mach numbers of 2-3 due to the limitations of existing engines. Commercial aircraft have been limited to sub-sonic flight with the exception of the expensive and now retired Concord. Missiles have been powered by inefficient solid rockets for short ranges and relatively expensive expendable turbojets for longer ranges. PDE systems could prove to be a replacement, in appropriate applications, to all the preceding engine concepts, especially when cost is a consideration. The PDE has the potential to combine high specific impulse with the capability to operate at both subsonic and supersonic Mach numbers. Alternative architectures are exploring hybrid combined cycle concepts which may even propel space vehicles en route to space. Although there has not been a developed PDE put into production, computational and experimental evaluation of the concepts predict that PDEs could possibly operate more efficiently than a ramjet and even low bypass gas turbine jet engines while possessing less cumbersome design with little or no moving parts and simpler geometry [3].

The relatively simple engine design and near absence of moving parts has caused PDEs to become an alternative propulsion concept for supersonic missions. The Naval Postgraduate School (NPS) has already conducted research demonstrating the use of both gaseous and liquid fuels in a PDE including ethylene, propane, and JP-10 [4,5]. These fuels have been used in a PDE at NPS with the aid of an ethylene/oxygen initiator to initiate a detonation in the primary fuel/air mixture. Although an operational PDE would not be competitive if penalized by the requirement to carry highly pressurized gaseous fuel and therefore, if to be competitive, it must be able to directly detonate liquid fuel-air

mixtures. An initiator is often a small “pilot” combustor filled with an easily detonable mixture used to initiate the detonation wave, as it can be difficult to detonate fuel-air mixtures directly.

A unique property of PDEs when compared to traditional engines is that they detonate the fuel-air mixtures where conventional air breathing engine platforms deflagrate their fuel-air mixtures. By deflagrating a fuel-air mixture, a conventional engine increases the temperature of the working fluid while imposing a small pressure drop due to flow expansion and losses while increasing the entropy substantially. Near the exit of the combustor, flow is left at a high temperature and almost equal pressure state that can then be expanded through a turbine or accelerated through a nozzle to produce work or thrust. Alternatively, a PDE detonates the fuel-air mixture through a supersonic combustion wave led by a shock wave in front that compresses the unburned mixture immediately prior to combustion. This method of combustion results in higher temperatures, higher pressures, and a relatively low entropy increase for the combustion products which can then be expanded or accelerated to produce work or thrust [6].

Due to the transient filling and combustion characteristics of PDEs they are inherently unsteady. Since the combustion is extremely rapid, as soon as the detonation exits the engine, the process must be repeated in order to maximize the overall energy conversion rate and net thrust. The thrust produced by the engine is directly dependant upon how often this combustion event can be repeated. Operating a PDE at higher frequencies has the additional benefit that at high frequencies the unsteady thrust is dampened by the inertia of the PDE and becomes quasi-constant. Therefore much emphasis is placed on minimizing the cycle time and thus, increasing the operating frequency.

The greatest challenge facing the continued development of PDEs is the reliable and rapid initiation of the detonations inherently required to operate the engine. This challenge has been identified as one of the critical and enabling technologies for PDEs. While methods exist to directly detonate a fuel-air mixtures they are either unrealistic or impose unacceptable losses to the system which will be discussed later. Transient Plasma Ignition is a new ignition technology that when combined with an initiator geometry

containing turbulence/generating shock reflecting devices can substantially improve the timescales associated with ignition and the initiation of a detonation. The strategy relies on first deflagrating the fuel-air mixture and then causing the deflagration to transition to a detonation and is commonly referred to as Deflagration-to-Detonation Transition or DDT. The acceleration process is often achieved by placing obstacles in the flow path of the deflagration wave. These obstacles cause turbulence and mixing of the unburned reactants and the combustion wave, as well as shock reflections thus increasing the effective flame surface and accelerating the deflagration to a detonation. The fluid dynamics, thermodynamics and chemistry behind this process are complicated and there are numerous efforts being carried out throughout the world to model the process and predict obstacle effects.

Previous work at NPS demonstrate successful operation of a PDE using gaseous ethylene/air mixture which used transient plasma ignition (TPI) for ignition and flow obstacles for detonation initiation. A PDE was designed for this research that has eliminated the requirement for supplementary oxygen as well as enabling the use of a JP-10, high-density liquid fuel. Air flows through segments of this PDE were simulated using Computational Fluid Dynamics and experimentally evaluated in the laboratory at simulated flight conditions, including supersonic cruising conditions.

II. BACKGROUND

A. DETONATION THERMODYNAMICS

A discussion on the thermodynamics and structure of detonations is required in order to adequately explain how a PDE operates. A detonation wave is a supersonic combustion wave that propagates through a gas, liquid or solid combustible mixture which involves a shock wave followed by a combustion front. The shock compresses the substance thereby increasing it pressure, temperature, and overall reaction rate. The temperature is locally increased beyond the auto-ignition condition for mixture and the energy released behind the shock further strengthens/reinforces the shock.

Detonation and deflagration combustion waves can be more easily understood if discussed in the frame relative to the wave. Figure 2 illustrates in a stationary one-dimensional (1-D) planar wave [6]. In this frame of reference, the unburned gas approaches the combustion wave at velocity u_1 with static thermodynamic properties ρ_1, T_1 and P_1. After combustion, the products move away from the combustion wave at velocity u_2 and with static thermodynamic properties ρ_2, T_2 and P_2. Combustion experiments by Friedman indicated quantitative differences in these values based on whether the combustion was deflagration or detonation [7]. A summary of these experiments can be seen in Table 1.

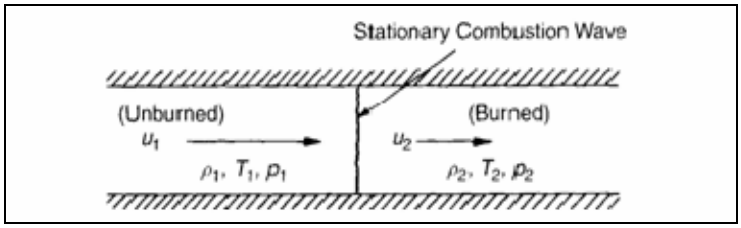

Figure 2. Schematic Diagram of a Stationary 1-D Combustion Wave (Deflagration or Detonation)

	Detonation	**Deflagration**
u_1/c_1	5-10	0.0001-0.03
u_2/u_1	0.4-0.7 (deceleration)	4-16
p_2/p_1	13-55 (compression)	0.98-0.976 (slight expansion)
T_2/T_1	8-21 (heat addition)	4-16 (heat addition)
ρ_2/ρ_1	1.4-2.6	0.06-0.25

Table 1. Qualitative Differences between Detonation and Deflagration

The characteristics listed in Table 1 reveal that a detonation results in a tremendous increase in pressure whereas a deflagration actually imposes a small loss in pressure due to flow expansion. The pressure increase, the slightly larger temperature increase and the lesser increase in entropy are what make the detonation a more efficient method of combustion. The increase in pressure removes the requirement for a costly and complicated high pressure compressor, therefore potentially decreasing the cost and complexity of a PDE system when compared to turbo-machinery.

Through the use of the conservation equations and an in depth thermodynamic analysis it can be shown that there is a relationship between a gases properties, pressure, density and ratio of specific heats, and the heat added to the gas [6,7]. This relationship, know as the Rankine-Hugonoit relation, is provided in Equation 1.

$$\frac{\gamma}{\gamma-1}\left(\frac{p_2}{\rho_2}-\frac{p_1}{\rho_1}\right)-\frac{1}{2}(p_2-p_1)\left(\frac{1}{\rho_1}+\frac{1}{\rho_2}\right)=q \qquad (1)$$

Using this equation and plotting P_2 versus $1/\rho_2$, for a fixed heat release per unit mass, the Hugonoit curve is created and is shown in Figure 3.

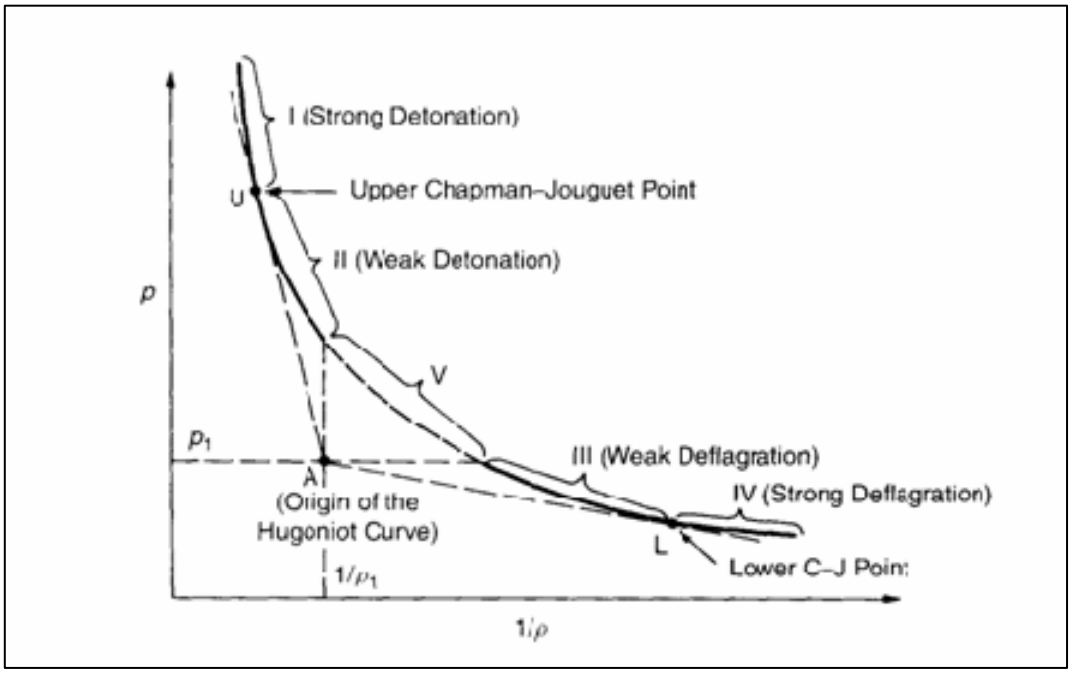

Figure 3. Hugonoit curve on *P*-versus-$1/\rho$ plane

The Hugonoit curve, essentially, represents all of the mathematically possible values for P_2 an ρ_2 for a given set of initial values of P_1, ρ_1, and q. The values are divided into five separate regions, region V is a mathematical solution only and is not physically valid. Region I represents the possible values for P_2 and ρ_2 for the products of a strong detonation while region II represents the possible values for P_2 an ρ_2 for the products of a weak detonation. Similarly, region III represents the possible values for P_2 an ρ_2 for the products of a weak deflagration while region IV represents the possible values for P_2 an ρ_2 for the products of a strong deflagration.

B. DETONATION INITIATION

The ability to achieve the thermodynamic benefits of a detonation depends on the ability to obtain a detonation. Two common methods exist to generate a detonation in fuel-air mixtures. One can either directly detonate the fuel-air mixture or transition a deflagration to a detonation using obstacles in the combustion flow field.

The direct initiation of a detonation employs the use of a high energy chemical or electrical ignition source which allows for an extreme release of energy over a relatively short period of time therefore causing the direct formation of the gas dynamic structure required for a detonation wave. The use of an extremely high power electrical ignition source, in excess of 1000 Joules, that contains sufficient energy to cause a detonation has been demonstrated in a laboratory but through the use of heavy bulky equipment. Considering the weight, volume, and power requirements of an ignition system capable of the required ignition energy for an airborne system, this is not a viable option. An alternative version of this first method involves the use of easily detonable supplementary gases. It was found that the gain in detonability was offset by the reduction in specific Impulse (I_{sp}) since the auxiliary oxygen used in the "initiator" gases must be considered as a "fuel" for I_{sp} calculations. Equation 2 shows that I_{sp} decreases for a given thrust level as mass flow rate of fuel and/or required initiator reactants increases. While both methods have there shortfalls, they have both been proven to be effective in achieving rapid and reliable detonations.

$$I_{sp} = \frac{Thrust}{\dot{m}_f} = \frac{Thrust}{\dot{m}_f + \dot{m}_{init}} \tag{2}$$

All gases and/or liquids carried onboard the vehicle are considered as fuel when calculating I_{sp}. Because the supplementary gases impose a negligible increase in thrust yet a substantial increase in mass flow of effective fuel, the I_{sp} is reduced. This method is further penalized by the fact that volume and weight allotments for the flight vehicle must be used for the auxiliary reactants.

The mechanism of DDT is explained well in Kuo where he summarizes the transition using the following steps from reference 3:

1. Generation of compression waves ahead of an accelerating laminar flame (see Figure 4). The laminar flame front is wrinkled at this stage.
2. Formation of a shock front due to coalescence of compression waves (see Figure 4).
3. Movement of gases induced by the shock, causing the flame to break into a turbulent brush (see Figure 4).

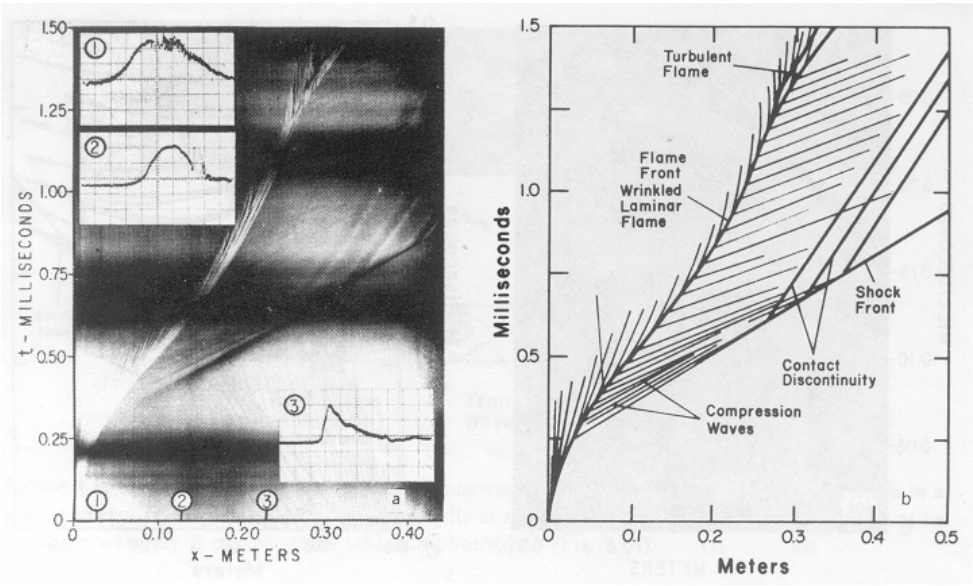

Figure 4. Streak Schlieren Photograph of the Development of Detonation

4. Onset of "an explosion in an explosion" at a point within the turbulent reaction zone, producing two strong shock waves in opposite directions and transverse oscillations in between. These oscillations are called transverse waves (see Figure 5). The forward shock is referred to as superdetonation and moves into the unburned gases. In the

opposite direction, a shock moves into the burned gases and is know as retonation.

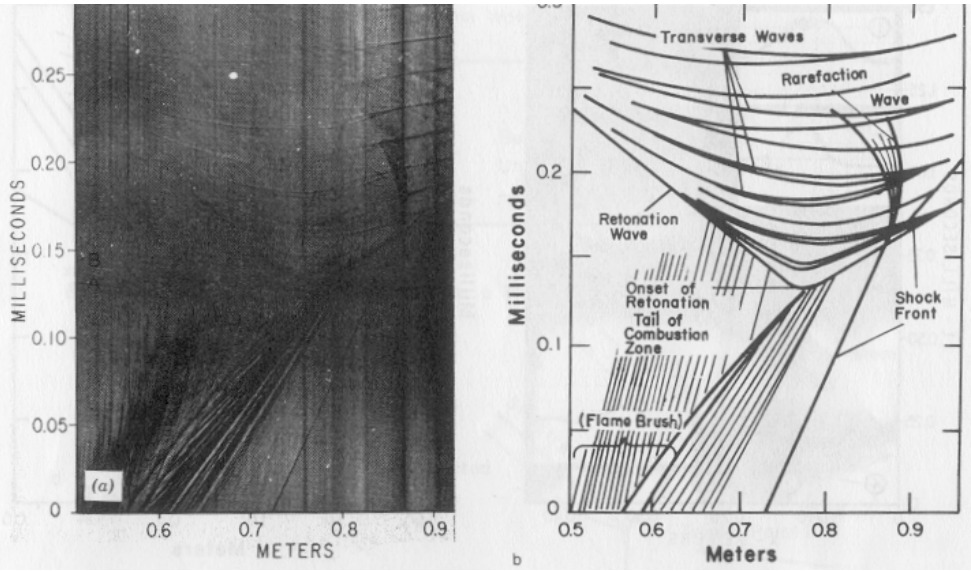

Figure 5. Streak Schlieren Photograph of the Onset of Retonation

5. Development of spherical shock at the onset of the "explosion in an explosion" with a center located in the vicinity of the boundary layer (see Figure 6).

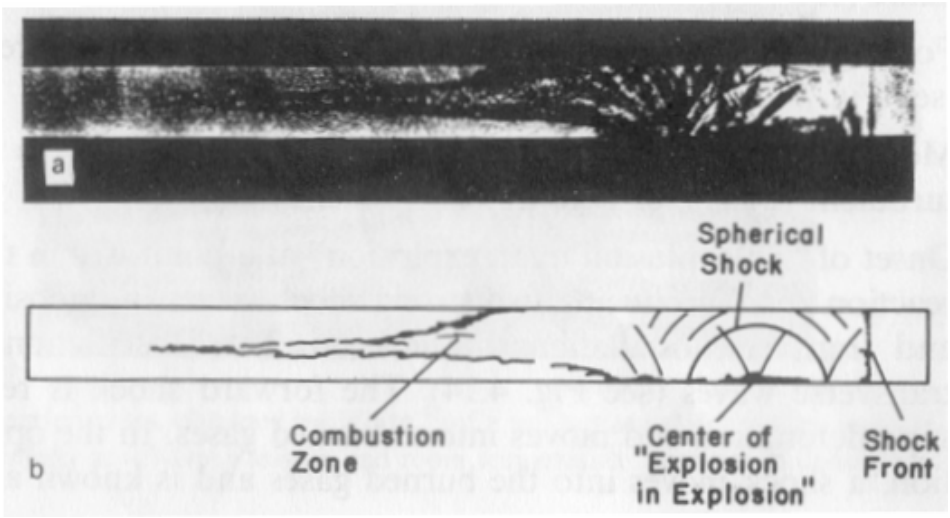

Figure 6. Flash Schlieren Photograph of the Onset of Retonation

6. Interaction of transverse waves with shock front, retonation wave, and reaction zone (see Figure 7).
7. Establishment of a final "steady wave" as a result of a long sequence of wave inter-reaction processes that lead finally to the shock deflagration ensemble: the self-sustained C-J detonation.

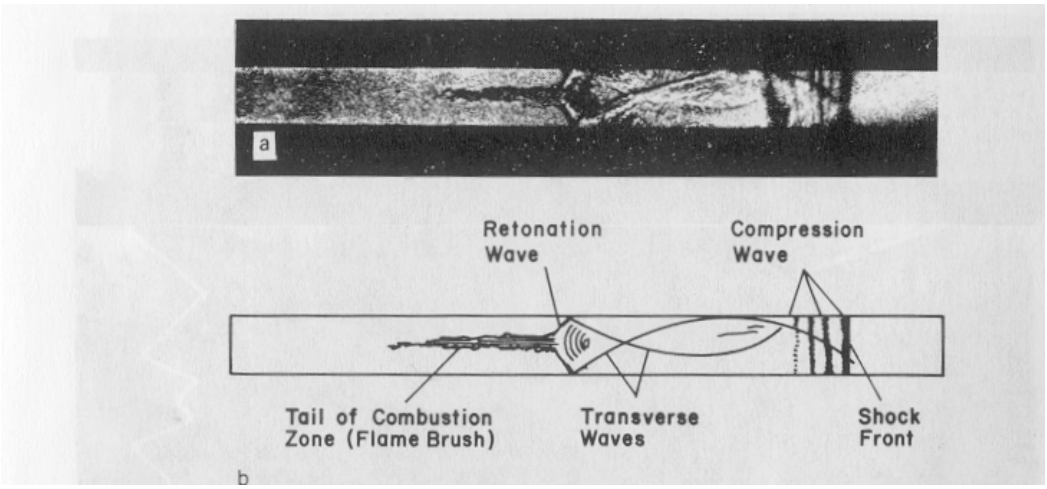

Figure 7. Flash Schlieren Photograph of Transverse Waves Set up at the Onset of Retonation

All detonations possess a particular structure. The understanding of the structure of a detonation wave has improved greatly due to experimental efforts in the 1960's. The original model assumed for a detonation wave was a 1-D structure. This structure is known as a 1-D Zeldovich–Neumann–Döring (ZND) detonation wave and is shown in Figure 8. The 1-D model consisted of a leading shock wave followed by an induction zone the shock wave where the reactants are at a higher pressure and temperature due to the compression heating. It is assumed that no reactions occur until a specified time after the shock wave. This assumption is valid as the thickness of the shock wave is only of the order of two to three molecular mean free path lengths (λ). Most of the reactions, and therefore heat release, were believed to occur in a thick deflagration zone after the shock wave. The induction zone is the region behind the shock where the reaction rates increase slowly and the pressure and density are almost constant. The reaction zone follows the induction zone and is where the properties quickly change as the reaction rate increases to an extremely high value. Following completion of the reaction the properties relax to near equilibrium values.

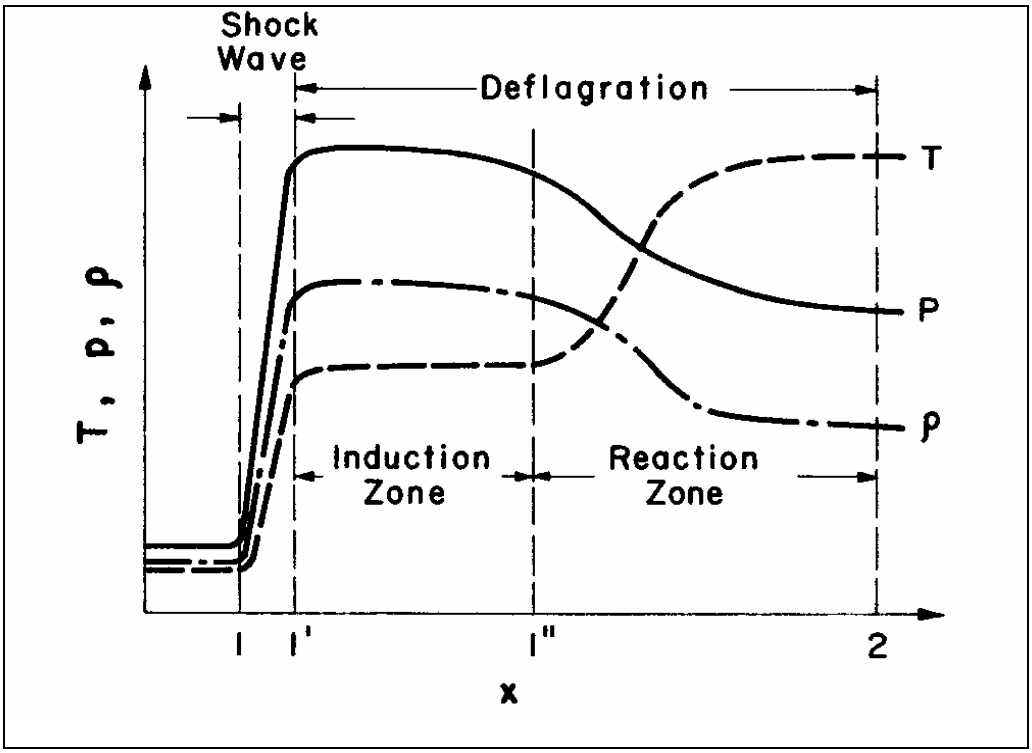

Figure 8. Variation of physical properties through a ZND detonation wave

In the early 1900's scientists realized that there was also a three dimensional (3-D) structure to detonation waves and detonations could not be simplified to 1-D structures. In reference 3, Kuo characterizes the 3-D detonation as follows:

> The detonation-wave structure is characterized by a non-planar leading shock wave which at every instant consists of many curved shock sections which are convex toward the incoming flow. The lines of intersection of these curved shock segments are propagating in various directions at high velocities (see Figure 9).

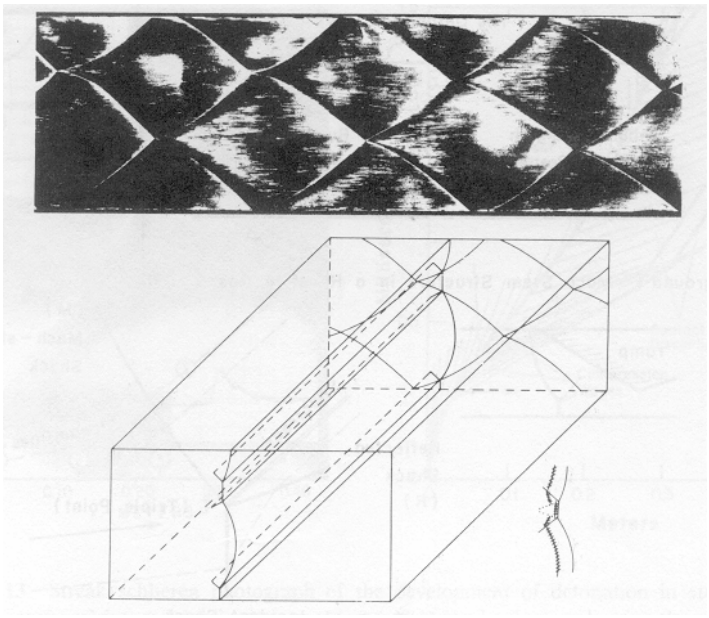

Figure 9. Smoked-foil record and schematic diagram of symmetric planar interaction

The third shock, R, (see Figure 10) of these intersections extends back into the reactive flow regime and is required for the flow to be balanced at the intersection of the two convex leading shock waves. In general, the flow in the neighborhood of the shock front is quite complex. The schematic diagram of symmetric planar interaction is shown in Figure 10.

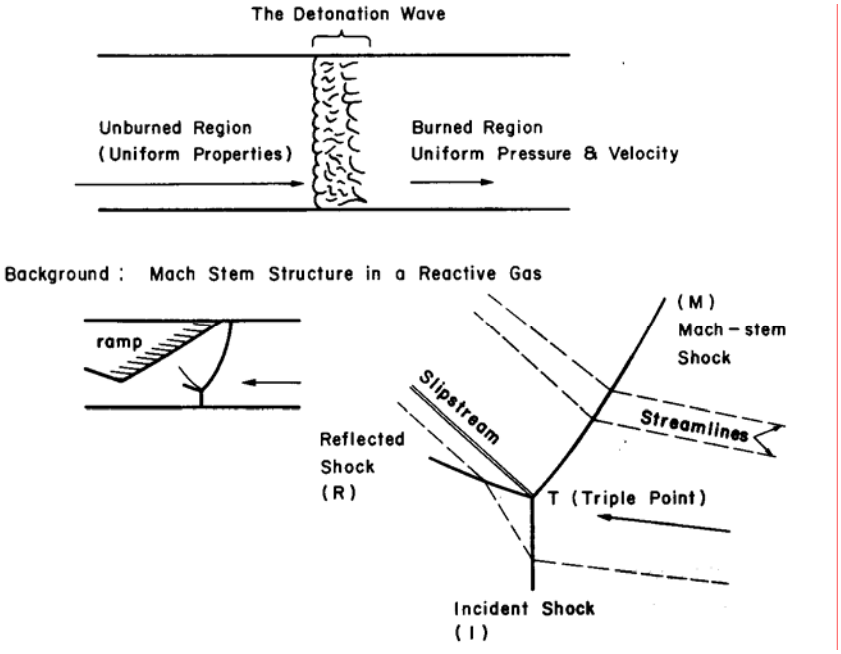

Figure 10. Schematic Diagram Showing the Shock-wave Pattern and Triple Point in a Two-dimensional Supersonic Flow Passing Through a Convergent Ramp Section

A detonation wave is the fundamental process within a PDE that enables the system to achieve higher thermal efficiencies. The benefits and challenges of the detonation, when used in propulsion, have been explained and can now be explored in the application to a PDE

C. PDE THERMODYNAMIC CYCLE

The PDE cycle differs from the turbo- and ramjets in that it detonates its fuel air mixture rather than using a deflagration process as in turbo- and ramjets. The PDE operates by detonating a volume filled with a fuel-air mixture through a detonation wave which propagates down the combustor. Recall that a detonation wave consists of two segments, a leading shock wave followed by a combustion wave. The shock wave compresses the air, through a non-isentropic process, thereby replacing the compressor stage required in a turbojet. The detonation wave is immediately follow by combustion wave which then combusts the now compressed air-fuel mixture. Similar to the ramjets, the PDE has almost no moving parts as it needs no compressor and therefore no turbine.

Due to the detonation process, the PDE cycle combusts the fuel-air mixture at approximately constant volume conditions whereas a turbo- or ramjet combusts its fuel-air mixture at approximately constant pressure. A constant volume combustion process is more thermodynamically efficient than one at constant pressure, in that at constant volume the combustion increases both the pressure and the temperature therefore releasing more energy, whereas a constant pressure the combustion process increases only the temperature. In order to explore the PDE cycle and compare it to the Brayton cycle in a Ramjet both cycles have been simulated using a combustion code named CEQUEL and compared with other propulsion methods in an I_{SP} plot seen in Figure 11 with varying flight Mach number. CEQUEL is described by its owners in this introductory statement [8]:

> CEQUEL stands for “Chemical EQUilibrium in excEL”, and is based on SEA’s CCET™ (Compressible Chemical Equilibrium and Transport properties) code. CCET was derived from NASA Glenns Gordon-McBride CEA (Chemical Equilibrium with Applications) code. Cequel

provides access to most of capabilities available in CCET, but as a function within Microsoft Excel. This eliminates the need to cut and paste from external thermodynamics codes' output files into Excel, and provides the additional power of allowing the output of one Cequel function to be used as the input to other Cequel functions. This allows the user to quickly evaluate many "what-if" scenarios as well as to utilize Excel's built in solvers and optimization routines.

NASA Johnson Space Flight Center funded the initial conversion of CCET into a dynamically linked library (DLL), and a limited VBA interface for a specific application. Since then, SEA has developed Cequel, a suite of general Excel functions for the TP, HP, SP, UV, SV, TV thermodynamic equilibrium point problems, and the rocket problem (area and pressure ratios). In addition, Cequel contains a non-reacting mixing function, which combines isobaric flows with different temperatures and species.

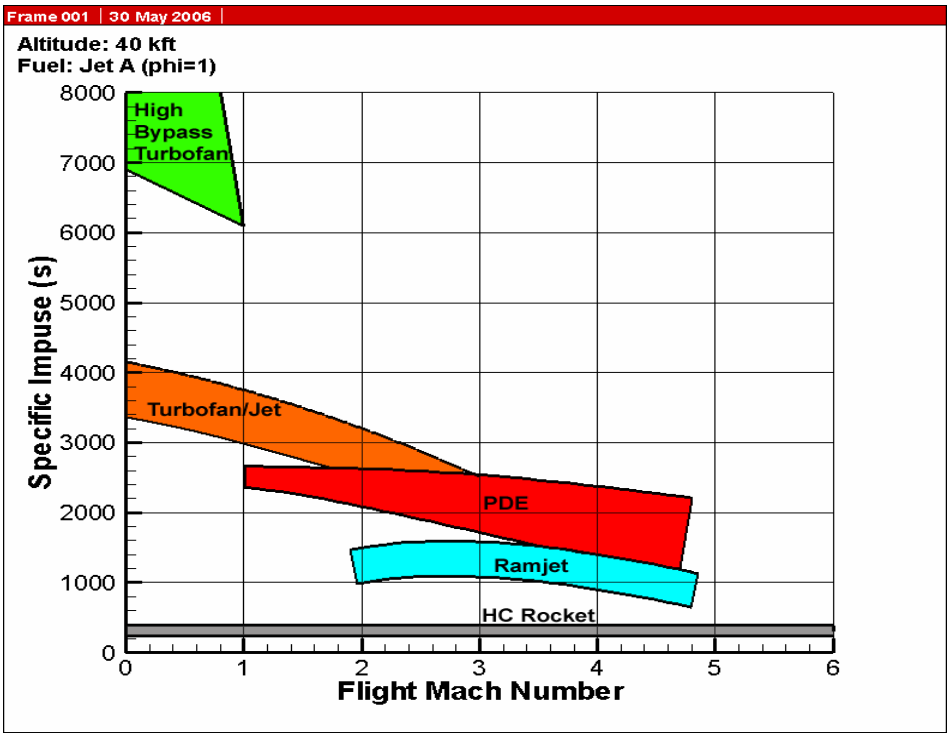

Figure 11. Comparison of Propulsion Technologies Using Combustion Simulation

The PDE is often compared to ramjets due to the benefits existing for supersonic inlet conditions. An analysis of the PDE and ramjet cycles was performed using CEQUEL for a flight Mach number of 4. Identical inlet losses, MIL-SPEC, and flight condition, M=4, were used in the analysis. A schematic of the various stages present in a PDE and ramjet are seen in Figures 12 and 13.

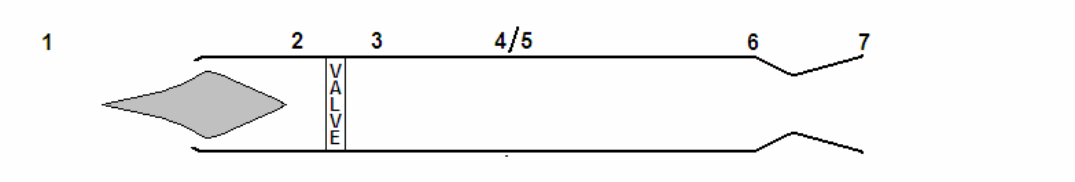

Figure 12. Schematic of a Generic PDE and Appropriate Stages

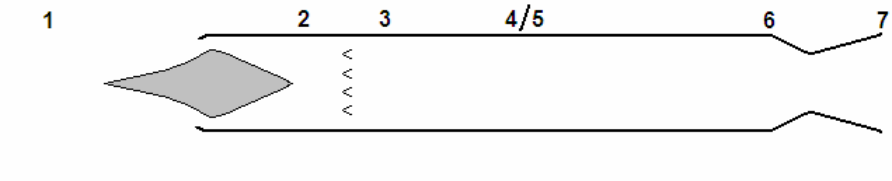

Figure 13. Schematic of a Generic Ramjet and Appropriate Stages

Stages 1,3,6 and 7 of the PDE are of specific interest to a cycle analysis. Stage 1 represents the conditions of the air flow in front of the flight vehicle. Stage 3 is the conditions of the flow after the inlet diffuser and following the valve system, if using a valved PDE. Stage 6 represents the conditions following the combustor after the detonation has completed and the flow properties have reached their equilibrium values. Finally Stage 7 represents the exhaust plane of the nozzle. Similarly, the stages of interest to the analysis of a ramjet are stages 1,2,6 and 7. Where stage 1 represents the condition of the air flow in front of the flight vehicle and stage 2 represents the condition of the flow after the inlet. Stage 6 represents the conditions following the combustor. Finally Stage 7 represents the exhaust conditions at the nozzle exit plane. The properties of the flow as determined using the CEQUEL combustion code at the four stages of interest have been tabulated (Table 2). Two methods of analyzing the cycles have been used and include a Temperature-entropy (T-s) diagram to determine the Isp of the engine and a Pressure-volume (P-v) diagram.

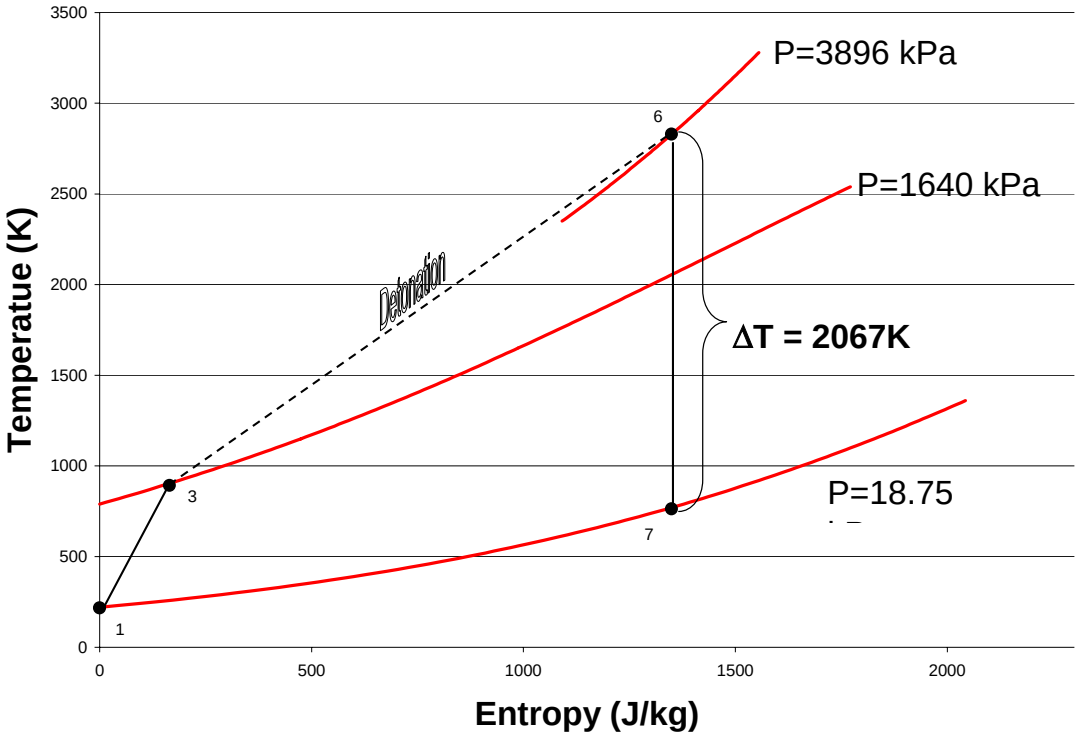

Figure 14. Temperature-Entropy Diagram for a Generic PDE at M=4

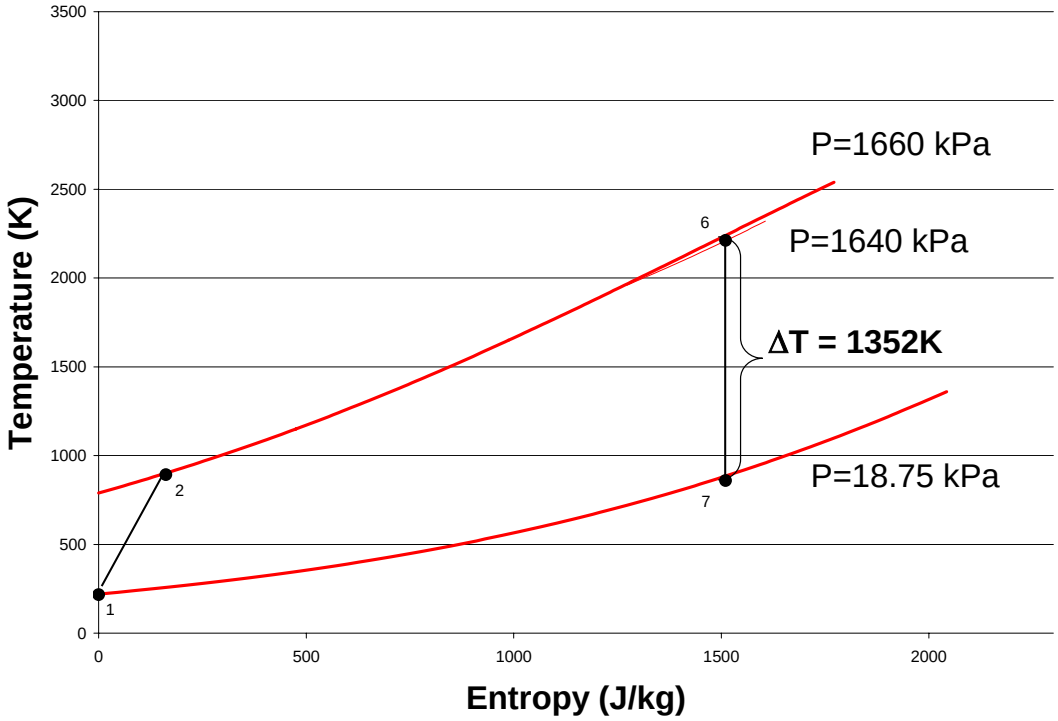

Figure 15. Temperature-Entropy Diagram for a Generic Ramjet at M=4

The specific work equations for both the PDE and the ramjet can be derived as follows;

$$\begin{aligned} w_{PDE} &= \int_6^7 p dv - \int_1^3 p dv - p_1(v_7 - v_1) \\ &= \frac{p_3 v_3 - p_1 v_1}{1-\gamma_{1-3}} + \frac{1}{2}\left(\frac{p_6 - p_3}{v_6 - v_3}\right)\left(v_6^2 - v_3^2\right) \\ &+ \left[p_6 - \left(\frac{p_6 - p_3}{v_6 - v_3}\right)v_6\right](v_6 - v_3) + \frac{p_7 v_7 - p_6 v_6}{1-\gamma_{6-7}} + p_1(v_1 - v_7) \end{aligned} \tag{3}$$

$$\begin{aligned} w_{Ramjet} &= p_2(v_6 - v_2) + \int_6^7 p dv - \int_1^2 p dv - p_1(v_7 - v_1) \\ &= p_2(v_6 - v_2) + \frac{\left(p_2 v_2 - p_1 v_1\right)}{1-\gamma_{1-2}} + \frac{(p_7 v_7 - p_6 v_6)}{1-\gamma_{6-7}} + p_1(v_1 - v_7) \end{aligned} \tag{4}$$

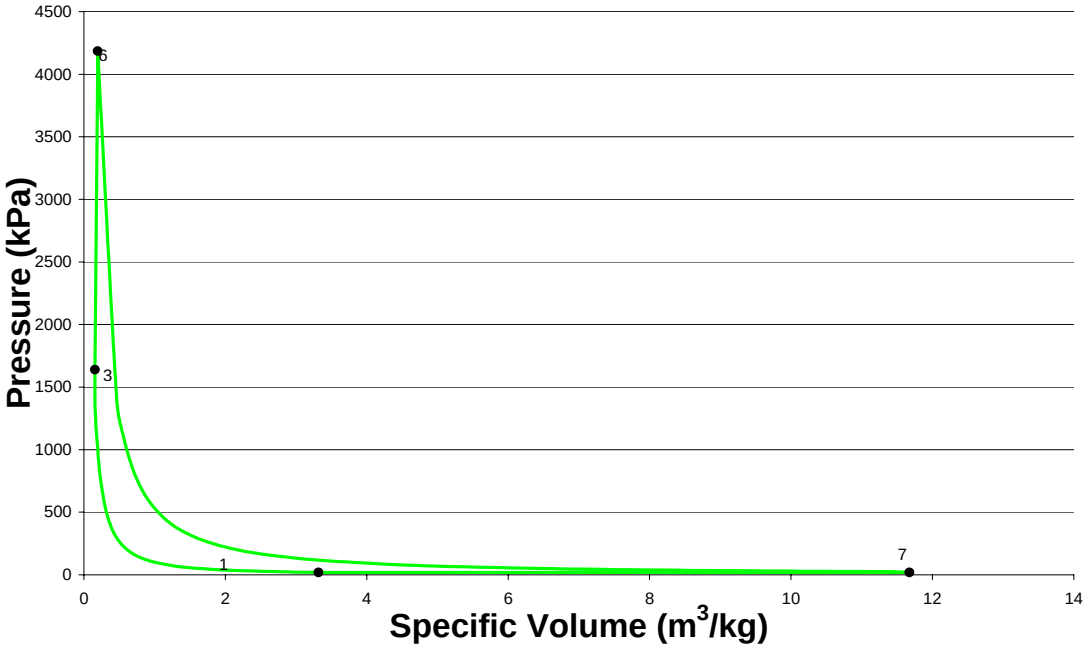

Figure 16. P-V Diagram for a Generic PDE at M=4

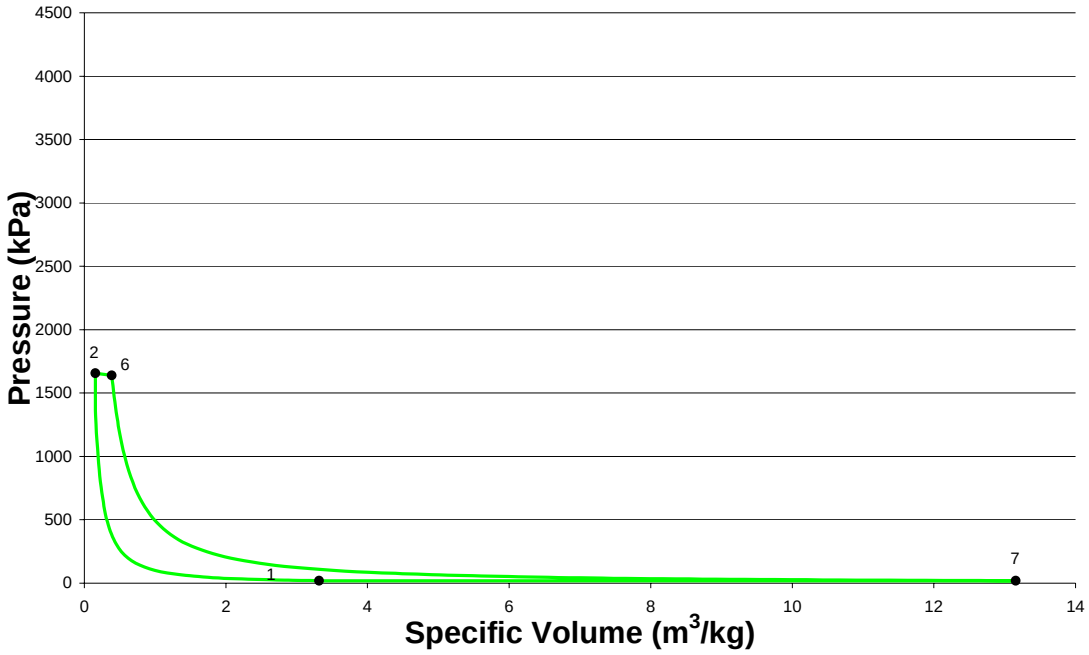

Figure 17. P-V Diagram for a Generic Ramjet at M=4

Assuming a quasi-steady approach allows the use of Equation 3. This equation and the entropy difference available to the nozzle can be used to determine the fuel based I_{SP}.The properties at each stage of each cycle in Tables 2 and 3 are used in Equation 3 to determine the I_{SP} from each cycle and can be seen in a T-s diagram in Figures 14 and 15 for the PDE and ramjet respectively. As depicted in the Figures the PDE demonstrates a higher temperature change at a flight Mach number of 4 and hence a higher I_{SP}.

$$I_{sp} = \frac{(1+f)u_7 - u_1}{f \times g} \quad \text{where,} \quad u_7 = \sqrt{C_P(T_6 - T_7)} \tag{3}$$

PDE Cycle					
	T	P	Gamma	S	v
1	216.6667	18.7485714	1.39	0	3.316697
3	892.67	1639.74	1.39	165.0445	0.156241
6	2829.66	4185.46901	1.295	1349.625	0.194031
7	762.66	18.7485714	1.32	1349.625	11.67474

Table 2. Flow properties for a PDE at M=4 at stages 1,3,6 &7

Brayton					
	T	P	Gamma	S	v
1	216.66	18.748	1.39	0	3.316696
2	892.6392	1657.13786	1.39	162.0074	0.154596
6	2211.825	1639.47778	1.24	1510.592	0.387193
7	859.3323	18.748	1.26815	1510.57	13.15492

Table 3. Flow properties for a Ramjet at M=4 at stages 1,2,6 &7

The properties at each stage of each cycle in Tables 2 and 3 are used in Equations 3 and 4 to determine the specific work from each cycle and can be seen in a P-v diagram in Figures 16 and 17 for the PDE and ramjet respectively. The PDE demonstrates its improved performance with a greater specific work at a flight Mach number of 4.

The results of this analysis are seen in Table 4 where each cycle is listed with its corresponding entropy change, net work, and fuel based I_{SP}. This table indicates that the PDE outperforms both the turbo- and ramjets thermodynamically.

	Entropy Change (kJ/kg)	**Net Work (kJ/kg)**	**Specific Impulse Isp (s)**
PDE	1.350	1803	1772
Ramjet	1.511	1092	1319

Table 4. Cycle comparison for PDE and ramjet engines at M=4

D. PERFORMANCE CONSIDERATIONS

A PDE can vary the thrust produced by two methods. The frequency of operation can be increased, where the aggregate impulse per cycle is relatively constant and the increase in frequency would therefore increase the impulse per unit time. The second method to vary thrust is by fill fraction where, for a given frequency, the volume of fuel-air mixture being processed per cycle can be altered by partially filling the PDE with fuel-air mixture. The mass flow per unit time of reactants will be varied therefore varying the thrust as seen in Equation 6.

$$Thrust = \dot{m}_a \left((1+f)u_7 - u_1 \right) \tag{6}$$

The PDE operational frequency may be increased if the total cycle time can be reduced sufficiently to achieve the desired frequency. Equation 7 shows the time components present in a PDE.

$$t_{cycle} = t_{refresh/\,fill} + t_{ignition\_delay} + t_{initiation} + t_{detonation} + t_{blowdown} + t_{purge} \qquad (7)$$

where, $t_{refresh/\,fill} = t_{refresh}$ or t_{fill} which ever is greatest, where $t_{refresh} = \frac{l_{initiator}}{M_{refresh} c}$ and $t_{fill} = \frac{l_{combustor}}{M_{fill} c}$, $M_{refresh}$ is the average Mach number at which the PDE initiator is refreshed with new reactants. This can be thought of as a non-dimensional refresh mass flow rate and is defined as:

$$M_{refresh} \equiv \frac{\bar{V}}{C_{CL}} = \frac{\dot{m}_{refresh} / \rho_{refresh} A_{initiator}}{\sqrt{\gamma R T_{CL}}} \quad (8), \text{ similarily } M_{fill} \equiv \frac{\bar{V}}{C_{CL}} = \frac{\dot{m}_{fill} / \rho_{fill} A_{combustor}}{\sqrt{\gamma R T_{CL}}} \quad (9)$$

Where $l_{combustor}$ is the length of the combustor portion of the PDE and $l_{initiator}$ is the length of the initiator which must be long enough to achieve transition to initiation of a detonation wave. The ignition delay, $t_{ignition\ delay}$, is the time between the ignition event and a fully developed flame and is dependant upon the stoiciometry, local flowfield, and ignition physics, $t_{ignition\ delay}$ is on the order of 3.5 ms for most practical hydrocarbon fuels.

$$t_{initiation} \approx \frac{l_{initiation}}{M_{detonation} c} \quad (10), \qquad t_{detonation} = \frac{l_{combustor}}{M_{detonation} c} \quad (11), \qquad t_{blowdown} \approx \frac{l_{PDE}}{c_{products}} \qquad (12),$$

and t_{purge} is the amount of time flow occurs between the last of the hot products and first of the new reactants and is design dependant such that it is sufficient to separate the hot products from the new reactants. Decreasing any of these preceding times can result in a higher possible operating frequency and thus a higher producible thrust. Of the six time segements that the cycle time depends on, only $t_{detonation}$ and $t_{refresh/fill}$ can realistically be decreased to substantially decrease the overall cycle time. Recall from Equation 11 that $t_{detonation}$ is directly proportional to the length of the combustor. Therefore, if one can decrease length of the combustor the frequency of operation can be increased. However, keeping the same cross-sectional area, a decrease in the length of the combustor would also cause a decrease in the volume of fluid being processed per cycle and hence have a decreasing effect on the thrust. The second method to decrease the cycle time would be to decrease the $t_{refresh/fill}$ parameter. This can be accomplished by simply increasing the mass flow rate at which the initiator and combustor are filled. This can be done to such a

point that the flow becomes choked. The pressure drop associated with refreshing the combustor at high subsonic Mach numbers outweighs the gain in frequency and the velocities in the ignition region often become sufficiently high to prevent ignition of the fuel-air mixture. Using a combination of these two methods the cycle time can be decreased to increase the thrust produced by the engine.

The thrust produced by the engine can also be modified by altering the length of the combustor or its diameter, or a combination of both. This increases the volume and therefore mass of fluid processed by the engine per cycle. As previously mentioned, the length of the combustor and the operating frequency are linked by an inverse relationship. Therefore there is little gain from increasing the length of the combustor. Increasing the diameter of the combustor is another way to increase the mass flow being processed by the engine. However, in order to support the 3-D structure of a detonation the flow field diameter is limited to a value that will support a detonation structure and is often near one cell size [6]. Once the detonation is established at a given diameter the flow field diameter can be stepped up to a new value as long as the step is sufficiently small enough not to ensure the detonation does not fail through the diffraction proccess. Obviously each of these discrete steps must occur over some length to allow the detonation to re-establish its strength before attempting another increase in diameter. These additional lengths in the flow field will, as previously explained previously, increase the over cycle time and decrease the maximum attainable frequency.

A combination of both methods for altering the thrust attainable from a PDE should be used together in an attempt to achieve an optimum configuration. This, of course, will depend upon the PDEs application whether that be for a long slender missile or a flight vehicle in which volume for payload is important. The PDE could be tailored to its application allowing for the specific concerns of each possible application.

THIS PAGE INTENTIONALLY LEFT BLANK

III. DESIGN & MODELING

The combustor design of the PDE evaluated during this research is intended to be used as the initiator unit in a split flowpath design. The initiator combustor possessed various turbulence devices which promote the DDT process, but at a performance penalty due to the relatively large pressure drop through the unit. Although approximately 25% of the total airflow will pass through the initiator unit, the remaining flow will by pass coaxially around the unit and be directed into the main combustor. Figure 18 shows a section view of the proposed design layout.

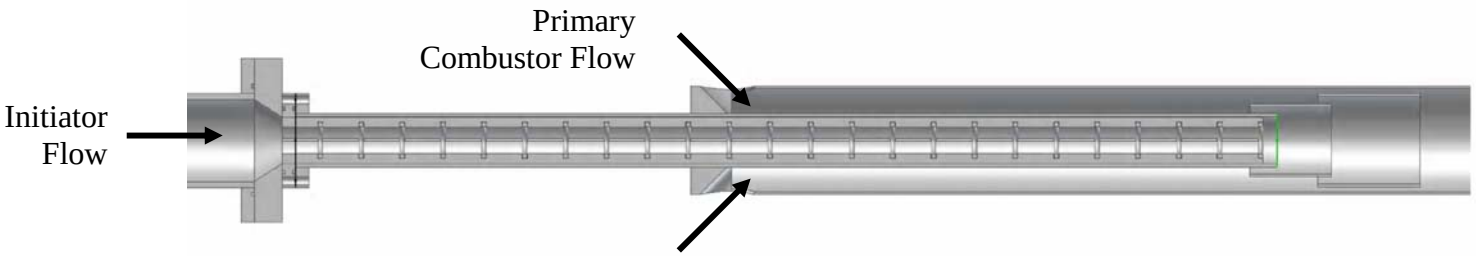

Figure 18. New PDE Initiator Design With Combustor Section View

The ignition system used was a Transient Plasma Ignition (TPI) developed at the University of Southern California (USC) by Martin Gundersen and his research group [9]. The interface for the TPI system was tailored to lend to the research goals of this paper.

A transient plasma discharge, sometimes called pulsed corona discharge, depicted in Figure 19 [10] has unique fundamental properties and benefits when compared to a traditional spark.

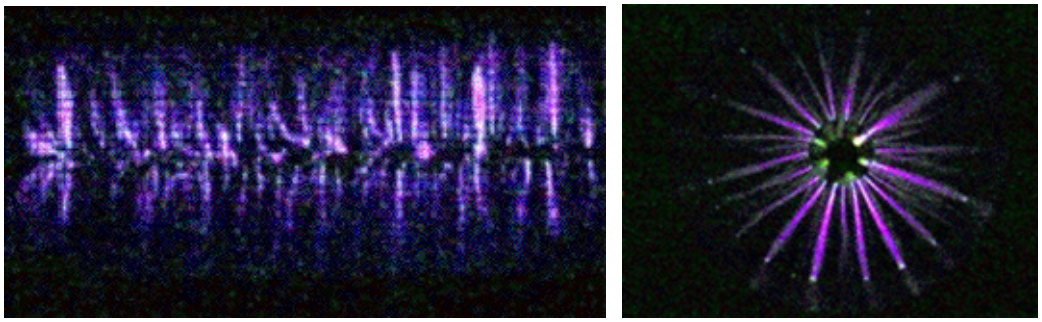

Figure 19. Corona from TPI

Due to the discharge physics, hundreds of "streamers" can readily ignite a mixture at tens to hundreds of regions simultaneously. Traditional capacitive discharge spark ignition discharges at a single location and typically contains electrons with energy levels of 1-3 eV. The TPI system delivers pulses of 70 to 100 kV within 50 to 100 ns at currents from 450 to 600 A, as depicted in Figure 20 [11], and creates electrons with energy levels of 10-30 eV. However, the total energy input is less than one Joule and is comparable to capacitive discharge systems.

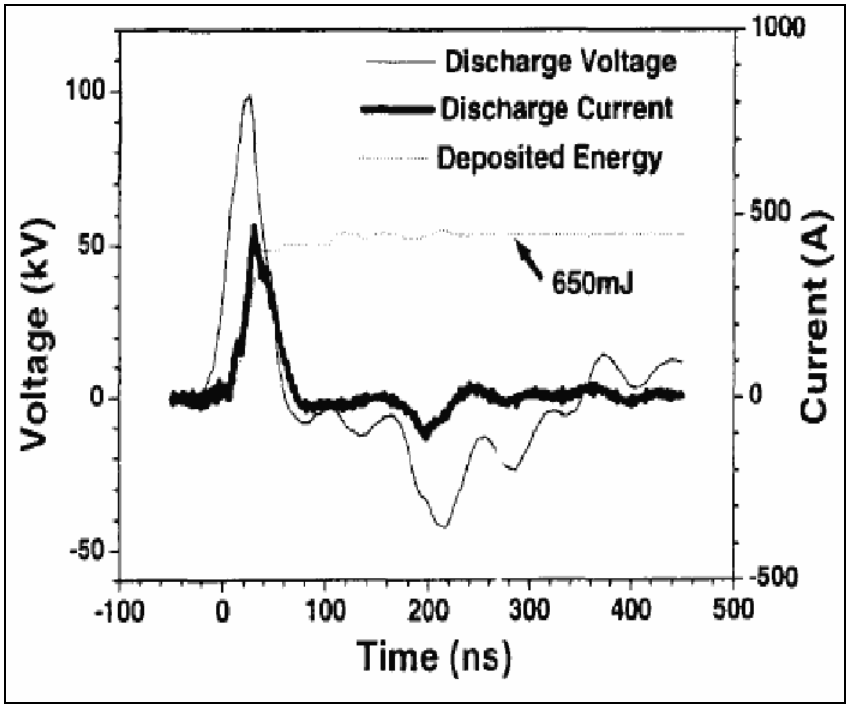

Figure 20. Voltage and Current from TPI

Results obtained during the early stages of this research indicated deficiencies in the TPI electrode holder design used in previous research at NPS. The previous TPI holder used at NPS was made of Macor, an insulating ceramic, with a threaded Macor cap to secure the TPI electrode. The air gap present within the mating threads of the two pieces of Macor resulted in an electrical path, between the TPI electrode and the ground, shorter than that between the bare electrode and the chamber wall. Due to this path the TPI would occasionally arc through the gap rather than discharge a corona at the electrode. Additionally, the insulator cap was under tension which is not favorable for ceramic

composites (Figure 21). A new TPI holder was then designed and can be seen in Figure 22. The new design eliminated the shorter electrical path through the thread gap and resulted in a design based on compression of the Macor, not tension.

Figure 21. TPI Holder Screw Cap Failure

Parts List			
ITEM	QTY	PART NUMBER	DESCRIPTION
1	1	ignitor	
2	1	Macor	
3	1	Teflon	
3	1	metal1	
5	1	Metal Insert	
6	1	metal2	

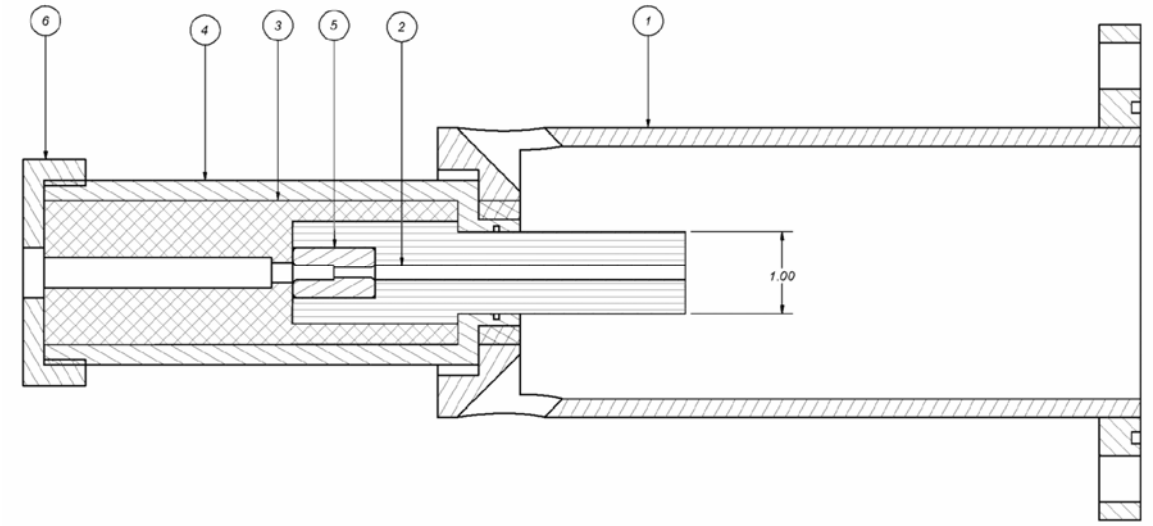

Figure 22. TPI Electrode Holder and Insulator Design Installed in Ignition Section

The PDE initiator designed for this research, as seen in Figure 23, was designed based on results from previous research obtained on a pre-existing engine [12]. Following the ignition section a spiral or ringed initiator can be installed. A hotwire anemometer

was used to explore the flow field present in the PDE used during previous research at NPS [12]. The data collected shows the exit velocity, exit turbulence and pressure loss though the PDE at varying flow rates. The velocity and turbulence at the exit plane centerline with varying flow rates and different flow conditioning screens (Figure 24) can be seen in Table 5.

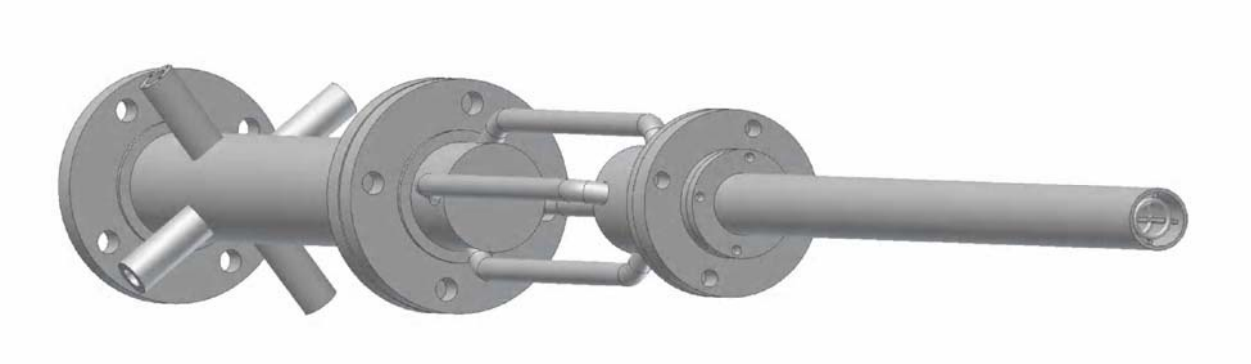

Figure 23. New PDE Initiator Design Architecture

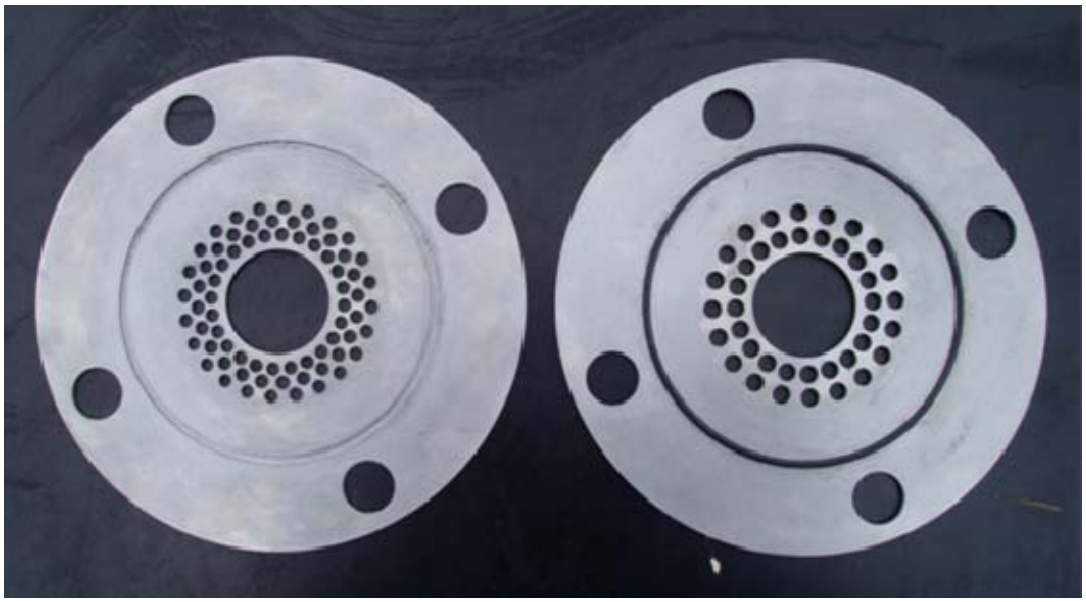

Figure 24. Flow Conditioning Screens

Clean		1/8" grid		3/16" grid		1/4" grid	
U (m/s)	TI (%)	U (m/s)	TI (%)	U (m/s)	TI (%)	U (m/s)	TI (%)
106.5279	10.96297	101.4373	12.01022	111.0715	9.067408	111.4635	9.242226

Table 5. Centerline Velocity and Turbulence Effects from Flow Conditioning Screens

The results indicated that the flow conditioning screens had little to no effect on the turbulence of the flow field and actually were detrimental to the ignition success rate since they removed the recirculation region at the head end of the combustor [13]. For this reason the screens were not incorporated into the new design.

Information was also obtained using an IR absorption spectroscopy diagnostic to determine the equivalence ratio of the fuel-air mixture for varying air flow rates for the use of 1 to 4 fuel injectors firing. Using the data, found in Table 6, the approximate fuel flow rate through each fuel injector was determined as a function of oil pressure. This effective fuel flow rate through each fuel injector was also determined for each of the four oil pressure settings and can be seen in Figure 25.

Date	Run	Injectors	Oil Press (kPa)	Equiv. Ratio	Air flow (kg/s)	Fuel flow per injector (kg/s)
25-Apr-06	14	4	5239	0.525214	1.2706	0.011178
25-Apr-06	15	4	5239	0.951066	0.6336	0.010093
25-Apr-06	16	4	5239	1.202596	0.4857	0.009784
25-Apr-06	17	4	5239	1.154576	0.5560	0.010752
25-Apr-06	18	4	5239	0.737	0.8792	0.010854
26-Apr-06	1	4	6031	1.236071	0.6339	0.013124
26-Apr-06	2	4	6031	0.904982	0.8800	0.013340
26-Apr-06	3	4	6031	0.769486	1.0763	0.013873
26-Apr-06	4	4	6031	0.979221	0.7814	0.012817
26-Apr-06	5	4	6893	1.054939	0.8798	0.015546
26-Apr-06	7	4	6893	0.949926	1.0764	0.017126
26-Apr-06	8	4	6893	1.235142	0.7815	0.016167
26-Apr-06	10	4	6893	0.882824	1.1737	0.017356
27-Apr-06	23	4	7754	1.68	0.63505	0.017870
27-Apr-06	24	4	7754	1.4	0.7816	0.018329
27-Apr-06	25	4	7754	1.21	0.8793	0.017821
27-Apr-06	26	4	7754	1.02	1.0747	0.018361
27-Apr-06	27	4	7754	0.89	1.2701	0.018934

Table 6. Fuel Injector Characterization for Varying Fuel Pressure

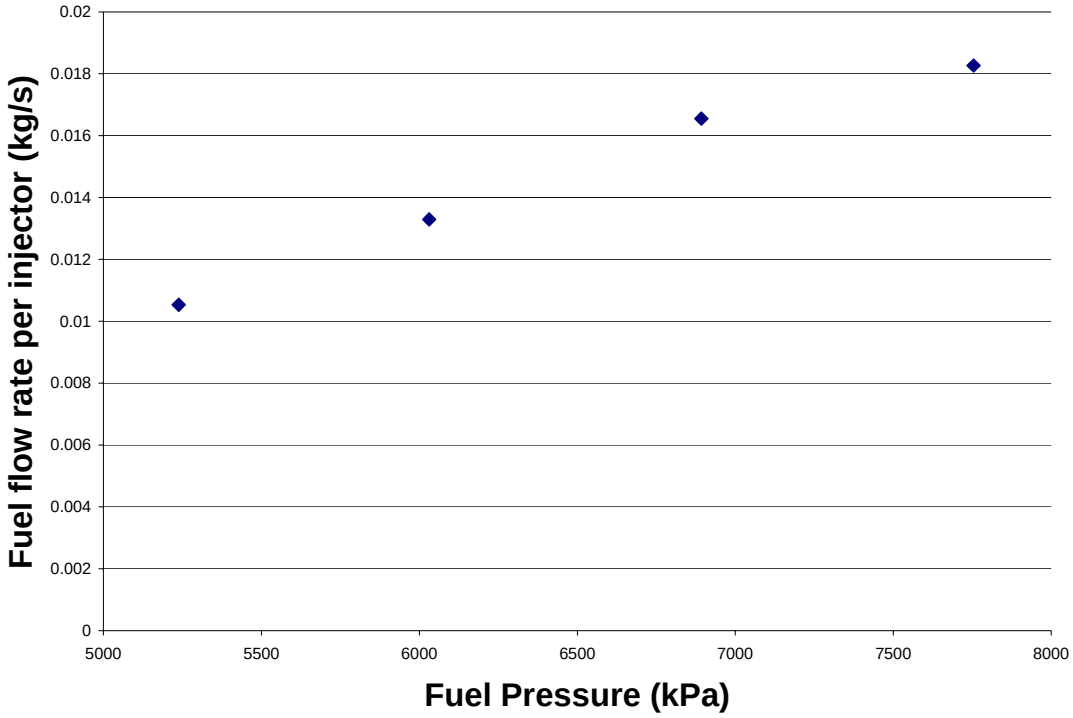

Figure 25. Fuel Injector Flow Rate at Varying Fuel Pressure

Previous research indicated that a JP-10 aerosol required a substantial convective time to vaporize, resulting in a minimum length manifold section to be designed to deliver a vaporized mixture to the combustor. After the flow reaches the engine, it enters an ignition section through four 45 or 60 degree arms, seen in Figure 26. The ignition section has a larger cross sectional area to decrease the flow velocity and thus aid the ignition process.

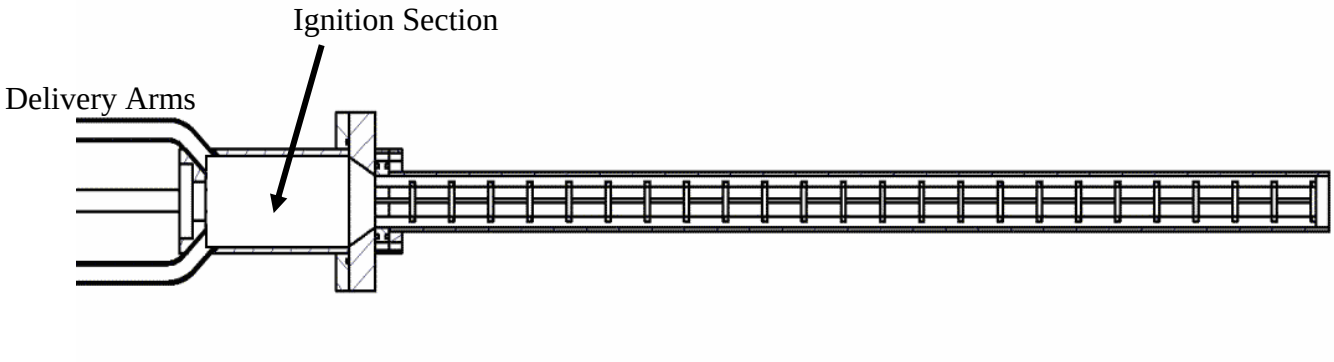

Figure 26. PDE Initiator Section View

After ignition, the combusting flow is accelerated into the initiator through a convergent section and into the smaller diameter initiator combustor containing ring obstacles or spiral which generate turbulence and cause shock reflections to occur which aid the detonation initiation process. The detonation exits the initiator and enters the main combustor in discrete diffraction steps, as seen in Figure 18, in order to keep the detonation from failing.

It was eventually determined that the geometry of the rings and the ring holders was preventing the formation of a detonation due to excessive blockage. The cell size required for a JP-10/air detonation was consequently too large to form in the in the space between the support spars holding the rings. The initiator was then redesigned using a spiral for turbulence generation to aid in the DDT process.

The proposed PDE design differs from previous designs due to the use of a fuel/air initiator section and a separate combustor section. Since, there are two separate flow paths; the design is referred to as a Split-Path Design. The steps of the operational cycle of this new design are shown in Figure 27:

1. The start of the engine cycle consists of a continuous airflow through all sections of the engine.
2. A fuel air mixture begins to enter each tube, the initiator and the combustor.
3. Then the initiator is filled completely with a fuel-air mixture and the combustor portion aft of the initiator exit is also simultaneously filled with the fuel-air mixture.
4. During step four, the ignition event occurs causing a deflagrating combustion wave to begin to move down the initiator.
5. The combustion wave is accelerated along the initiator due to the existing turbulence devices until it transitions to a strong detonation.
6. The strong detonation from the initiator then diffracts and enters the combustor through sections of discrete diameter size increases such that the detonation is allowed to enter a larger diameter section without

completely failing and is then given sufficient length to recover the strength of the initial detonation wave. The detonation then travels the length of the combustor to the combustor exit.

7. After the detonation has exited the combustor, a rarefaction wave is formed and propagates toward the head end of the engine.

8. Finally, at step eight, the rarefaction wave has traveled the length of the entire engine reducing the pressure to the initial value and the volume is now prepared for the cycle to repeat.

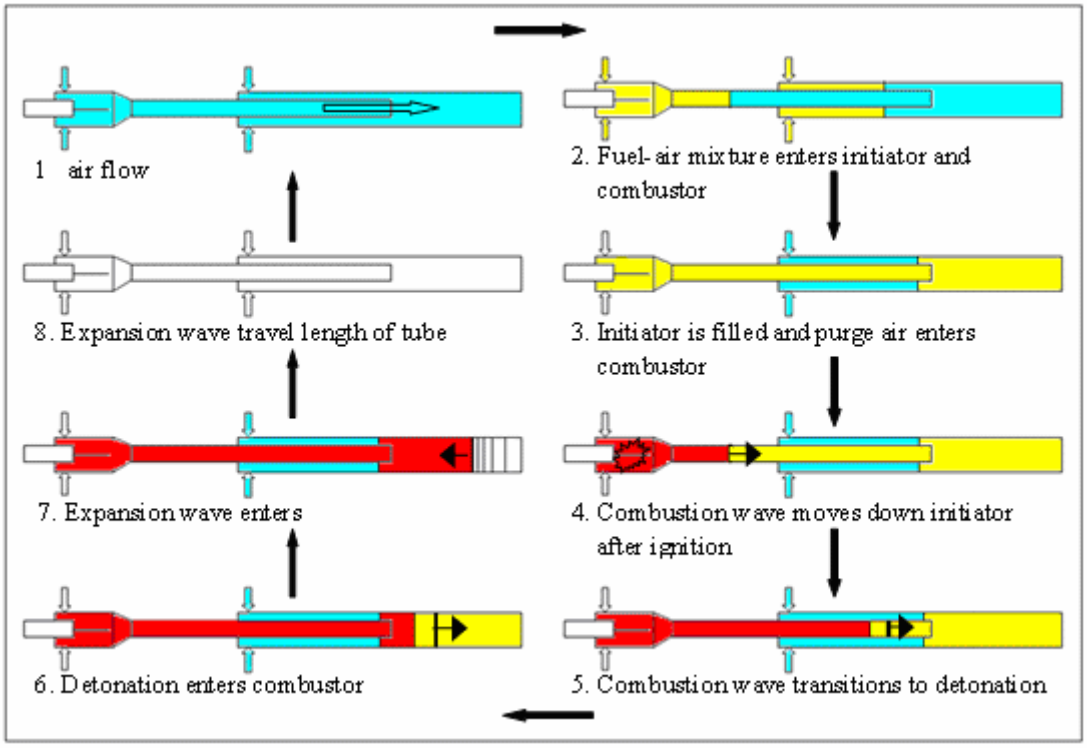

Figure 27. New PDE Design Cycle Steps

The split-path PDE design introduces many potential benefits for the overall system. It allows the use of a relatively low energy ignition source to obtain a deflagrating combustion wave which can then be accelerated through an obstacle field. The losses associated with the obstacle field are then localized to a small portion of the overall flow path and should minimize the overall system performance loss. Another

advantage to the split-path design is the fact that the co-flowing main combustor mixture convectively cools the initiator section.

The airflow through various configurations of the initiator unit and split-path geometry was modeled using three computational packages developed by CFDRC and sold by ESI Group. The software, CFD-GEOM, is a geometry and grid generation system, with an extensive set of geometry creation and manipulation, CAD import, and mesh generation capabilities. CFD-GEOM provides meshes for ESI Group's CFD solver packages CFD-ACE+ and CFD-FASTRAN. The software allows the user to build a computational domain based on the geometry of the desired model. CFD-GEOM was used to create the axis-symmetric geometries of three possible configurations for the initiator, of which the lower boundary of each model representing the axis. These geometries were then processed using GEOM's grid generation system to generate the three grids seen in Figures 28, 29 and 30 used to model the designed initiator, the ramped initiator and the clean initiator respectively.

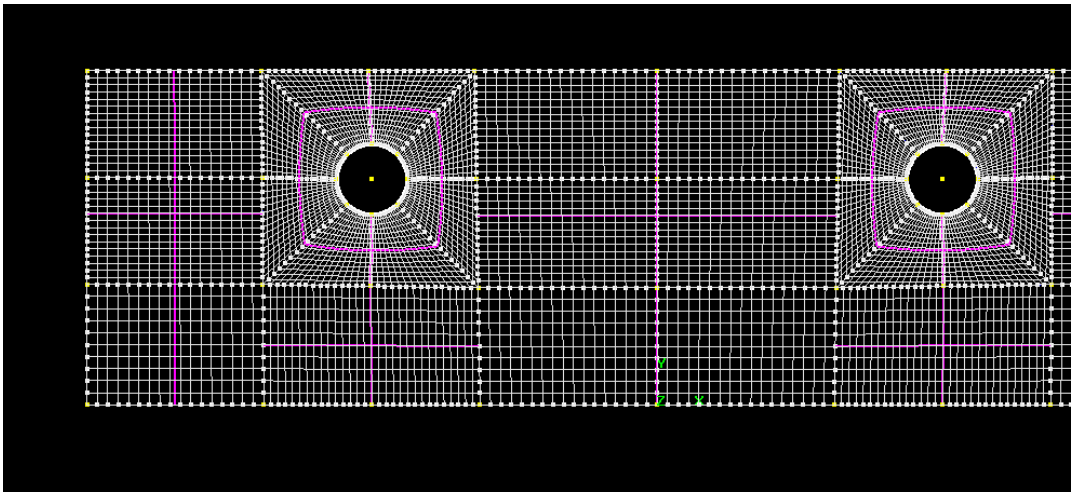

Figure 28. Grid Model of Initiator with Ring Turbulence Generators

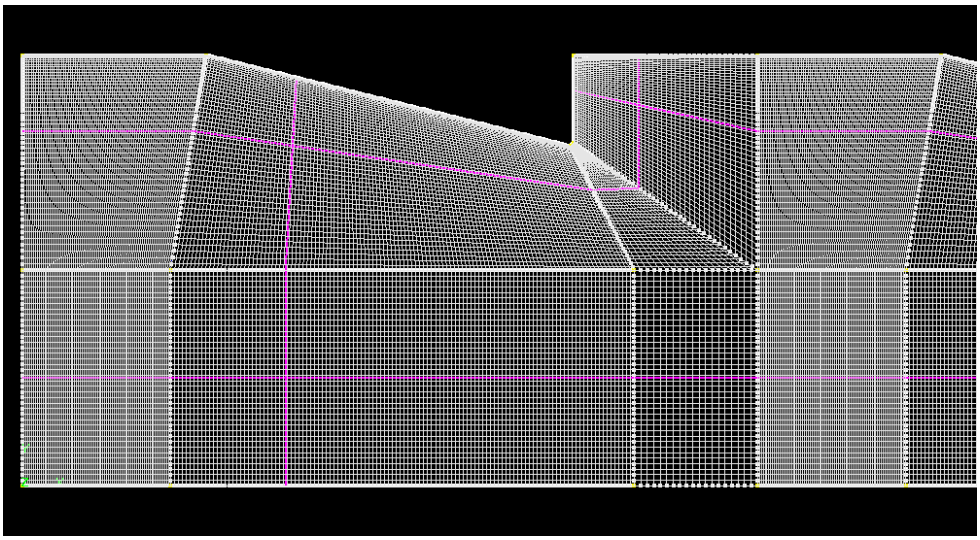

Figure 29. Model of Initiator with Ramp Turbulence Generators

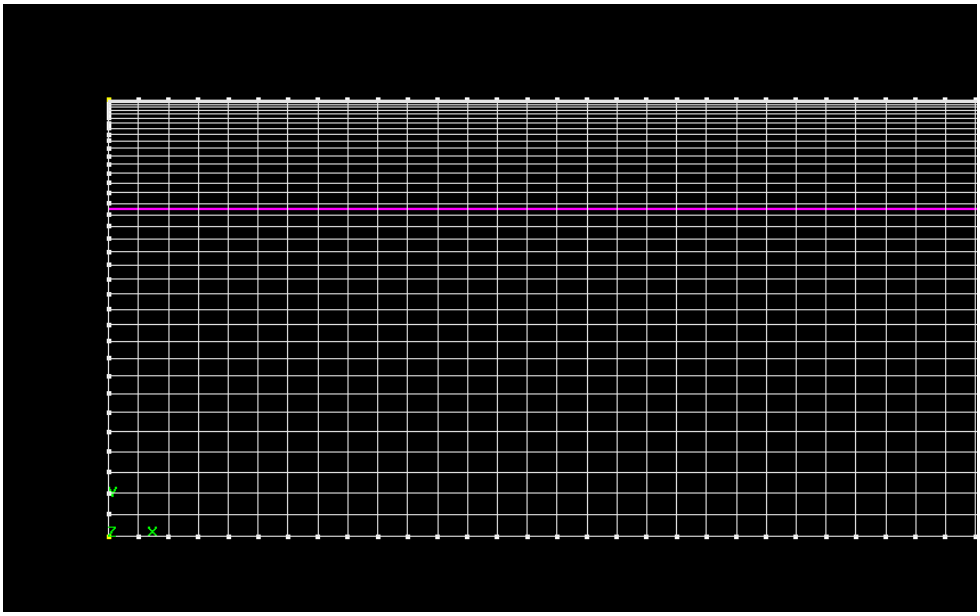

Figure 30. Grid Model of Initiator with No Turbulence Generators

Figure 28 shows the decreased grid spacing near the 3/16” ring cross-section since high flow gradients in that region were anticipated. Similarly, in Figure 29, the grid density was increased in the region near the end of the 3/16” ramp to accommodate flow gradients that were suspected to be large due to the sudden change in geometry. Finally, the grid density in the clean initiator model and the initiator with ramps model is increased toward the upper boundary as flow gradients near walls are always large due to boundary layer effects. These models were created to give results on qualitative trends.

A model of the initiator with a spiral was not created due to the inherent requirement for a 3-D model.

A model of the initiator and combustor combination was also created (Figure 31). This was done to examine the propagation of a detonation or shock wave through the initiator and into the combustor via the discrete diameter steps.

The boundary conditions for all the models consisted of a symmetry boundary, wall boundaries, an inlet boundary and an outlet boundary. Once the models were complete they were exported to a *.DTF file that can be read by the solver program, CFD-ACE.

The steady state CFD simulations were performed using the flow module of CFD-ACE. It allows the user to model various gas or liquid systems. The code solves the Navier-Stokes differential equations discretized over a finite volume allowing internal and external flows at sub-sonic velocities to be simulated yielding a numerical solution of the flow fields.

The conditions used for the simulations performed for this research are tabulated in appendix A, CFD Settings. The settings for each simulation were selected based on the expected values through the engine flow path and values of which were known to be of interest. The solver settings were selected in the interest of obtaining quickly converging and accurate solutions. The turbulence field within the modeled flow was also explored. Turbulent flow is the common flow condition encountered in a large number of applications in various industries. In general, any moderate to high Reynolds number flow problem will involve turbulence. Turbulence often has a strong influence on momentum as well as heat and mass transfer. Due to the diverse range of turbulent flow problems a wide choice of turbulence models are available in CFD-ACE+ and CFD-FASTRAN. These include Reynolds Averaged Navier Stokes (RANS) models as well as Large Eddy Simulation (LES) models. For this research, the standard k-ε model was used exclusively [14]. The setup and simulation for the transient CFD simulations were performed using CFD-FASTRAN, a density-based finite-volume solver for compressible flows. The solver incorporates higher-order numerical schemes and advanced physical models for application to flow problems.

The actual set-up conditions for the transient simulations performed for this research are also tabulated in appendix A, CFD Settings. The settings for each simulation were selected based on the actual expected values through the engine and values of which were known to be of interest. CFD-FASTRAN solves the full Navier-Stokes equations using a density-based finite-volume formulation and higher order differencing schemes for the accurate prediction of subsonic, transonic or hypersonic flows. CFD-FASTRAN employs state-of-the-art turbulence models for predicting the effects of turbulence within boundary layers and within separation regions [15]. The flow field of the simulation using the PDE model was initiated with an initial velocity of 200 m/s, a pressure of 150 kPa and a temperature of 600 K. A portion of the model was a driver section used to set up a shock wave inside the initiator. The driver section had an initial velocity of 0 m/s, a temperature of 2000K and a pressure of 2 MPa. A portion of the model is show in Figure 31. The figure shows the grid spacing present in the main combustor, the discrete diameter change regions, and initiator region which has the same grid space at the driver region.

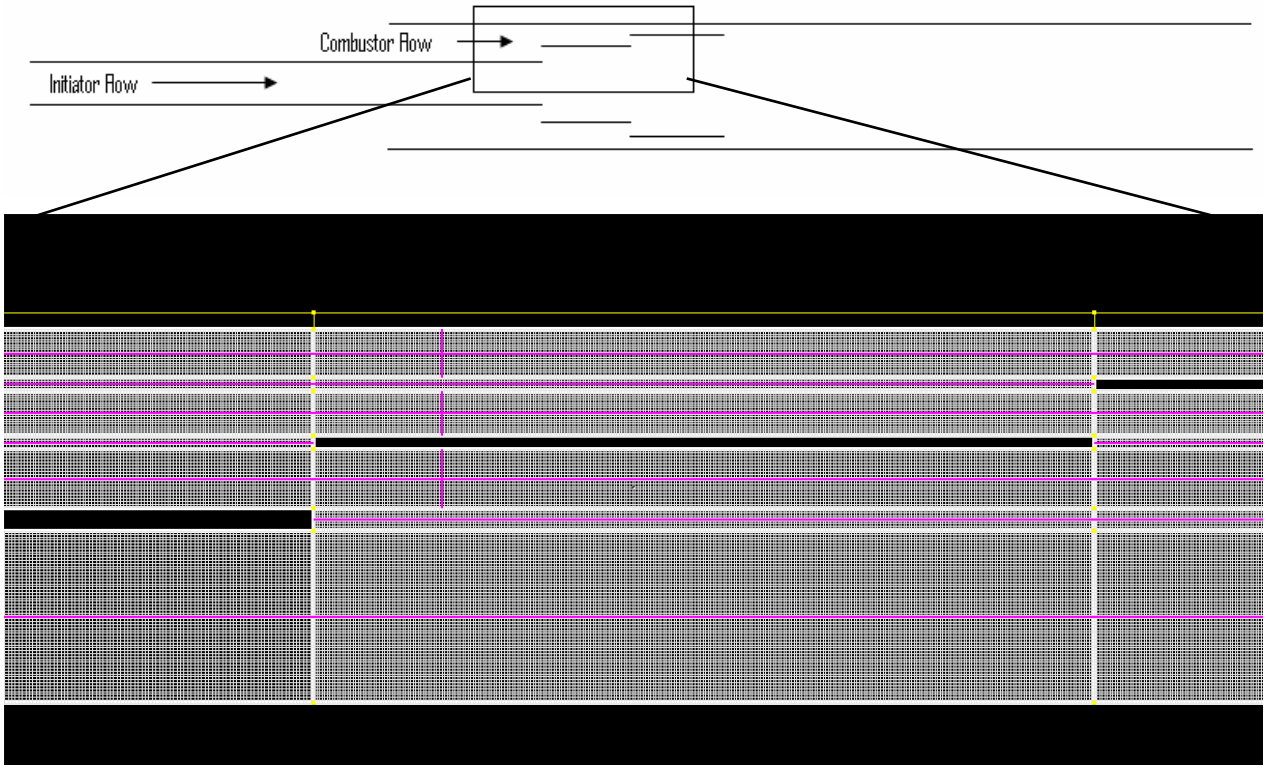

Figure 31. Grid Model of PDE with No Turbulence Generators

VI. EXPERIMENTAL SETUP

A. PDE

The initiator section of the PDE is shown in Figure 32 and consisted of an ignition section and a reduced diameter obstacle field. The ignition section had an inner diameter of 7.8 cm and a length of 91.4 cm. This section housed the TPI electrode and provided a concentric geometry relative to the electrode, to allow for a reliable transient plasma corona discharge. This section also allowed for a relatively slower flow field, to aid the ignition process. Following the ignition section, a convergent section reduced the diameter to the initiator where obstacles were used to accelerate the deflagration wave to greater velocities thereby reducing the DDT timescale. The fuel air mixture entering the PDE initiator was provided by the upstream fuel manifold which injects JP-10 into the flow through up to four prototype fuel injectors. The prototype fuel injectors used pressurized oil provided by an oil pump to hydraulically actuate a plunger within the injector which physically injected the JP-10. The oil pump provided oil pressure ranging from 5000 kPa (750 psi) to 10000 kPa (1500 psi).

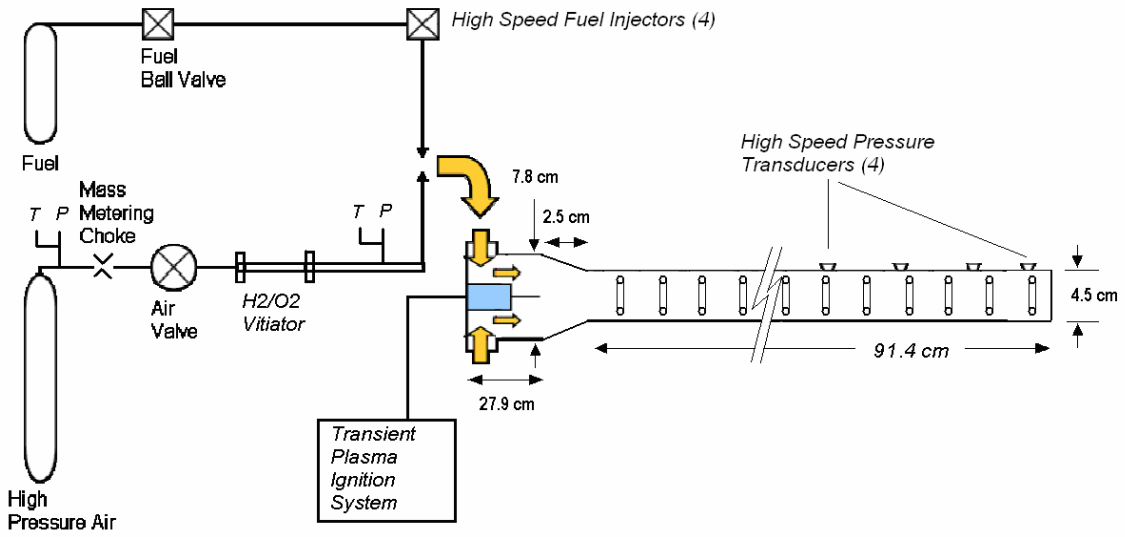

Figure 32. PDE Initiator Experimental Set-up

B. VITIATOR

A vitiator was used to heat the air entering the PDE to simulate combustor inlet flow conditions at different flight conditions, including supersonic cruise velocities. The vitiator burned a hydrogen/air mixture to produce high temperature air. Oxygen was then introduced into the air delivery system downstream of the vitiator to restore the oxygen that was consumed in the combustion process, thereby correcting the mass percentage of oxygen to that of "standard" air. The vitiator was started by a hydrogen/air torch, sparked by a high voltage transformer and spark plug. The vitiator is shown in Figure 33.

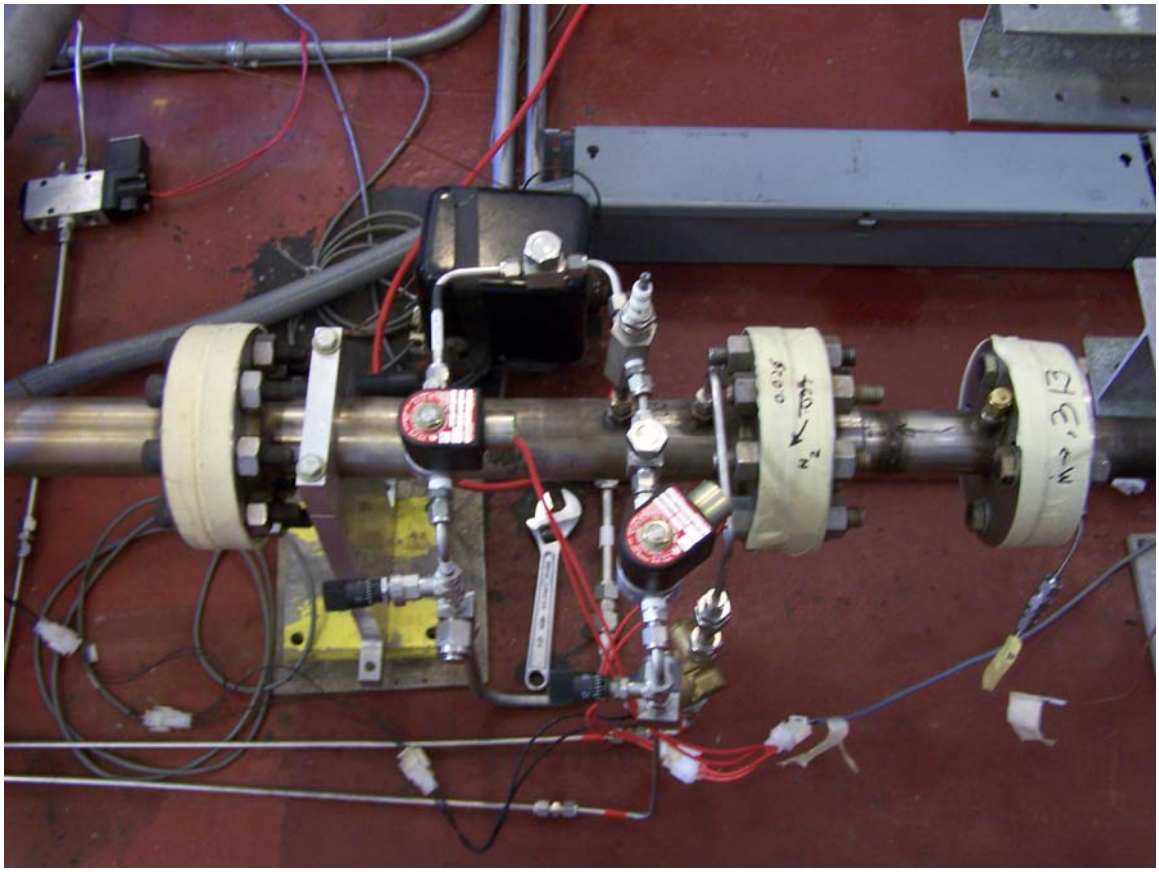

Figure 33. H_2/O_2 Vitiator

The operating temperature range of the vitiator was from 473 K to 800 K resulting in air entering the combustion chamber as high as 600 K. The vitiator, used in conjunction with high pressure air supply, provides the ability to deliver air flow at the specific pressures and temperatures required to simulate the combustor inlet flow conditions for the flight Mach number range of interest. For example, providing an air flow at 250 kPa and 490 K corresponds to the combustor inlet flow conditions of a PDE operating at an altitude of 13000 m (40000 ft) and flying at Mach 2.5 with a Mil-Spec (MIL 5007-D) Inlet (87 % pressure recovery).

C. TEST CELL AND PDE CONTROL

Control of the test cell and PDE was accomplished using a PC located inside the control room. This PC controlled the test cell by running National Instruments Labview 8.0, which was linked to a NI PXI-1000B controller inside the test cell through the internet and the PXI IP address. Additionally, within the control room was a BNC pulse generator, used to send fuel valve and ignition trigger signals to the solid state relays in the test cell. Master switches for 28 VDC and 110 VAC power were located in within the control room, and the capacity to shutdown the test cell in the event of an emergency. The control of all the supply gases was accomplished through TESCOM ER3000 regulator control units and software.

All ball valves and solenoid valves could be controlled through the Labview control and would immediately close if the facility was disabled through software or if the emergency stop button was manually depressed. The unswitched 110 VAC power was used principally for instrumentation such that pressure transducers and temperatures could always be monitored. A schematic diagram of the facility control and the Labview graphical user interface are presented in Figures 34 and 35 below, while the wiring tables and diagrams are included in the Appendix C. The Electrical Relay assignments for these controls can be seen in Table 14 in appendix C and the test cell operating procedure is contained in appendix D.

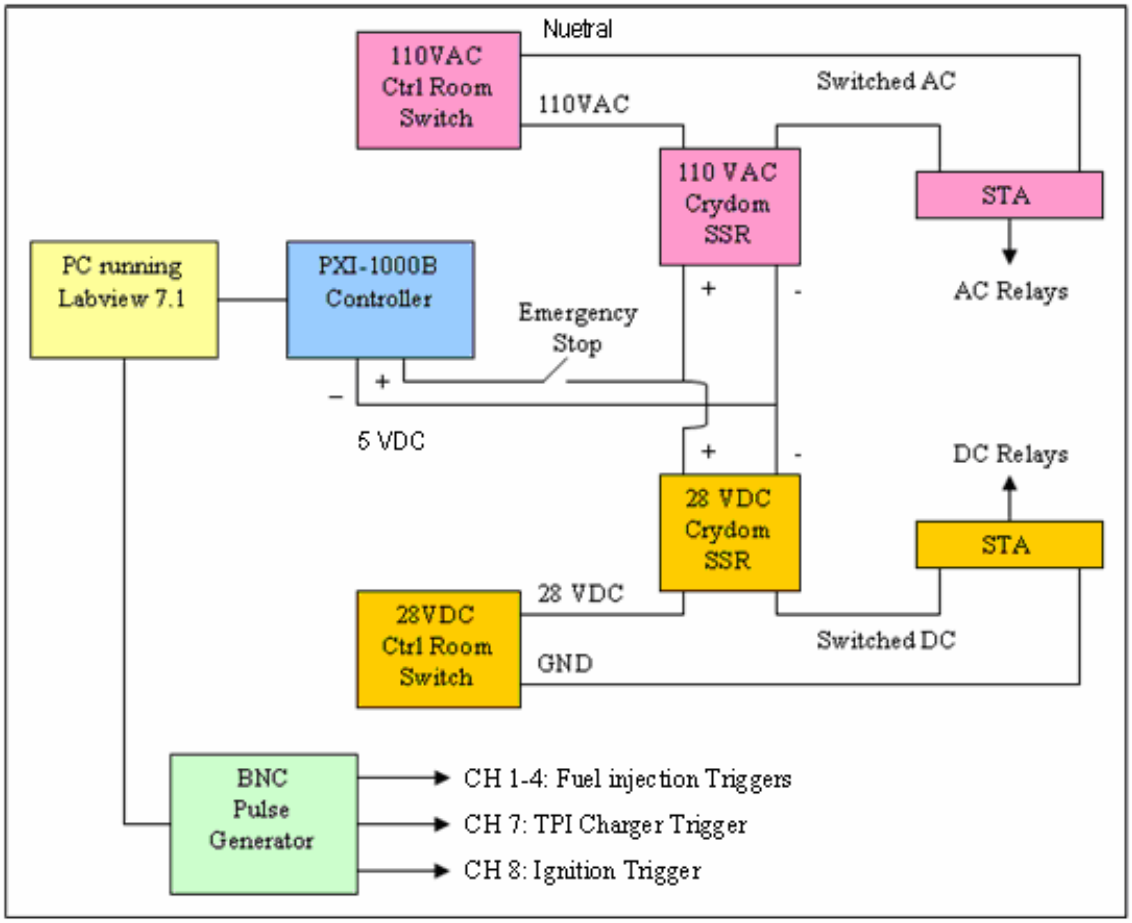

Figure 34. Facility Control Schematic

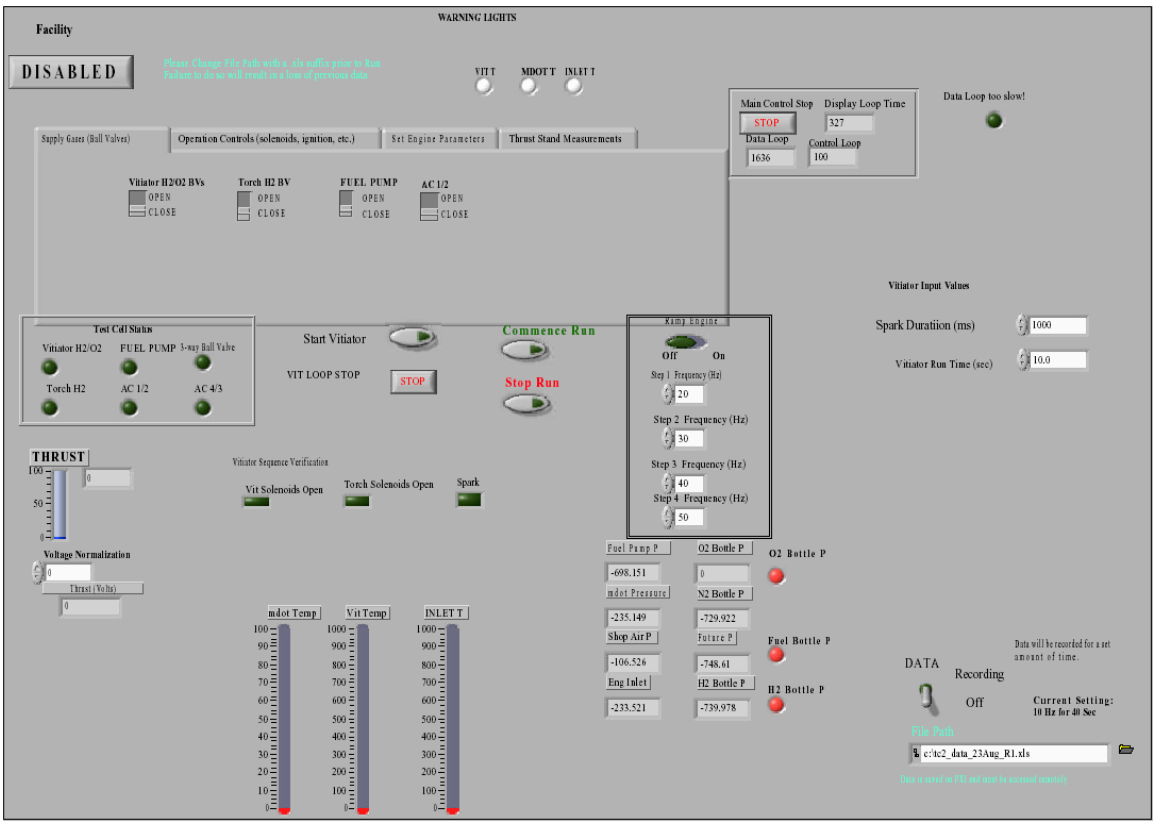

Figure 35. Test Cell #2 Graphics-User Interface

D. DATA ACQUISITION

Data acquisition was accomplished by the control PC which was linked to the PXI-1000B. Installed in the PXI-1000B was a PXI-6031E monitoring 16 channels at 1 kHz which included the temperatures at the main air choke, the engine combustor, and the line pressures of the supply gases as well as the thrust from the linear displacement sensor. High speed data was acquired at 500 kHz per channel using a PXI-6115 which monitored 4 Kistler pressure transducers mounted on the initiator portion of the PDE three of which are seen in Figure 36. The four Kistler pressure transducers were installed inside cooling jackets and were able to measure pressure at four of twelve possible locations (Figure 36). A Waverunner Oscilloscope was used to visually monitor the output of the pressure transducers as well as measure the output voltage and amperage of the TPI to verify a corona discharge was being achieved. Tables of the data acquisition wiring are included in Appendix C.

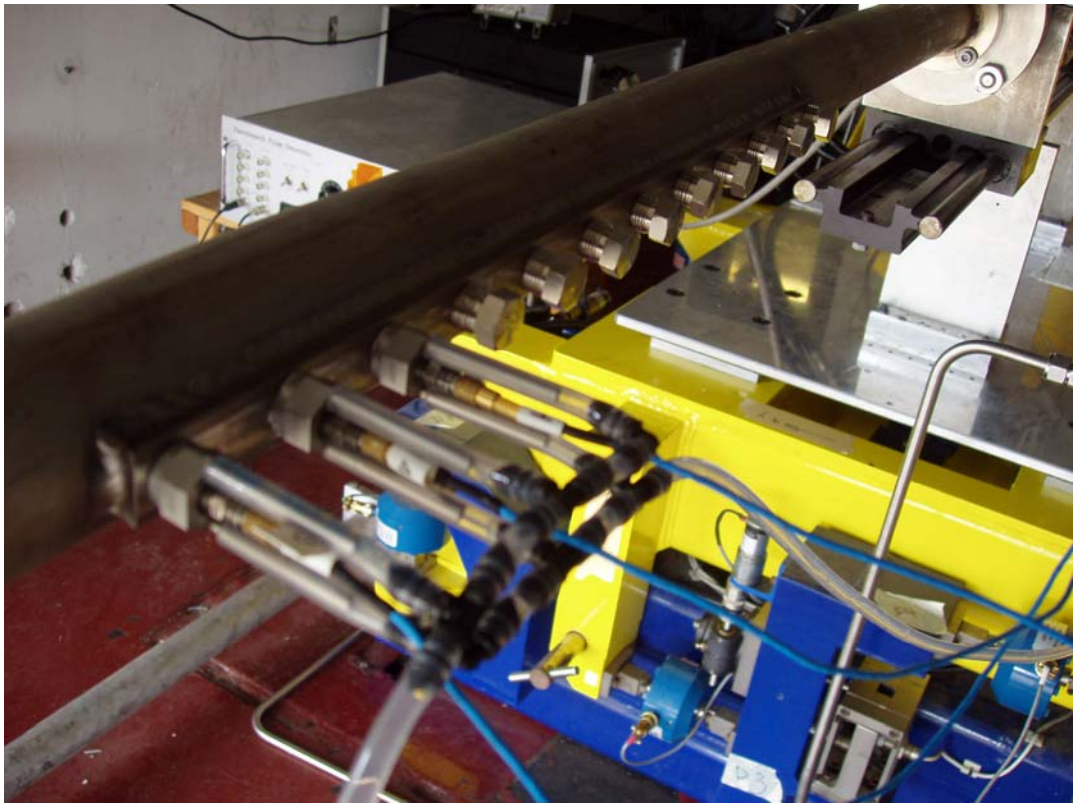

Figure 36. Kistler High Speed Pressure Transducers

VII. RESULTS

Computational and experimental results were obtained during this research. The computational methods and modeling of the proposed flow fields generally agreed well with the experimental results with the exception of the turbulence data. The discrepancies between the two methods can be attributed to simplifications made to the modeled geometry such that each model could only be created in a 2-D axis-symmetric geometry varying in radius and depth only.

A. CFD

The CFD simulations indicated that an initiator with a series of low profile ramps, vice a spiral or rings, would generate a greater value of turbulent kinetic energy. However, the simulations indicate ramps will also have a slightly greater pressure drop through the initiator. Since TKE is an important parameter for flame acceleration, this indicates that an initiator with ramps would perform better than its ringed counterpart if the length of the obstacle field could be shortened to reduce the total pressure loss while simultaneously reducing detonation initiation times.

Spatial results for turbulent kinetic energy (TKE) are presented in Figure 37 for a $M_{refresh}$ number of 0.25. The centerline TKE and turbulence intensity (TI) results of the steady-state simulations within the initiator designs can be seen in Figure 38 for varying refresh Mach numbers. The results indicate that TKE tapers off toward higher refresh Mach numbers with an initiator using ramps to induce the turbulence, whereas the TKE continually increases as refresh Mach number increases for an initiator employing rings. The turbulence intensity does not vary greatly with refresh Mach number but did decrease slightly for both the ramp configuration and the ringed configuration.

Clean Initiator

Initiator with Rings

Initiator with Ramps

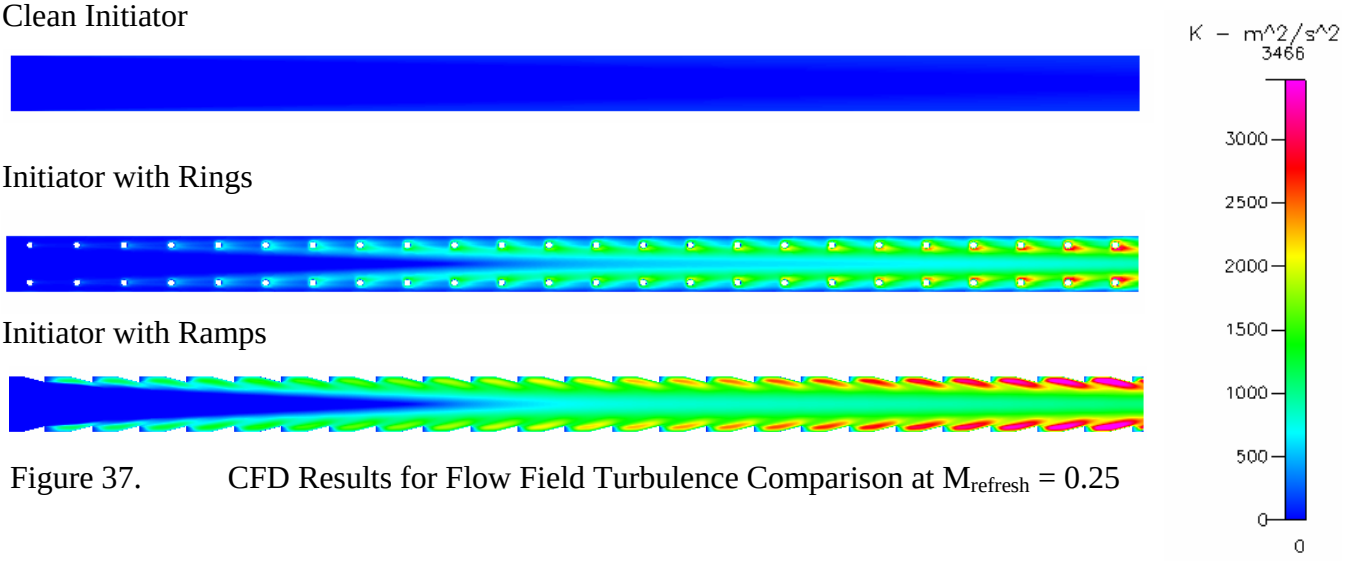

Figure 37. CFD Results for Flow Field Turbulence Comparison at $M_{refresh}$ = 0.25

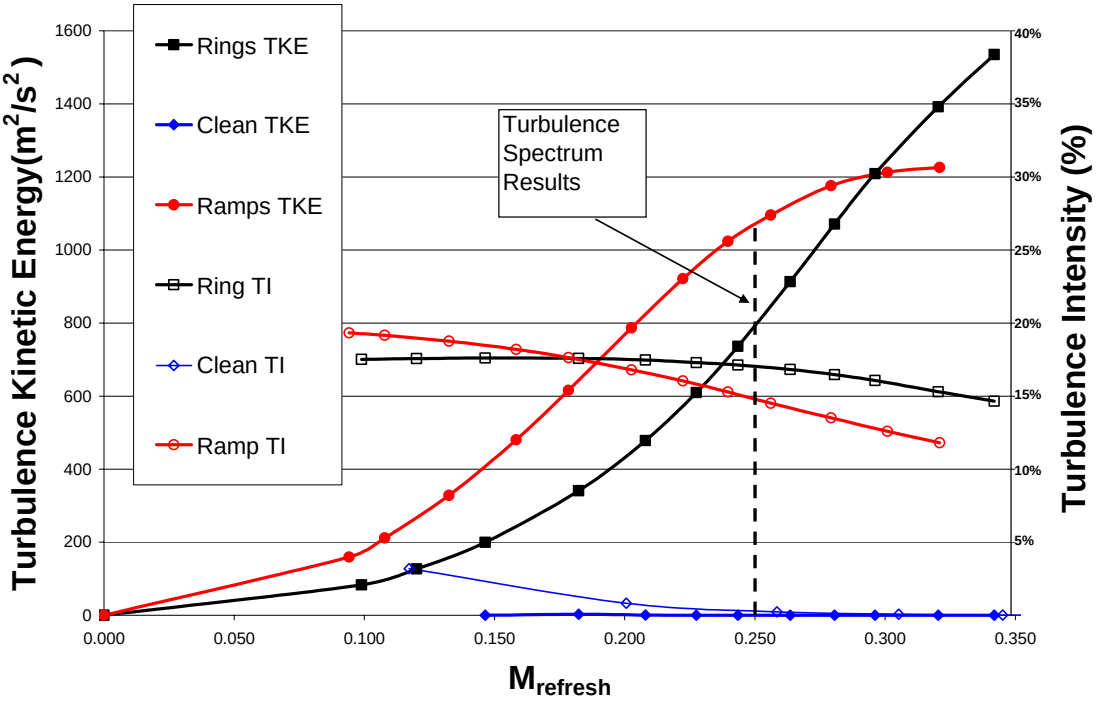

Figure 38. Exit Centerline CFD Results for Turbulence Generated by Obstacles

The pressure loss along the one meter section of each initiator configuration was also measured in each of the simulations performed, the results of which can be seen in Figure 39. The pressure loss was also simulated for the initiator with rings configuration

and characterized with the conditions representative of post-detonation flowing through the initiator at steady state. The computational results revealed that the initiator with ramps possessed the highest pressure drop followed by the ringed configuration with refresh conditions. Surprisingly, the ringed configuration with post-detonation conditions flowing through it resulted in lower total pressure loss. This was believed to be due to the fact the drag through the obstacle path was due to primarily pressure drag vice viscous drag. Although the viscosity was greater in the gas with post-detonation properties, the high pressure compresses the gas causing it to flow at lower velocities and result is less pressure drag. Obviously the initiator in the clean configuration resulted in the lowest pressure drop.

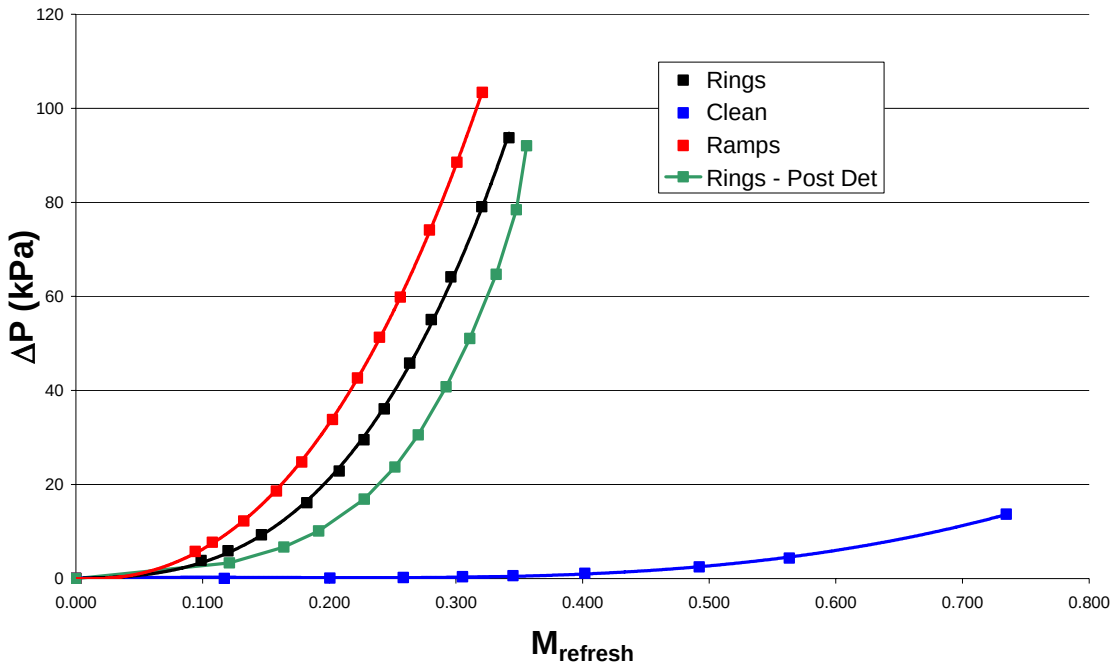

Figure 39. CFD Results for Pressure Drop Over Obstacles

The total pressure drop results were also correlated to the mass flow rate through each initiator configuration to demonstrate that the data represented as a 3rd order polynomial with a R-squared values very close to unity, as seen in Figure 40. This does

not occur when the data is presented against refresh Mach number because refresh Mach number is non-linear in this application.

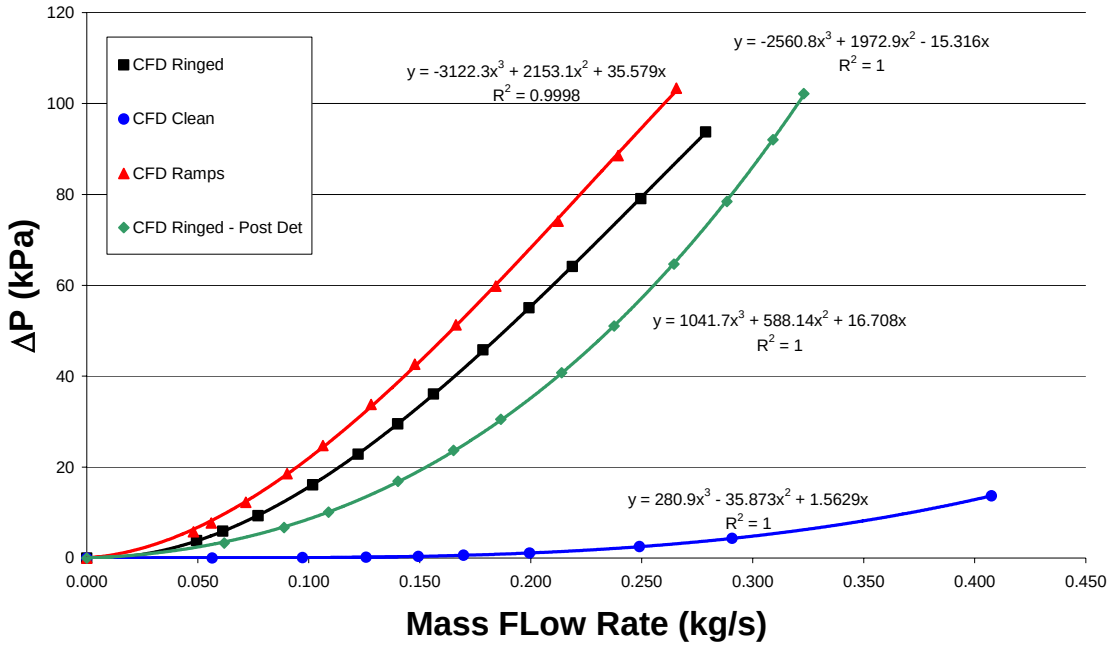

Figure 40. CFD Results for Pressure Drop Over Obstacles Versus Mass Flow Rate

The simulation results of the shock wave propagating through the initiator and into the combustor via the three discrete diameter step can be seen in Figures 41 and 42. The structure of the shock wave is seen in Figure 41 immediately after exiting the initiator. The features that should be noticed are the lambda foot at the base of the renewed shock in the first diameter step as well as the re-formation of the normal shock wave as it progresses aft.

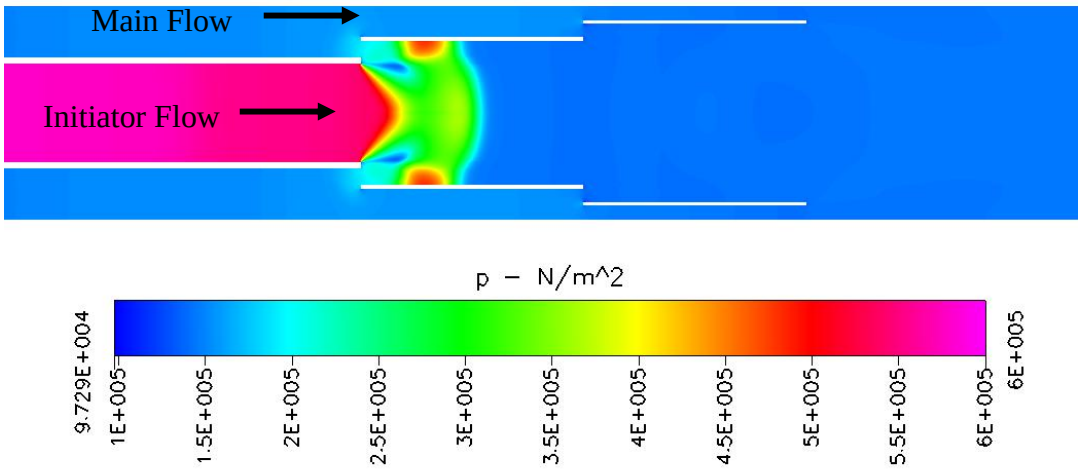

Figure 41. CFD Results for Shock Propagation from Initiator

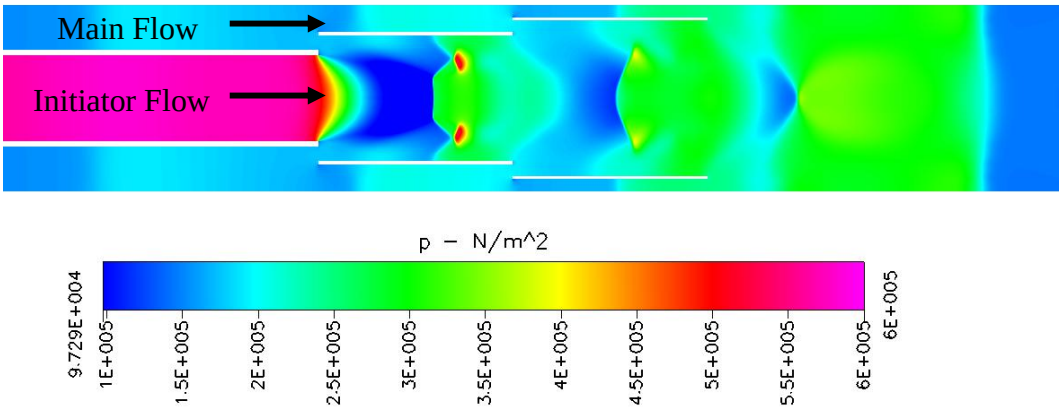

Figure 42. CFD Results for Pressure Shock Propagation to Combustor

B. EXPERIMENTAL

The performance of the PDE design was tested using a 6 degree of freedom (6DOF) thrust stand as well as a displacement thrust measurement, pressure transducers, thermocouples and a hotwire anemometer. The effects of the pressure loss through the initiator were also examined. Additionally, a hotwire anemometer was used to determine the velocities and turbulence present in the flow so that they could be compared with the computational results as well as the observed detonability. Through pressure measurements along the initiator the verification and location of detonations were determined.

Velocity, pressure, and turbulence measurements were taken at varying flow rates through the ringed initiator. The experimental measurements have indicated that the actual TKE and TI values within the initiator, shown in Figure 43, were much lower than that predicted by the CFD indicating inaccuracies in the simulations. The results indicate that TKE increases with increased flow rate but tapers off toward higher refresh Mach numbers in excess of approximately 0.16 kg/s. Accordingly, the TI decreases as flow rate increases.

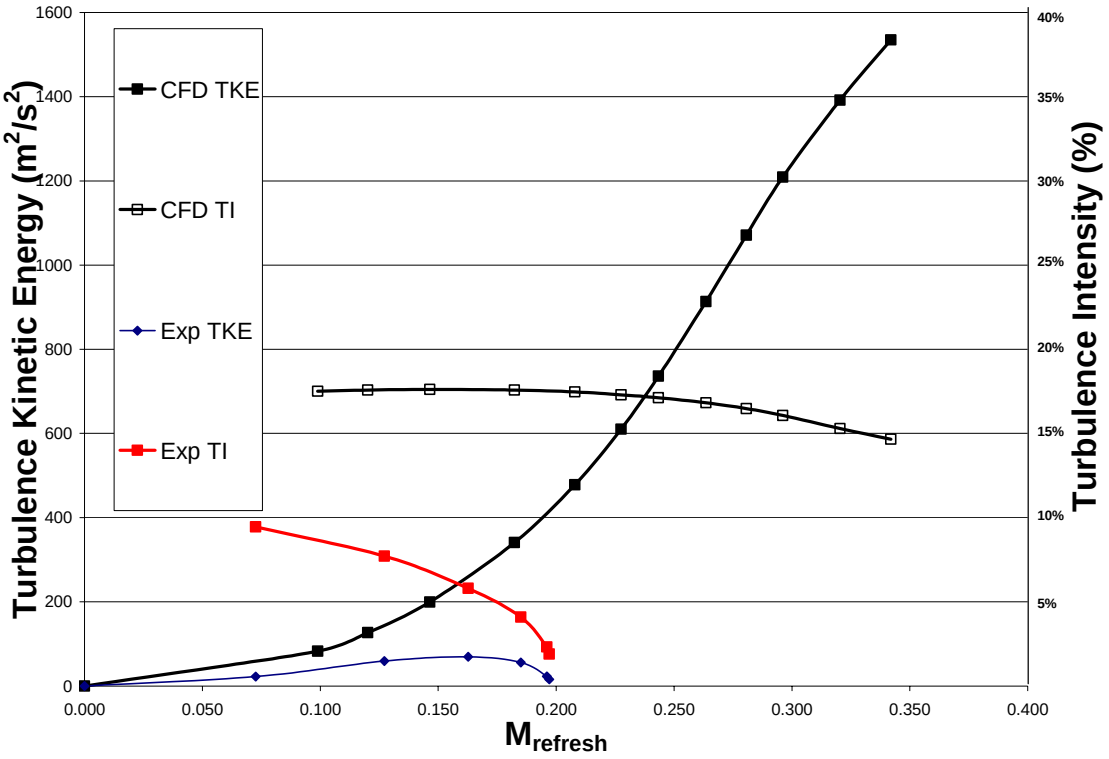

Figure 43. Exit Centerline Laboratory Result for Turbulence Induced by Rings

The pressure loss measurements along a one meter section of the initiator with rings were much greater than that seen during the CFD simulations but very similar in nature. It was observed in the experimental measurements that the flow chokes at a lower $M_{refresh}$ number than that indicated by the CFD results and can be seen in Figure 44. This was due to the initiator model having a lesser blockage area ratio and less surface area than that of the actual initiator because of the longitudinal supports which held the rings in place. The large blockage ratio and substantial surface area caused the initiator to choke at a lower mass flow rate than that indicated by the CFD and hence a lower $M_{refresh}$

number. Pressure loss measurements were also taken from the initiator with rings with hot air flow. The pressure loss measurements for this case were slightly greater than that measure for cold flow. This is explained by the fact that at higher temperatures the flow densities are lower and hence the flow velocities are larger leading to increased internal pressure drag as well as increased viscosity at the elevated temperatures resulting in increased viscous drag.

Figure 44 shows that the pressure loss measurements across a three foot section of the initiator with a spiral installed were less than that measured from the initiator with rings. Choking was not observed at the $M_{refresh}$ numbers at which this configuration was tested. Pressure loss measurements were also taken from the initiator with a spiral with hot air flow. The pressure loss measurements for this case were slightly larger than that measure for cold flow in the spiral as seen in the initiator with rings.

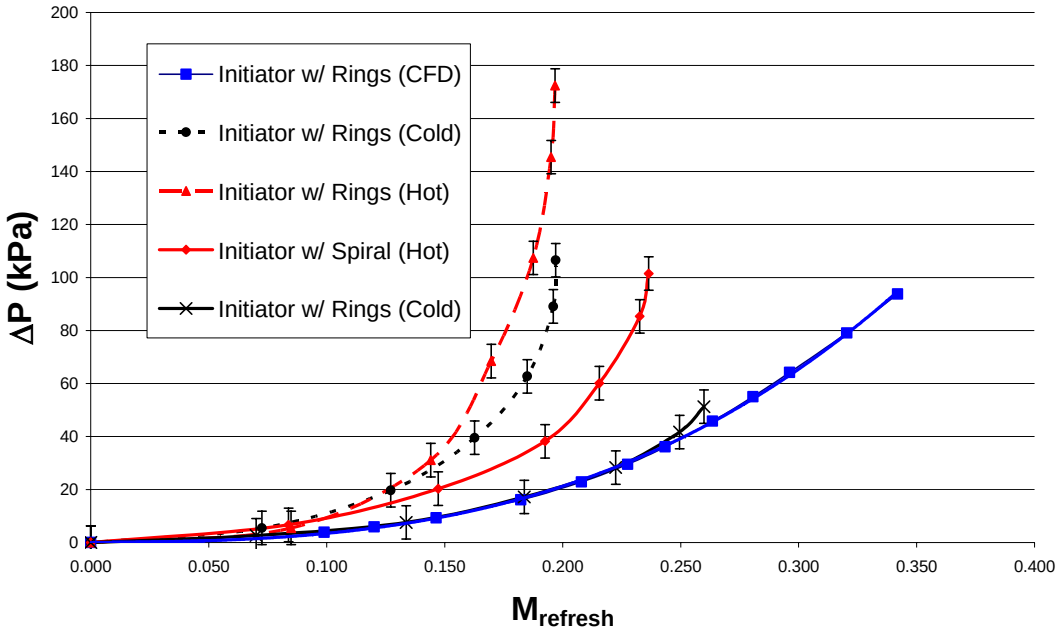

Figure 44. Laboratory Result for Pressure Drop over Obstacles

During hot-fire testing using the initiator with rings, it was observed that at higher flow rates, around 0.2 kg/s, the pressure in the ignition zone was on the order of 2 atm

and the ignition success occasionally became erratic. Subsequently, further testing was completed at various flow rates as well as pressurized static testing and it was confirmed that this phenomenon was prevalent at higher ignition zone pressures. Ignition success was achieved on the ringed initiator configuration at rates up to and including 20 Hz. Although detonations were not verified, as explained in the design section of this thesis, it is known that with ignition present detonation would have formed given the required initiator length and internal geometry.

VIII. SUMMARY AND CONCLUSIONS

This research demonstrates a practical and possible design for a PDE which would minimize the overall total pressure losses by localizing the largest losses in the system to a small portion of the flow. The design uses an initiation strategy which employs the DDT approach to detonation initiation with a TPI used for ignition and localizing losses associated with the DDT approach. No supplementary gases or gaseous fuels are required and conventional ignition energy levels may be used.

The lack of agreement between the turbulence data from the simulations and the actual turbulence measurements made in the laboratory indicate that the turbulence model used in the simulations did not accurately represent the flow. Whereas, the pressure data from the CFD simulations had better agreement with the laboratory measurements made. Although, the pressure losses observed in the actual laboratory test were greater than those found in the simulations. The deficit of pressure seen in the simulations can be attributed to the fact that the simulations did not take into account any of the geometry used to hold the rings inside of the initiator and therefore likely needed to be corrected for the increased surface area and blockage ratios.

The ignition tests revealed that the TPI has erratic ignition at higher engine flow rates due to the higher ignition zone pressures which affects the discharge mechanisms. It has been concluded that this was due to the fact that the increased pressure causes an increase in the dielectric resistance of the air. This, therefore, causes the path of preferential discharge to be through the electronics housing box rather than between the TPI electrode and the PDE ignition zone walls. Additionally, recirculation zones near the ignition region are needed to increase the residence time for the mixtures and provide reliable ignition at high flow rates.

THIS PAGE INTENTIONALLY LEFT BLANK

IX. FUTURE WORK

Future work in this research area should examine the feasibility of an initiator unit with ramp-like obstacles. Turbulence & velocity profiles should be made and compared to the results of the CFD simulations already performed during this research. The ability of a ramped initiator to produce DDT should be explored and documented. Research is also needed to observe the effects of refresh Mach number and cycle frequency on the detonability of the engines fuel-air mixture as well as the overall thrust and specific impulse of the entire system with the main combustor portion.

Ongoing efforts in this research could also benefit from further CFD simulations. In particular, a model of the ringed initiator with detonation products in the head could be created to simulate the transient shock reflections present during the DDT process. This would help to better understand and visualize the DDT process in this engine which could therefore aid in redesign efforts to create a more effective and efficient initiator. A 3-D model is also required to more accurately simulate the flow through the engine and produce results that more closely match what has been seen in the actual laboratory tests. Further simulations are also required to discover a turbulence model that closely resembles the turbulence field in the PDE evaluated in this thesis. This should be done with the help of CFD experts at NPS as well as with technical support from CDFRC.

Finally, the selection and incorporation of an alternative fueling strategy should be considered which could provide a more versatile range of operation. The current fuel injectors limit the operation of the engine to an aggregate flow rate of approximately 0.20 kg/s due to the current lateral fuel injection set-up. The current fuel injection method also limits the ability to decrease the engine flow so that it is only possible to decrease the fuel-air ratio by discrete increments.

THIS PAGE INTENTIONALLY LEFT BLANK

APPENDIX A: CFD SETTINGS

Initiator simulation (refresh)

Problem Settings		
Modules:	Flow	
	Turbulence	
Model Options		
Shared:	Steady state	
	Axisymmetric	
Flow:	Reference Pressure:	0 Pa
Turb:	Turbulence Model	K Epsilon
Volume Conditions		
Physical Properties:	Property Mode	Fluid, Gas
	Density Evaluation Method	Ideal Gas Law
	Viscosity Evaluation Method	Constant, 7.7E-5 kg/m-s(Default)
Boundary Conditions		
Inlet:	Mode	Total Pressure
	Pressure	Varied
	Temperature	533.15 K
	Relative Pressure	Constant, 0 Pa(Default)
	Kinetic Energy	0 m^2/s^2 (Default)
	Dissipation Rate	0 m^2/s^3 (Default)
Wall:	x-direction velocity	0 m/s (Default)
	y-direction velocity	0 m/s (Default)
Symmetry:		Maintain default settings
Interface:		Maintain default settings
Outlet:	Mode	Fixed Pressure
	Relative Pressure	101325 Pa
	Temperature	533.15 K
	Kinetic Energy	0 m^2/s^2 (Default)
	Dissipation Rate	0 m^2/s^3 (Default)
Initial Conditions		
Initial Condition:	User specified	
IC Applied:	For all volumes	
Shared:	Temperature	Constant, 533.15 K
Flow:	x-direction velocity	0 m/s (Default)
	y-direction velocity	0 m/s (Default)
	Pressure	101325 Pa
Turb:	Kinetic Energy	0 m^2/s^2 (Default)
	Dissipation Rate	0 m^2/s^3 (Default)
Solver Control		
Iterations:	Max Iterations	15000
	Convergence Criteria	0.0001 (Default)
	Min Resdiual	1E-18 (Default)
Spatial Differencing:	Velocity	Upwind (Defaullt)
Solvers:	Velocity	CGS+Pre (Default)
	P Correction	AMG
	Turbulence	CGS+Pre (Default)
Relax:	Velocities	0.2
	P Correction	0.2
	Turbulence	0.2
	Pressure	1
	Density	1
	Viscosity	1
Limits:		Maintain default settings
Advanced:		Maintain default settings
Output:	Steady state results	specified interval (50 iterations)
Print:	Mass flux summary	YES

Table 7. CFD-ACE Solver Setting for All Initiator Pre-detonation Simulations

Problem Settings		
Modules:	Flow Turbulence	
Model Options		
Shared:	Steady state Axisymmetric	
Flow:	Reference Pressure:	0 Pa
Turb:	Turbulence Model	K Epsilon
Volume Conditions		
Physical Properties:	Property Mode	Fluid, Gas
	Density Evaluation Method	Ideal Gas Law
	Viscosity Evaluation Method	Constant, 1.846E-5 kg/m-s(Default)
Boundary Conditions		
Inlet:	Mode	Total Pressure
	Pressure	1.00E+06
	Temperature	2800 K
	Relative Pressure	Constant, 0 Pa(Default)
	Kinetic Energy	0 m^2/s^2 (Default)
	Dissipation Rate	0 m^2/s^3 (Default)
Wall:	x-direction velocity	0 m/s (Default)
	y-direction velocity	0 m/s (Default)
Symmetry:		Maintain default settings
Interface:		Maintain default settings
Outlet:	Mode	Fixed Pressure
	Relative Pressure	varied
	Temperature	2800 K
	Kinetic Energy	0 m^2/s^2 (Default)
	Dissipation Rate	0 m^2/s^3 (Default)
Initial Conditions		
Initial Condition:	User specified	
IC Applied:	For all volumes	
Shared:	Temperature	Constant, 2800 K
Flow:	x-direction velocity	0 m/s (Default)
	y-direction velocity	0 m/s (Default)
	Pressure	varied
Turb:	Kinetic Energy	0 m^2/s^2 (Default)
	Dissipation Rate	0 m^2/s^3 (Default)
Solver Control		
Iterations:	Max Iterations	15000
	Convergence Criteria	0.0001 (Default)
	Min Resdiual	1E-18 (Default)
Spatial Differencing:	Velocity	Upwind (Defaullt)
Solvers:	Velocity	CGS+Pre (Default)
	P Correction	AMG
	Turbulence	CGS+Pre (Default)
Relax:	Velocities	0.2
	P Correction	0.2
	Turbulence	0.2
	Pressure	1
	Density	1
	Viscosity	1
Limits:		Maintain default settings
Advanced:		Maintain default settings
Output:	Steady state results	specified interval (50 iterations)
Print:	Mass flux summary	YES
Graphic:		Maintain default settings
Monitor:		Maintain default settings

Table 8. CFD-ACE Solver Setting for Designed Initiator Post-detonation Simulations

Problem Settings			
Problem Type:		Transient Compressibile Flow	
Model Options			
Global:		Axisymmetric	
Flow:		Gas Model	Ideal Gas
		Viscous Model	Turbulent (Navier Stokes)
Ideal Gas Properties:		Molecular Weight	28.97 g/mol
		Gamma, (C_p/C_v)	1.4
		Viscosity, Mu	Sutherlands Law
		Conductivity, Pr	0.7
		Turulent Conductivity, Pr_t	0.9
		Turbulence Model	Baldwin Lomax
Volume Conditions			
Physical Properties:		Property	Fluid
Boundary Conditions			
Wall:		Heat Transfer	Adiabatic
		Flow Condition	No slip
		Wall Roughness	0.00000081 m
Symmetry:			Maintain default settings
Interface:			Maintain default settings
Inlet:			Fixed Total T and P
Outlet:		BC Subtype	Fixed Pressure 101325
Initial Conditions			
Flow:		Initial Condition from:	Constant
		U	200 m/s (Default)
		V	0 m/s (Default)
		Static Pressure	150,000 N/m^2
		Static Temperature	600 K
Solver Control			
Control:		Time Accurate	
	Simulation:	Max Number of Cycles	2500
		Start Time	0 s (Default)
		Max Time	0.05 s
	Time Step:	Based on CFL Number	
		Initial CFL	0.001
		Final CFL	10
		Ramping Cycles	100 (irrelevant for transient)
Spatial:	Flow	Min Resdiual	1E-18 (Default)
		Velocity	Upwind (Defaullt)
		Flux Splitting	Roe's FDS
		Spatial Accuaracy	Higher Order
	Entropy Fix	Linear Waves	0.3
		Nonlinear Waves	0.3
Solvers:	Flow	Time Integration	Implicit
		Implicit Scheme	Point Jacobi (Fully Implicit)
		Subiterations	40
		Tolerance	0.0001
		Discretization	Backward Euler
Linear Relaxation:		No settings	
Advanced:		Freeze flow field	Unchecked
Output			
Limits:			Maintain default settings
		Viscosity	1
Output:	Solution Data	Specified Interval	50 cycles/steps
		Unique files	
	RSL, Force, etc	Overwrite	
Print:		Aero Force Summary	Unchecked
		Aero Force by Section	Unchecked
Monitor:		Monitor Points	Unchecked

Table 9. CFD-FASTRAN Solver Settings for Designed Initiator During Detonation Simulations

THIS PAGE INTENTIONALLY LEFT BLANK

APPENDIX B: CFD RESULTS

			Centerline				r=0.0020 (exit plane)				r=0.0151(exit plane)				Comments
Mass flow/rad (kg/s/rad)	Mass flow (kg/s)	Mrefresh	P_{totin} (kPa)	P_{totout} (kPa)	Pressure drop(kPa)	ΔP rate (kPa/m)	TKE (m2/s2)	TI (%)	Velocity (m/s)	Vel' (m/s)	TKE (m2/s2)	TI (%)	Velocity (m/s)	Vel' (m/s)	
0.0444	0.279	0.342	250	156	94	103	1535	14.66	378	55.4	4376	64.97	144.0	93.6	
0.0397	0.250	0.320	225	146	79	86	1392	15.29	345	52.8	3336	59.62	137.0	81.7	
0.0348	0.219	0.296	200	136	64	70	1209	16.07	306	49.2	2388	54.85	126.0	69.1	
0.0317	0.199	0.281	185	130	55	60	1071	16.47	281	46.3	1896	52.63	117.0	61.6	
0.0284	0.179	0.264	170	124	46	50	913	16.82	254	42.7	1459	50.48	107.0	54.0	
0.0249	0.156	0.243	155	119	36	39	736	17.13	224	38.4	1071	48.21	96.0	46.3	
0.0223	0.140	0.228	145	115	30	32	610	17.29	202	34.9	836	47.16	86.7	40.9	
0.0195	0.122	0.208	135	112	23	25	478	17.47	177	30.9	618.2	46.02	76.4	35.2	
0.0162	0.102	0.182	125	109	16	18	341	17.57	148.6	26.1	415.9	44.85	64.3	28.8	
0.0123	0.077	0.146	115	106	9	10	199	17.61	113.4	20.0	228.1	43.59	49.0	21.4	
0.0098	0.061	0.120	110	104	6	6	127	17.57	90.7	15.9	139.6	42.84	39.0	16.7	
0.0079	0.049	0.099	107	103	4	4	83	17.51	73.6	12.9	88.57	42.25	31.5	13.3	
0.0000	0.000	0.000	101.3	101	0	0	0	0	0	0.0	0	0	0.0	0.0	

Table 10. CFD Results for Initiator with Rings

			Centerline				r=0.0020 (exit plane)				wall (exit plane)				Comments
Mass flow/rad (kg/s/rad)	Mass flow (kg/s)	Mrefresh	P_{totin} (kPa)	P_{totout} (kPa)	Pressure drop(kPa)	ΔP rate (kPa/m)	TKE (m2/s2)	TI (%)	Velocity (m/s)	Vel' (m/s)	TKE (m2/s2)	TI (%)	Velocity (m/s)	Vel' (m/s)	
0.0649	0.408	0.735	175	161	14	15	0	5E-04	393	0.0	1031	40.91	111.0	45.4	
0.0463	0.291	0.563	140	136	4	5	0	5E-04	307.153	0.0	611.7	47.33	73.9	35.0	
0.0396	0.249	0.492	130	128	2	3	0	6E-04	271.1	0.0	471.4	50.25	61.1	30.7	
0.0318	0.199	0.402	120	119	1	1	0	0.004	224.6	0.0	317.4	54.54	46.2	25.2	
0.0270	0.170	0.345	115	114	1	1	0	0.021	194.9	0.0	234.3	57.57	37.6	21.6	
0.0238	0.149	0.305	112	112	0	0	0	0.064	173.7	0.1	182.5	60.08	31.8	19.1	
0.0200	0.126	0.258	109	109	0	0	0	0.227	148.6	0.3	129.6	63.38	25.4	16.1	
0.0155	0.097	0.201	106	106	0	0	0	0.821	116.9	1.0	76.4	68.29	18.1	12.4	
0.0090	0.057	0.117	103	103	0	0	3	3.194	70	2.2	25	82.22	8.6	7.1	
0.0000	0.000	0.000	101.3	101	0	0	0	0	0	0.0	0	0	0.0	0.0	

Table 11. CFD Results for Clean Initiator

			Centerline				r=0.0020 (exit plane)				r=0.0176 (exit plane)				Comments
Mass flow/rad (kg/s/rad)	Mass flow (kg/s)	Mrefresh	P_{totin} (kPa)	P_{totout} (kPa)	Pressure drop(kPa)	ΔP rate (kPa/m)	TKE (m2/s2)	TI (%)	Velocity (m/s)	Vel' (m/s)	TKE (m2/s2)	TI (%)	Velocity (m/s)	Vel' (m/s)	
0.0423	0.266	0.321	275	172	103	113	1226	11.8	419.5	49.5	4054	45.02	200.0	90.0	
0.0381	0.239	0.301	250	161	89	97	1213	12.59	391.1	49.3	3641	48.05	177.6	85.3	
0.0338	0.212	0.279	225	151	74	81	1176	13.52	358.8	48.5	3164	50.93	156.2	79.5	
0.0293	0.184	0.256	200	140	60	65	1096	14.52	322.4	46.8	2792	57.04	131.0	74.7	
0.0265	0.166	0.240	185	134	51	56	1024	15.29	296	45.3	2271	55.33	121.8	67.4	
0.0235	0.148	0.222	170	127	43	47	921	16.03	267.7	42.9	1897	56.87	108.3	61.6	
0.0204	0.128	0.203	155	121	34	37	787	16.79	236.2	39.7	1505	58.37	94.0	54.9	
0.0169	0.106	0.178	140	115	25	27	616	17.64	198.9	35.1	1098	59.93	78.2	46.9	
0.0144	0.090	0.158	130	111	19	20	481	18.19	170.4	31.0	818.6	60.94	66.4	40.5	
0.0114	0.072	0.132	120	108	12	13	328	18.76	136.6	25.6	535.6	61.99	52.8	32.7	
0.0089	0.056	0.108	113	105	8	8	212	19.16	107.4	20.6	335.8	62.75	41.3	25.9	
0.0076	0.048	0.094	110	104	6	6	159	19.32	92.4	17.9	249.9	63.15	35.4	22.4	
0.0000	0.000	0.000	101.3	101	0	0	0	0	0	0.0	0	0	0.0	0.0	

Table 12. CFD Results for Initiator with Ramps

			Centerline				r=0.0020 (exit plane)				r=0.0151 (exit plane)				Comments
Mass flow/rad (kg/s/rad)	Mass flow (kg/s)	Mrefresh	P_{totin} (kPa)	P_{totout} (kPa)	Pressure drop(kPa)	ΔP rate (kPa/m)	TKE (m2/s2)	TI (%)	Velocity (m/s)	Vel' (m/s)	TKE (m2/s2)	TI (%)	Velocity (m/s)	Vel' (m/s)	
0.0514	0.323	0.355	1000	898	102	112	1363	17.58	297	52.2	1591	44	128.2	56.4	
0.0492	0.309	0.356	1000	908	92	101	1208	17.6	279.3	49.2	1390	43.79	120.4	52.7	
0.0459	0.288	0.348	1000	922	78	86	1012	17.64	255.1	45.0	1142	43.45	110.0	47.8	
0.0421	0.265	0.332	1000	935	65	71	820	17.63	229.8	40.5	910.16	43.1	99.0	42.7	
0.0378	0.238	0.311	1000	949	51	56	634	17.59	202.4	35.6	690.1	42.75	86.9	37.2	
0.0341	0.214	0.292	1000	959	41	45	499	17.57	179.9	31.6	534.9	42.42	77.1	32.7	
0.0297	0.187	0.270	1000	969	31	33	368	17.51	155	27.1	387	42.03	66.2	27.8	
0.0263	0.165	0.252	1000	976	24	26	283	17.46	136.3	23.8	292.9	41.73	58.0	24.2	
0.0223	0.140	0.228	1000	983	17	18	200	17.39	114.9	20.0	202.1	41.37	48.6	20.1	
0.0173	0.109	0.192	1000	990	10	11	118	17.23	89	15.3	115.4	40.73	37.3	15.2	
0.0141	0.089	0.164	1000	993	7	7	78	17.13	72.7	12.4	73.8	40.23	30.2	12.1	
0.0099	0.062	0.121	1000	997	3	4	38	16.83	51.8	8.7	33.3	38.86	21.0	8.2	
0.0000	0.000	0.000	1000	1000	0	0	0	0	0	0.0	0	0	0.0	0.0	

Table 13. CFD Results for Initiator with Rings Post-detonation Conditions

APPENDIX C: WIRING TABLES

AC Relays:

Relay Number	Logic Input (Port/Bit)	Controls:
AC 1/0	1/0	Main Air 3-way Ball Valve (Air Isolation Valve)
AC 1/1	1/1	Vitiator (O2/H2) Solenoid Valves
AC 1/2	1/2	Spare
AC 1/3	1/3	Torch (H_2/Air) Solenoid Valves
AC 2/0	1/4	Torch Ignition
AC 2/1	1/5	Torch (H_2) Ball Valve
AC 2/2	1/6	Fuel Pump
AC 2/3	1/7	Vitiator (O_2/H_2) Ball Valves
AC 4/3	2/1	Spare

Table 14. Electrical Relay Assignments

Low Speed Data

Channel	Data
Device 4 ACH 32	Inlet Temperature
ACH 33	Vitiator Temperature
ACH 34	Future Temperature
ACH 35	mdot Temperature
ACH 36	Oil Pressure
ACH 37	mdot Pressure
ACH 38	Shop Air Pressure
ACH 39	N2 Pressure
ACH 48	H2 Pressure
ACH 49	Future Pressure
ACH 50	Engine Inlet Pressure
ACH 51	Fuel Pump Pressure
ACH 52	Eng 3 Pressure
ACH 53	O2 Bottle Pressure
ACH 54	Future Pressure
ACH 55	Thrust

High Speed Data

Table 15. Data Acquisition Assignments

High Speed Data

Channel	Data
BNC CH 1	TPI Voltage
BNC CH 2	TPI Amperage
BNC CH 3	Kistler High Speed Pressure 1
BNC CH 4	Kistler High Speed Pressure 2
BNC CH 5	Kistler High Speed Pressure 3
BNC CH 6	Kistler High Speed Pressure 4
BNC CH 7	Kistler High Speed Pressure 5
BNC CH 8	Kistler High Speed Pressure 6

Table 16. High Speed Data Wiring

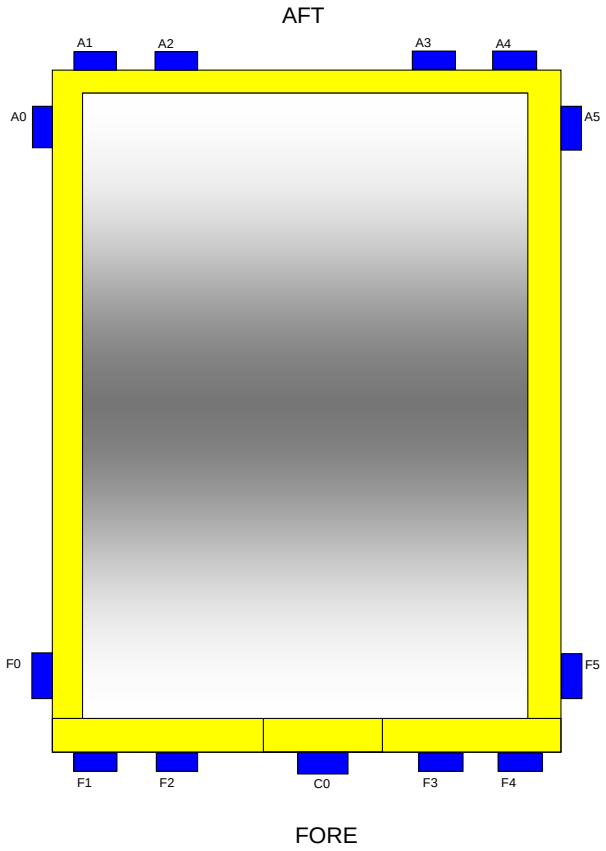

Figure 45. Thrust Stand Load Cell Wiring Diagram

Thrust Stand	PXI slot 7
SCXI 1520	(see thrust stand diagram for load cell #'s)
Slot 1 ACH0	Load Cell A0
ACH 1	Load Cell A1
ACH 2	Load Cell A2
ACH 3	Load Cell A3
ACH 4	Load Cell A4
ACH 5	Load Cell A5
ACH 6	Load Cell A6
ACH 7	Load Cell A7
Slot 2 ACH0	Load Cell F0
ACH 1	Load Cell F1
ACH 2	Load Cell F2
ACH 3	Load Cell F3
ACH 4	Load Cell F4
ACH 5	Load Cell F5
ACH 6	Load Cell F6
ACH 7	Load Cell F7
Slot 3 ACH0	Load Cell C0
ACH 1	blank
ACH 2	blank
ACH 3	blank
ACH 4	blank
ACH 5	blank
ACH 6	blank
ACH 7	blank

Table 17. Thrust Stand Load Cell Data Acquisition Assignments

THIS PAGE INTENTIONALLY LEFT BLANK

APPENDIX D: TEST CELL #2 SOP

Test Cell #2
Standard Operating Procedures (S.O.P)
Engine Start UP
(last modification date 24 November 2006)

Prior to starting preparations

1. Notify all lab personnel of live test cell.
2. Turn ON control console
3. Turn ON warning lights
4. Notify the Golf Course (x2167) (Only required if Hot Fire Test is conducted)

Preparing Test Cell

1. Push the Emergency Stop IN (secured)

1. Turn ON BNC Cabinet Power Strip.
2. On Control Computer, open LABVIEW and ensure that the execution target contains the PXI address. Open control panel and run the program.
    a. RT Target address: 131.120.20.49
    b. Control Program Path
        i. Open
        ii. Test Cell #2 Manual Control v19
        iii. Enter Run Path Name
            1. If this is not completed prior to running you will lose the data file that was created with the default name.
3. Turn ON 24 VDC in the control room cabinet
4. OPEN Main Air (HP Air Tank Valve) and High Pressure Air
    a. Blue hand valve should be opened slowly as not to shock the lines
    b. Node 4 air valve in test cell #1
5. OPEN H_2 & O_2 six packs
6. Enter Test Cell #2 and OPEN all the supply gas bottles that are going to be used
7. OPEN both JP-10 valves
8. Ensure that PXI Controllers, Amps, Kisslers, and Power strips in 2 the black cabinets are ON.
9. Turn ON 24 VDC power supply for Test Cell #2 TESCOM Control Power.
10. OPEN Shop Air, Purge Air (High Pressure Air) and Main Air
11. CLOSE 440 VAC knife switch for Oil Pump
12. TURN ON Cooling Water
13. TURN ON TPI (do not exceed 85 on heater control knob)
14. CONNECT Vitiator Spark Plug (if being used).
15. If required, set up any visual data recording equipment.
16. Evacuate all non-essential personnel to the control room
17. RUN the control

Running the Engine

1. Set Main Air, Secondary/Purge Air, and all other gases pressures (ER3000) ON RPL00
    a. Set Main Air and Purge Air (ER3000)
        i. 001 Main Air
        ii. 004 Secondary Air
    b. Supply Gases in Test Cell #2 TESCOM Node Address
        i. 020 Vit H20
        ii. 21 Vit O2
2. **DISCONNECT CH 7 & 8**
3. Set All Engine Control Parameters (on BNC Pulse Generator)
    a. Send Engine Parameters to BNC
4. **RECONNECT CH 7 & 8**
5. Twist Emergency Stop Button clockwise (TEST CELL IS NOW LIVE)
6. ENABLE the Test Cell on the VI.
7. OPEN required ball valves.
8. Verify Golf Course is clear
9. Sound the Siren
10. When area is clear, START record VCRs
11. Fuel Pump On
12. TURN ON Data Recording Switch
13. Manually engage Main Air flow
14. Start Vitiator

**********WARNING**********

The next step will result in the commencement of a run profile and ignition.

* Note: The 3-Way Ball Valve has a control in the Vitiator sequence. If the Vitiator is used then the 3-Way Ball will not divert through the engine until 375º F and will dump overboard at the end of the run at 175º F.

15. COMMENCE RUN
    a. High Speed DAQ will be triggered and the engine profile will commence
16. STOP RUN.
    a. Pulse generation will be stopped.
17. TURN OFF Data Recording Switch
18. Wait for main air to divert
19. Ensure all BV are closed
20. Fuel pump off
21. Stop Main Air Flow
22. DISABLE the Test Cell on the VI.
23. Push Emergency Stop Button IN

Test Cell #2
Standard Operating Procedures (S.O.P)
Engine Shut DOWN
(last modification date 24 November 2006)

1. SET all supply gases to ZERO, Nodes 1,4,20 & 21
2. STOP control code.
3. Push Emergency Stop Button IN
4. Turn OFF Power Strip in BNC Timing Cabinet
5. If Gas Turbine ignitor used DISABLE BEFORE turning off 24 VDC
6. TURN OFF 24 VDC power supply (check with other test cells first)
7. CLOSE Janesbury Valve (check with other test cells first)
8. REMOVE Vitiator Spark Plug head
9. SECURE TESCOM 24VDC power. (check with other test cells first)
10. CLOSE Shop Air, High Pressure Air, and Main Air
11. CLOSE 440 VAC Knife switch
12. TURN OFF Cooling Water
13. CLOSE Supply gases
14. CLOSE JP-10 supply valves
15. TURN OFF TPI
16. CLOSE H_2 & O_2 six packs
17. VENT H_2 & O_2 lines
18. STOW Cameras and other equipment used in testing.
19. CLOSE Test Cell #2.
20. TURN OFF Warning Lights.

THIS PAGE INTENTIONALLY LEFT BLANK

APPENDIX E: ENGINEERING DRAWINGS

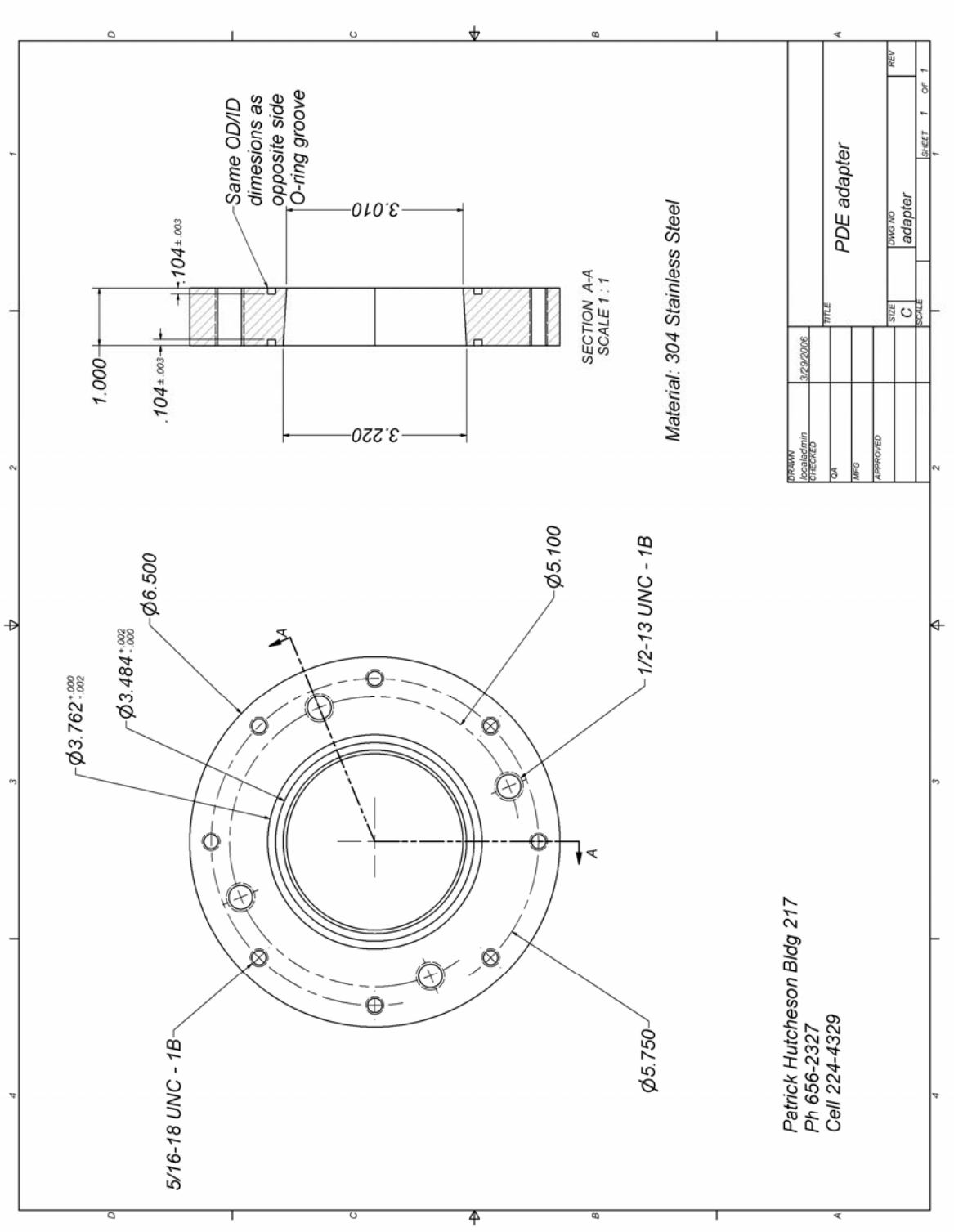

Figure 46. PDE Engine Adapter

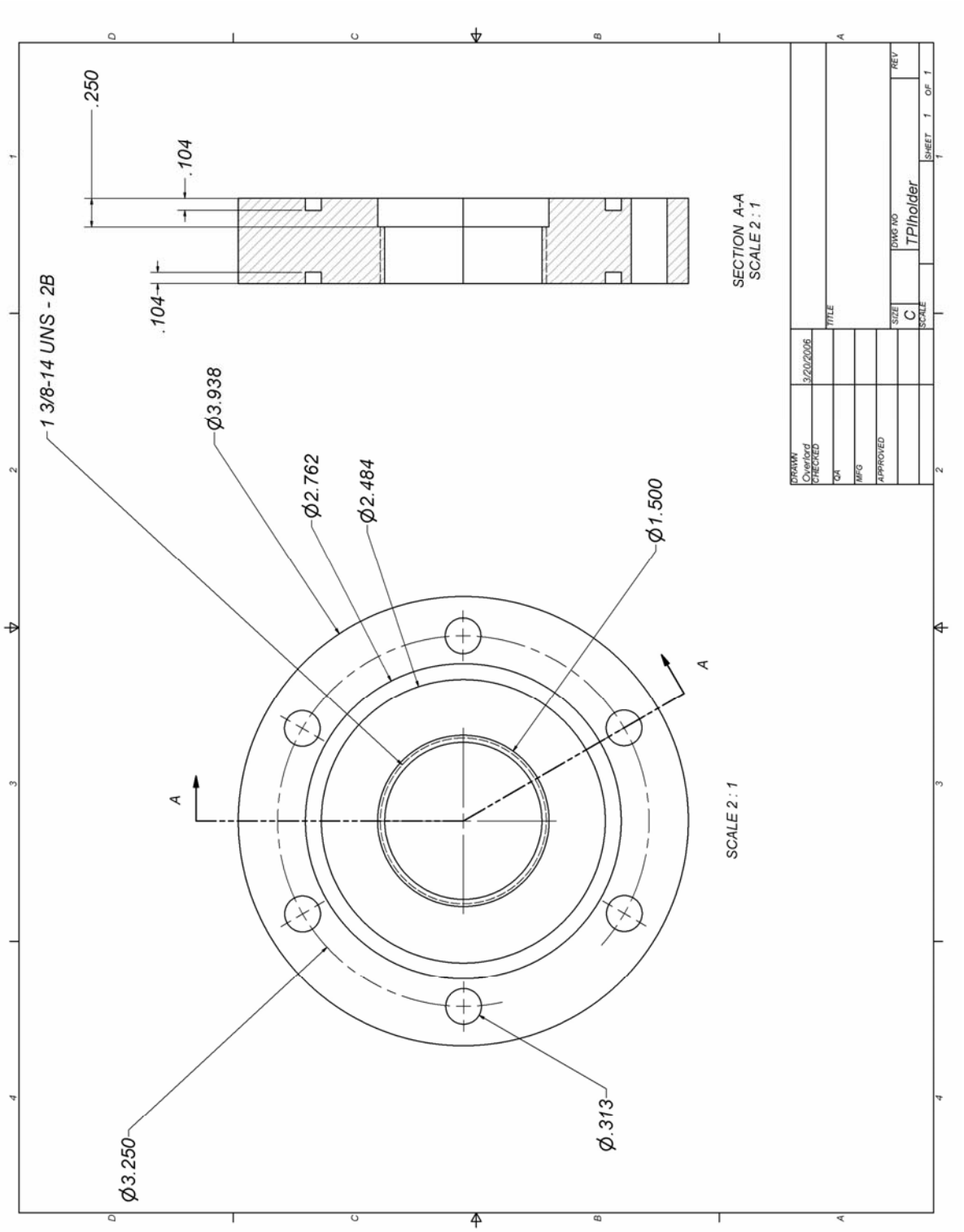

Figure 47. TPI Holder

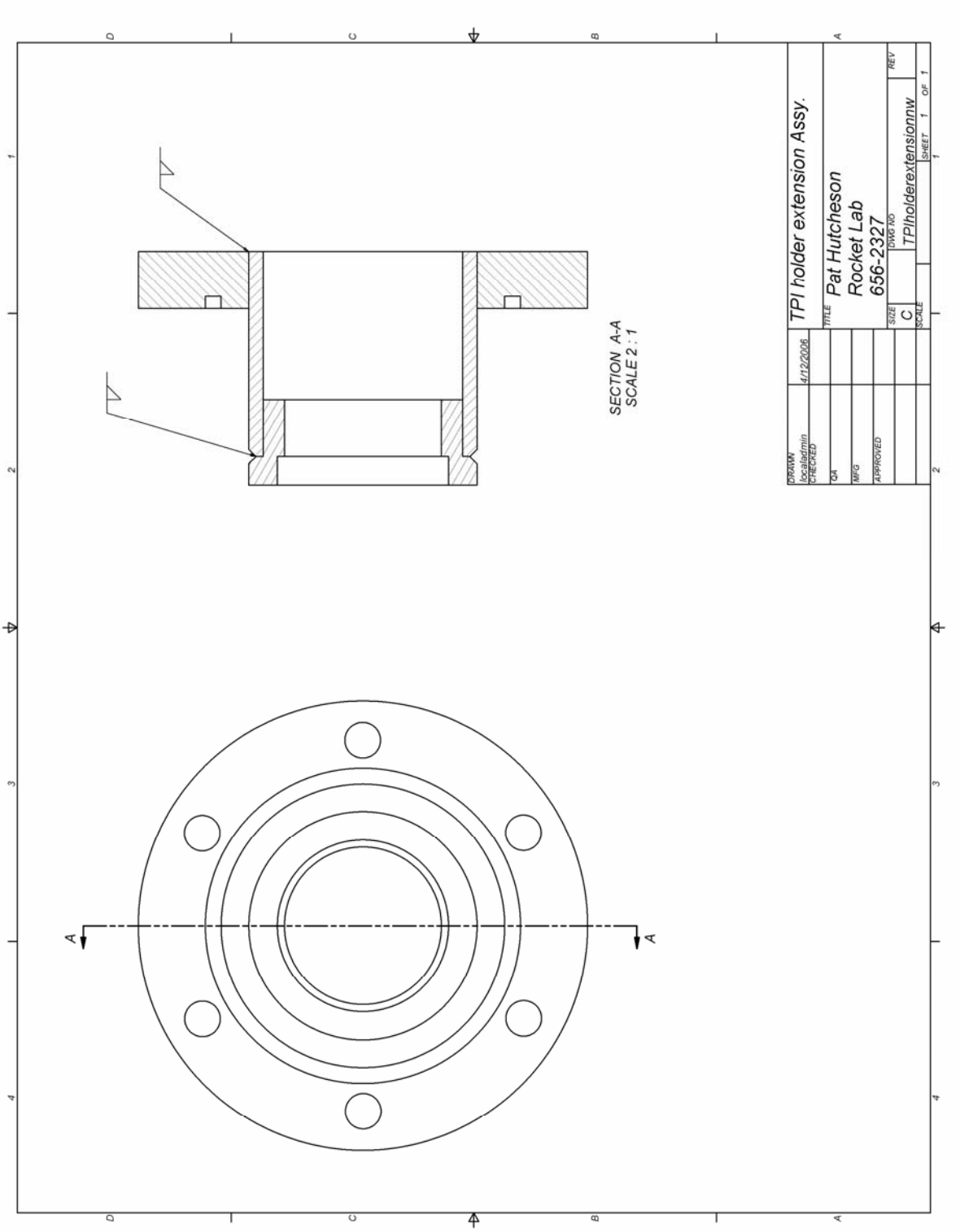

Figure 48. TPI Holder Extension Assembly

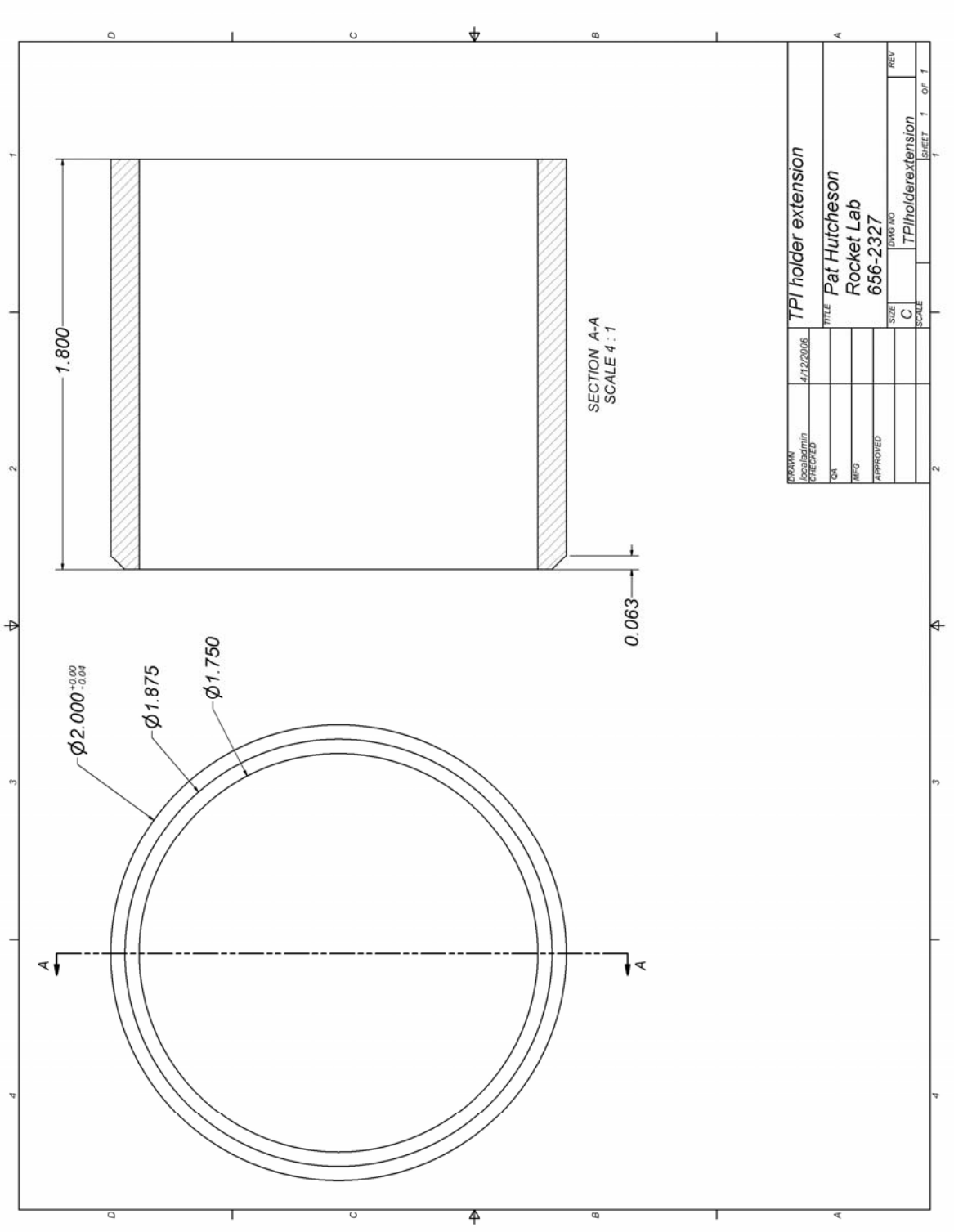

Figure 49. TPI Holder Extension Assembly

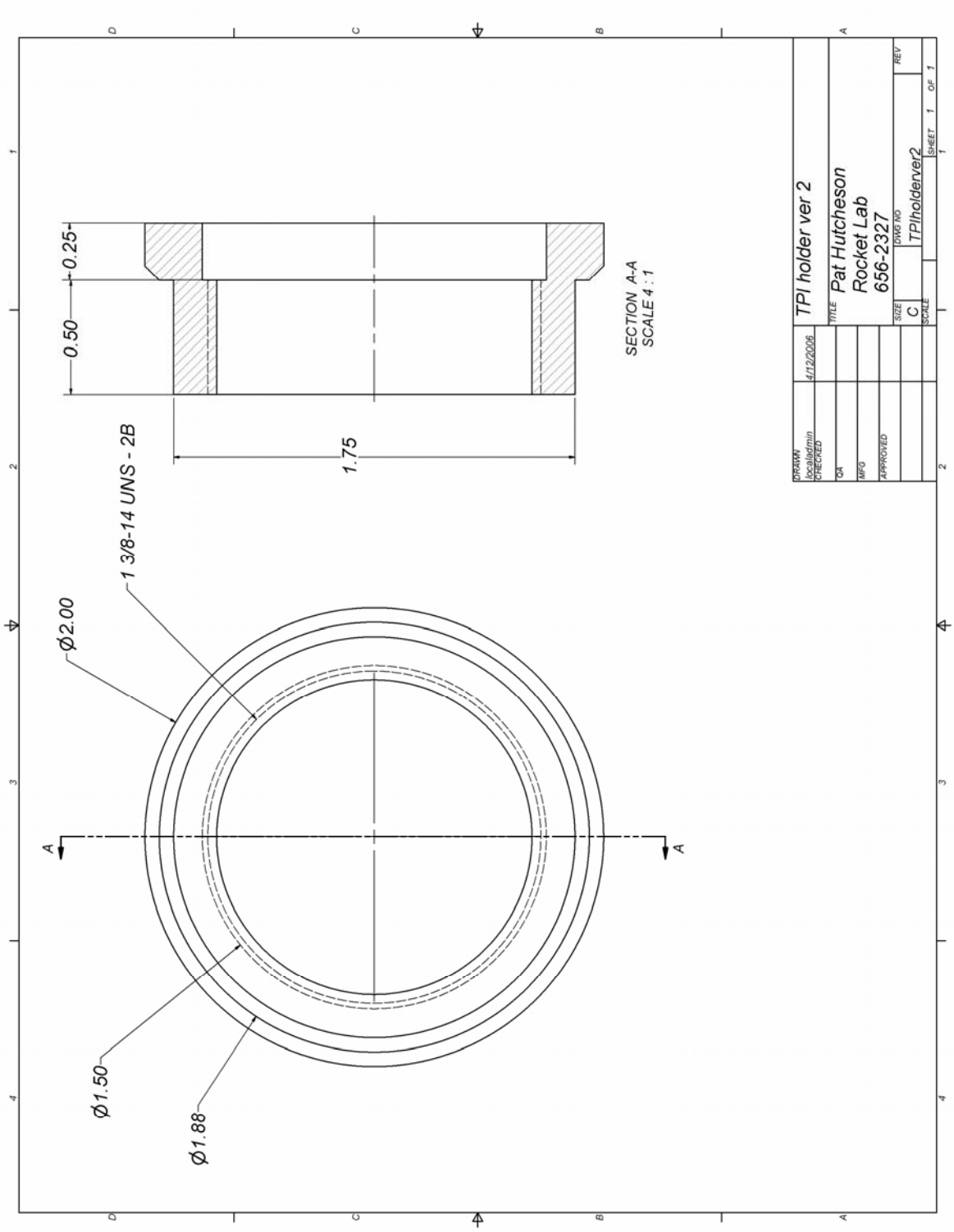

Figure 50. TPI Holder (version 2)

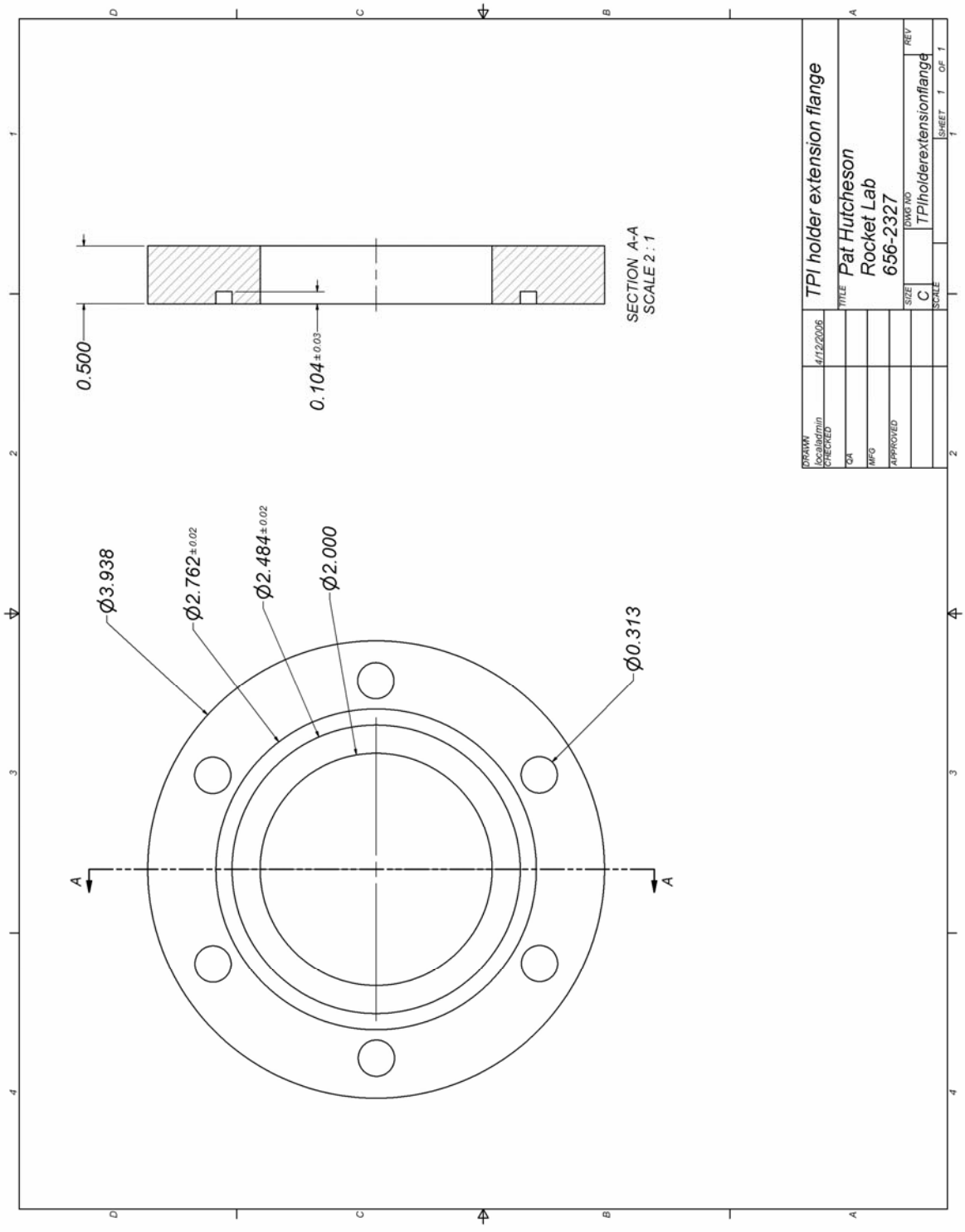

Figure 51. TPI Holder Extension Flange

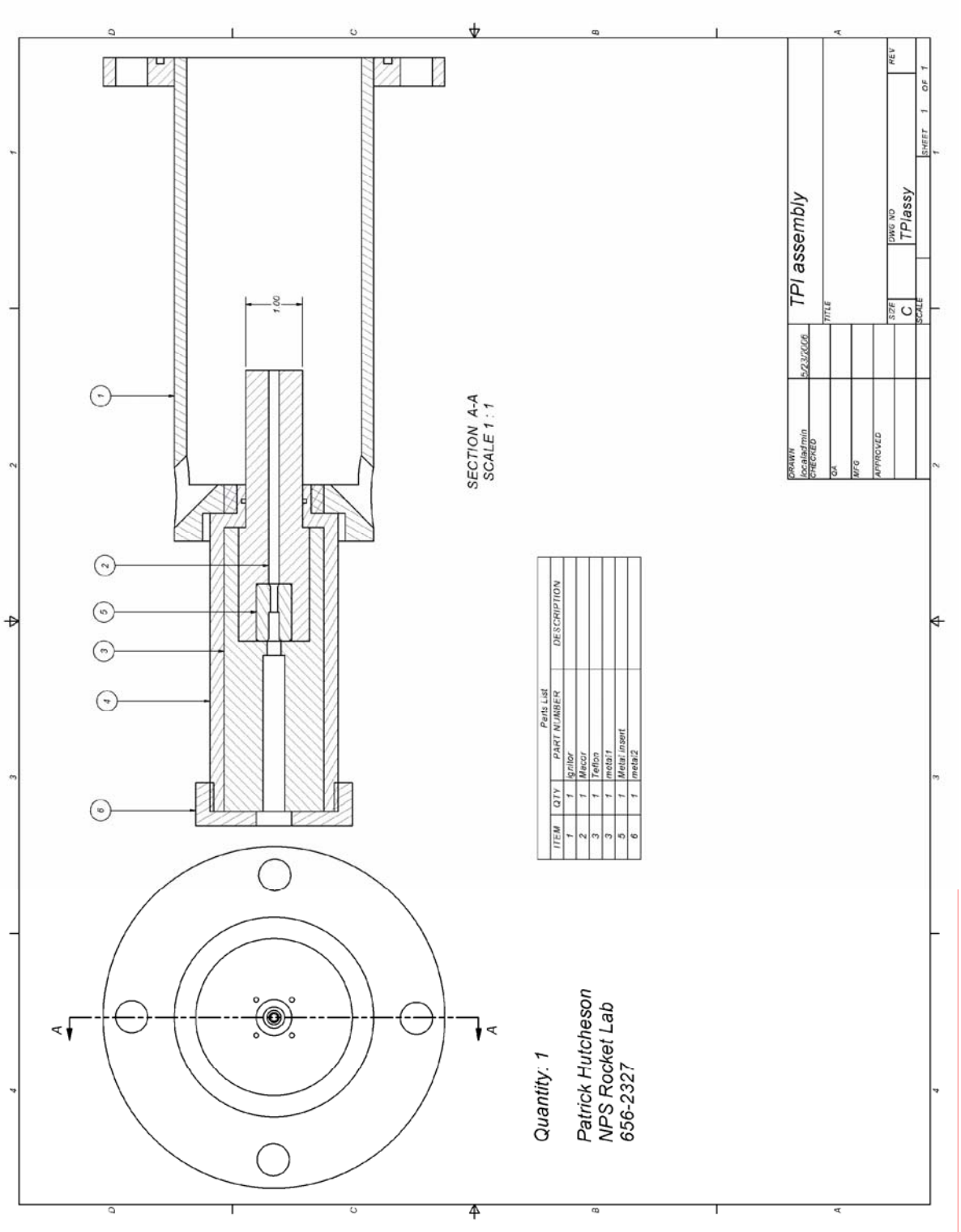

Figure 52. New TPI Assembly

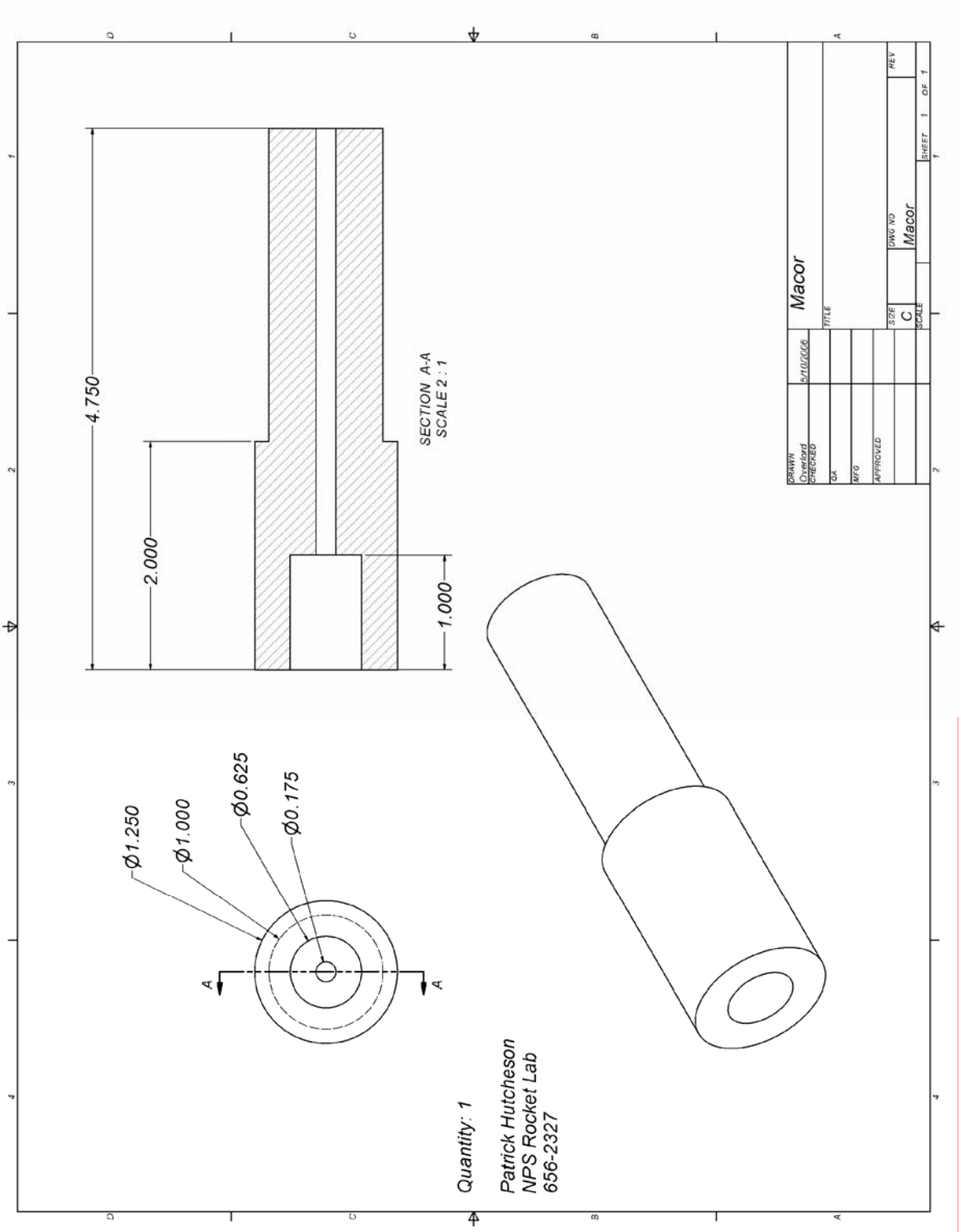

Figure 53. Macor Insulator

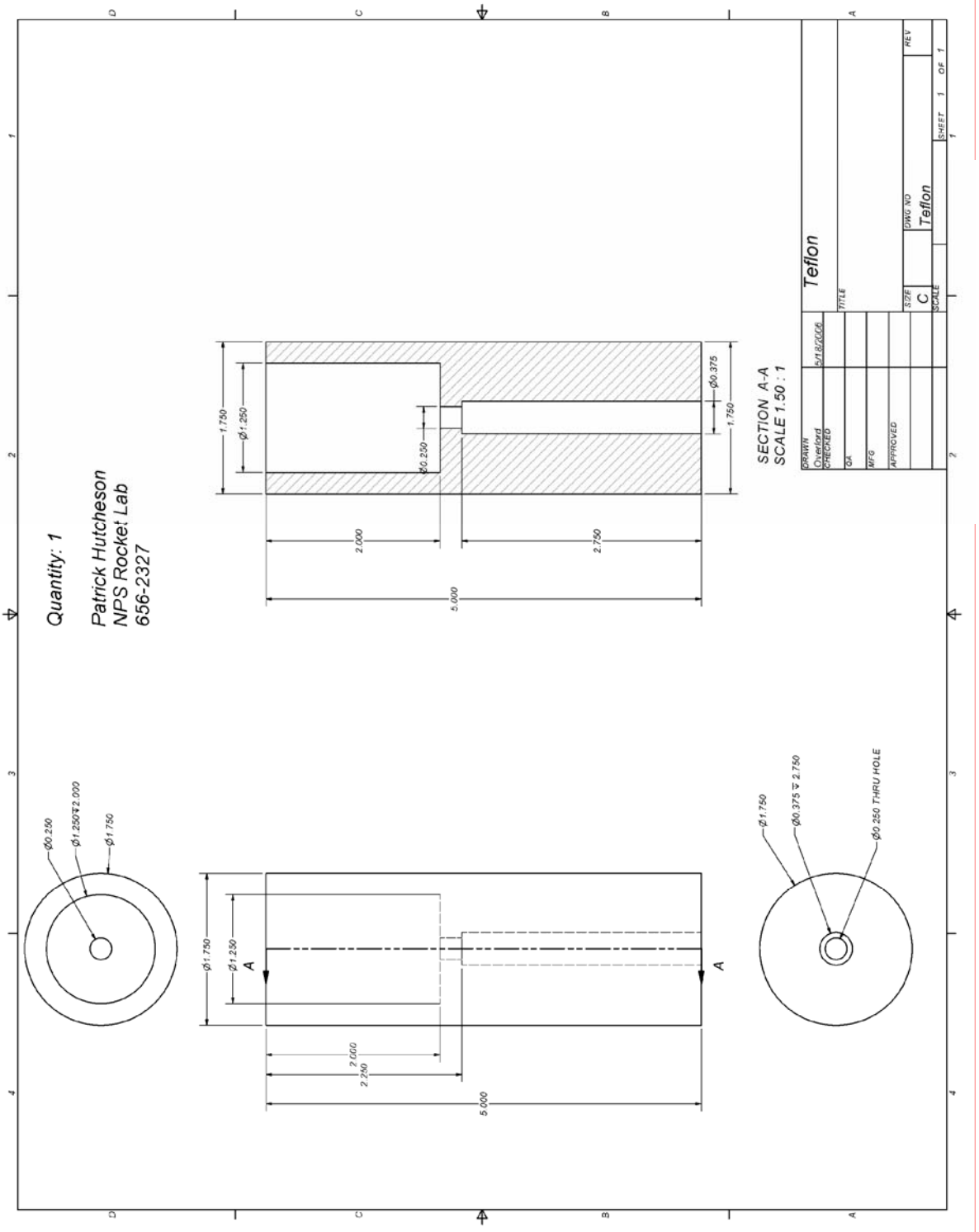

Figure 54. Nylon\Teflon Insulator

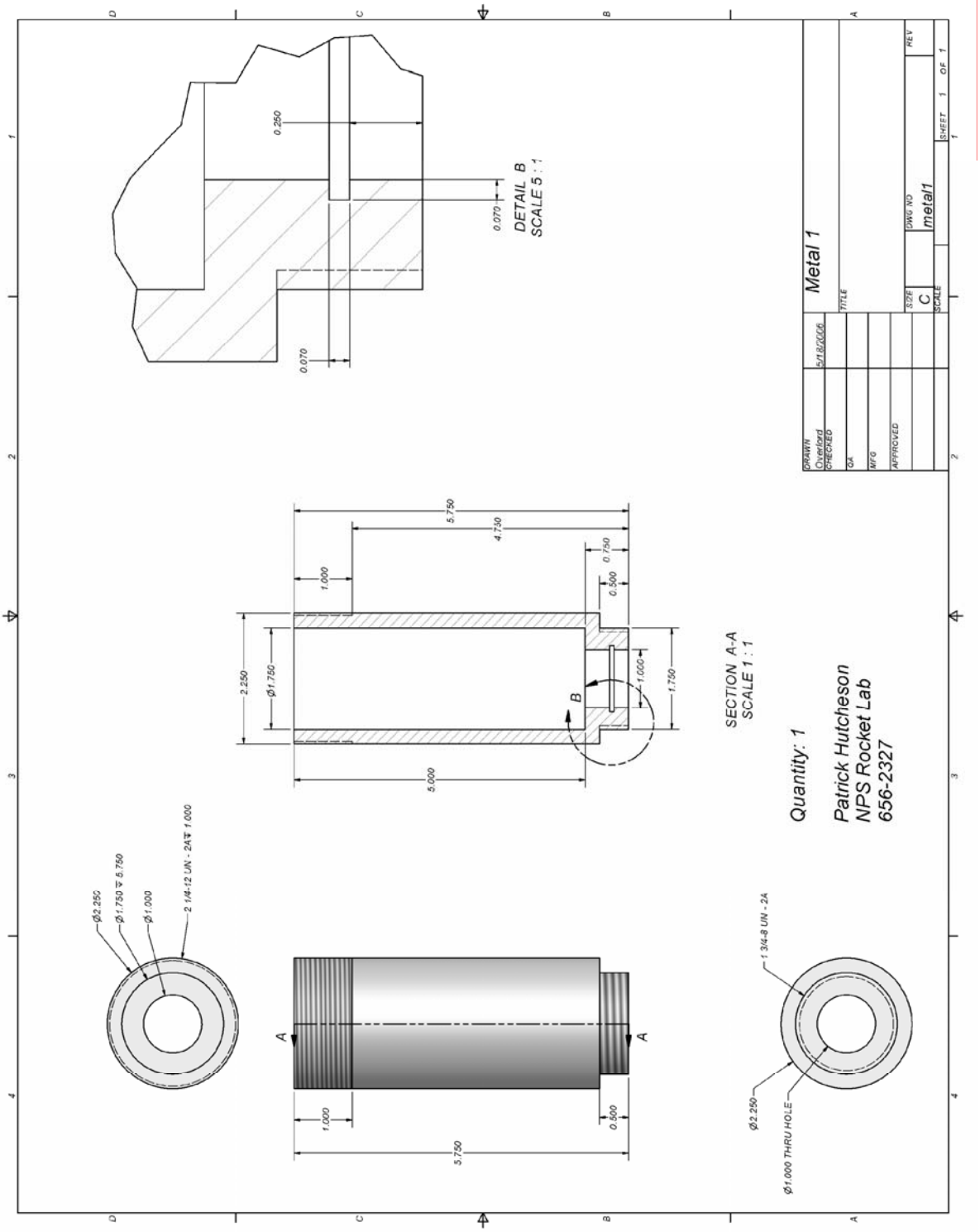

Figure 55. New TPI Metal Holder

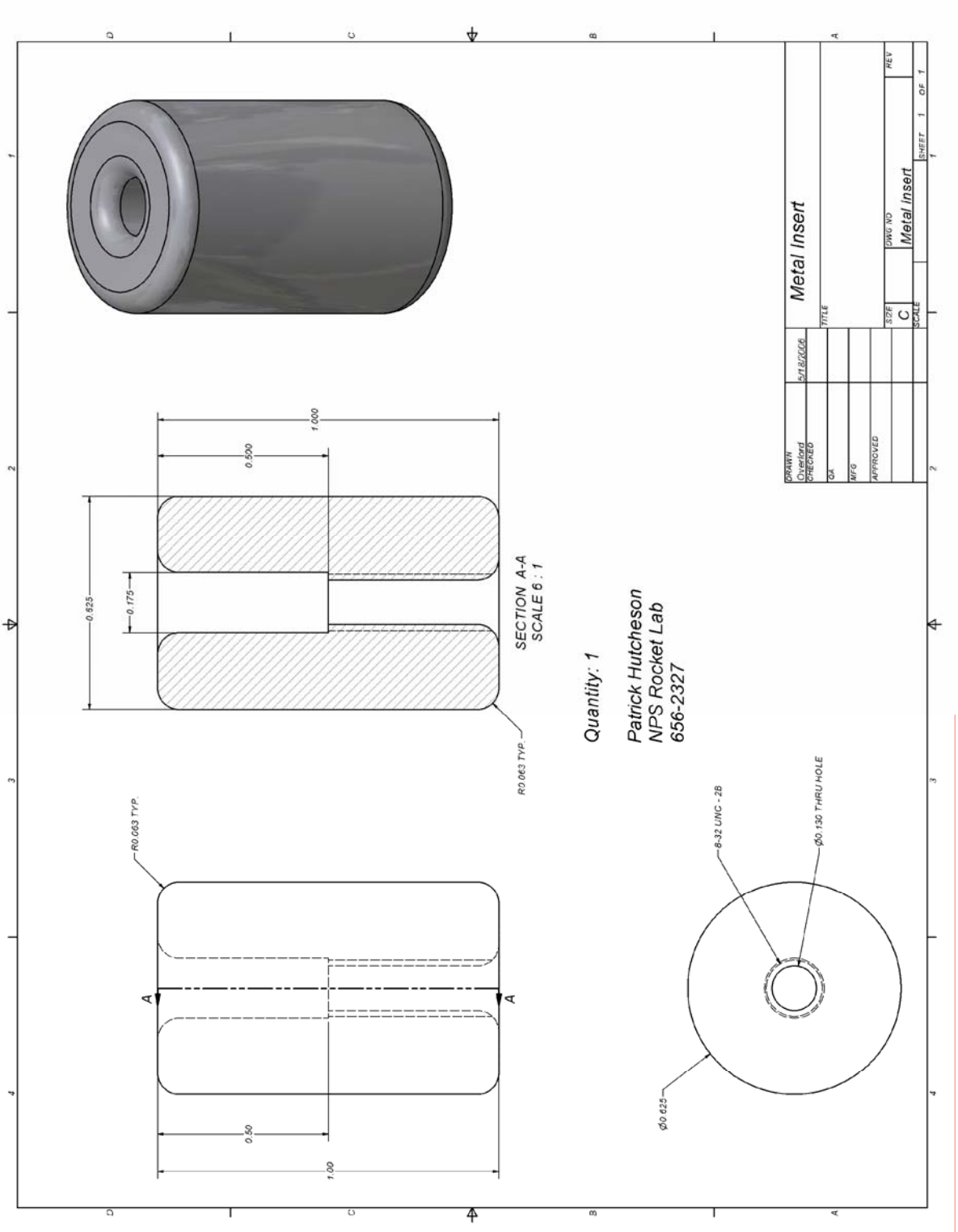

Figure 56. Metal Insert

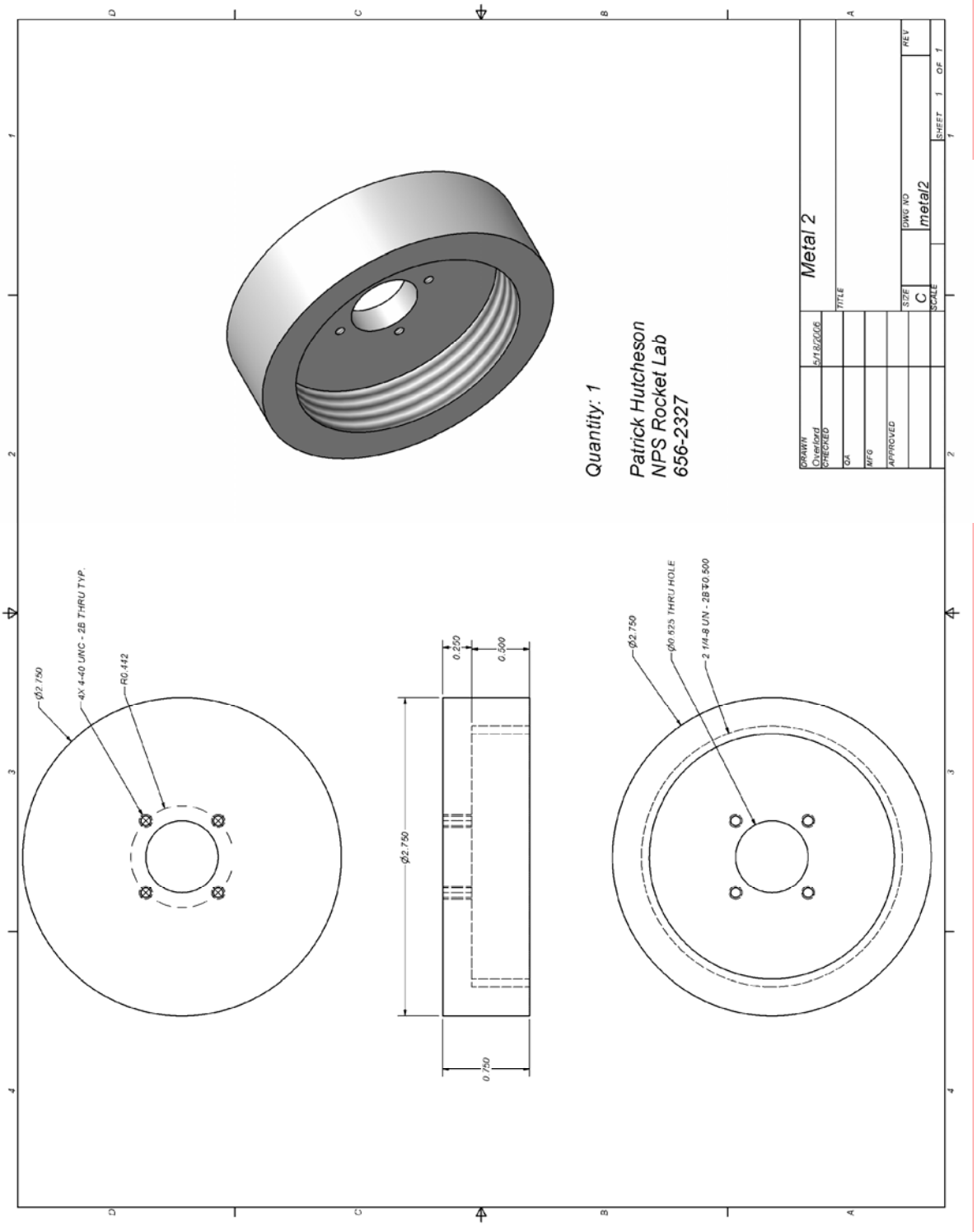

Figure 57. Metal Cap

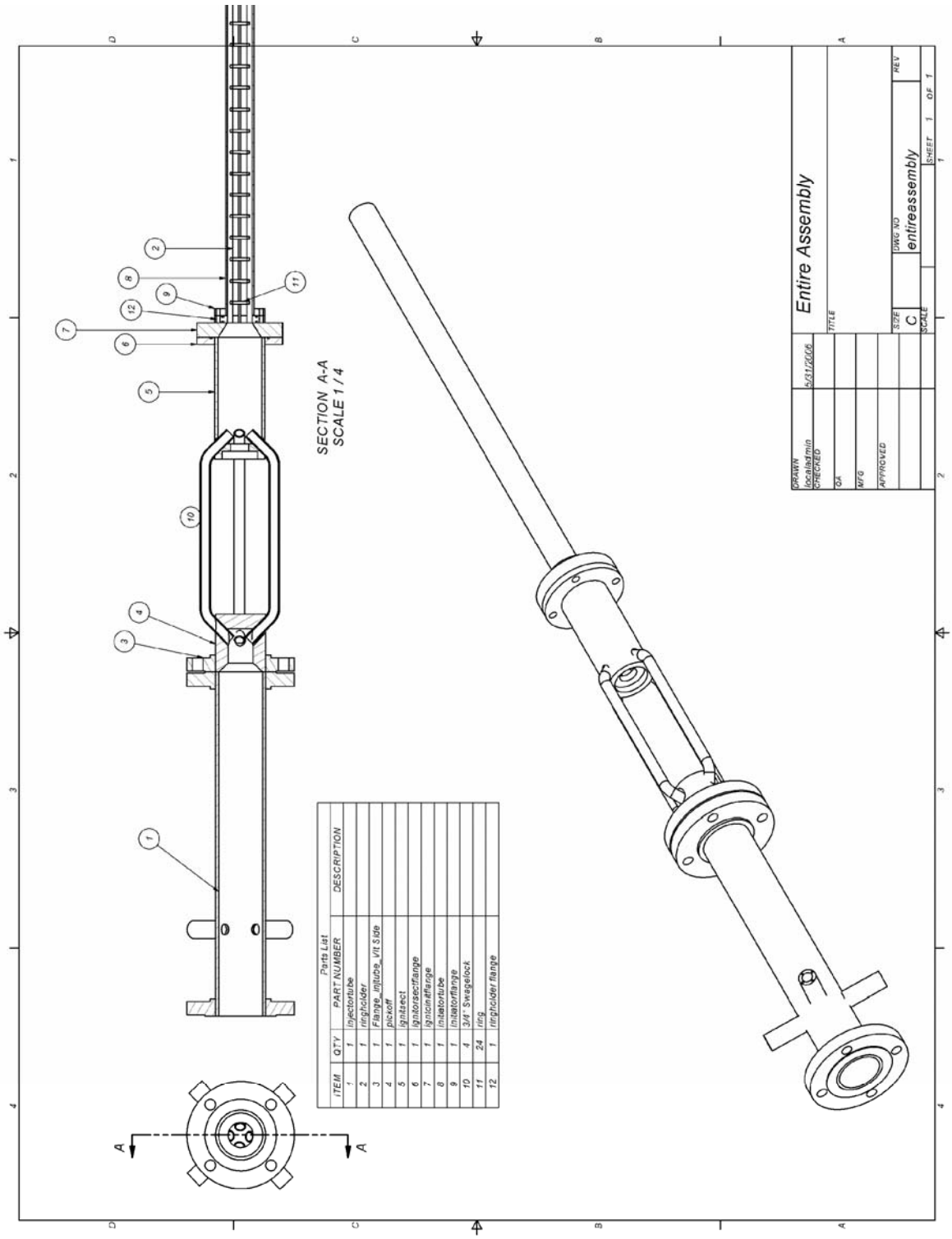

Figure 58. New PDE Design Entire Assembly

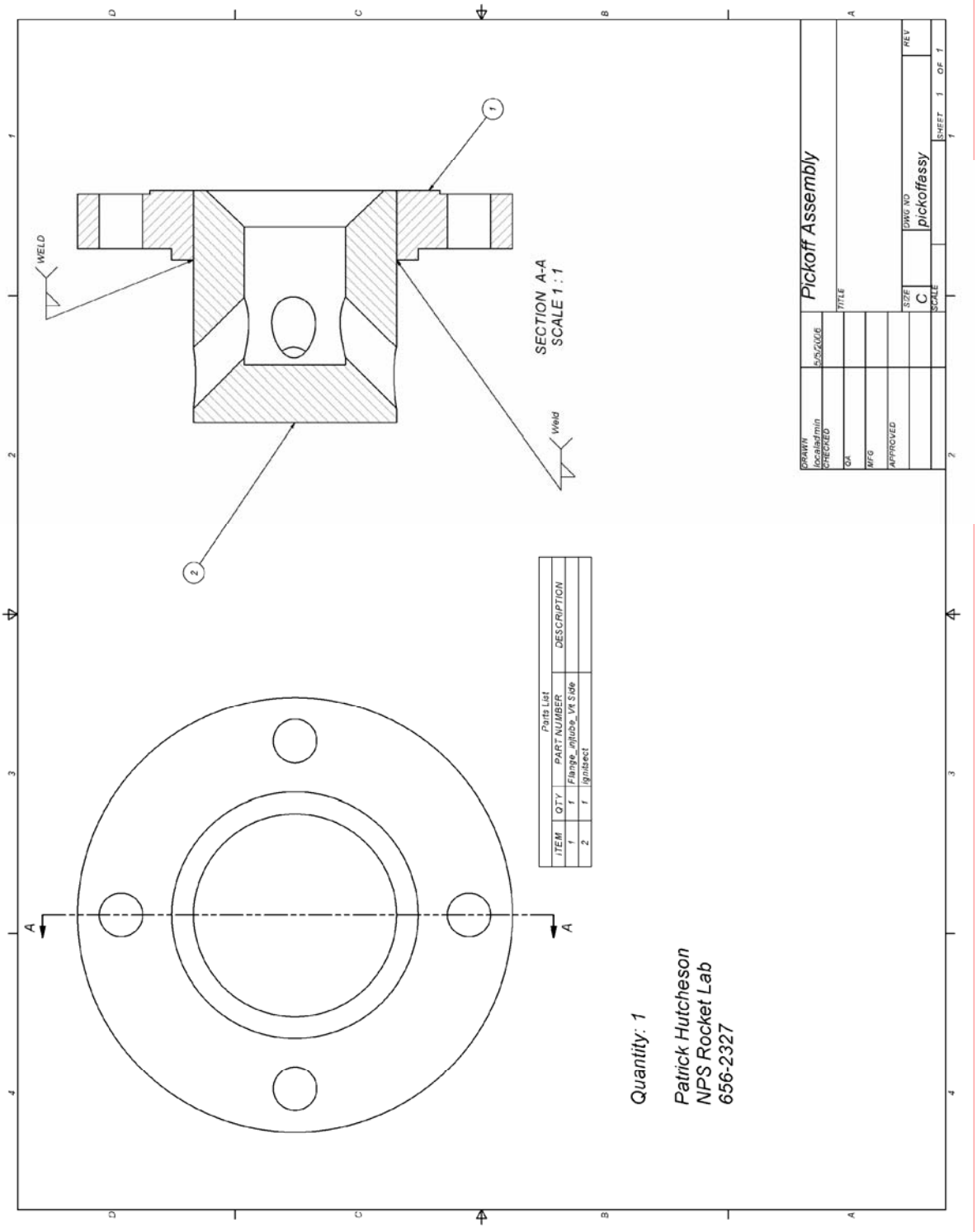

Figure 59. Pickoff Assembly

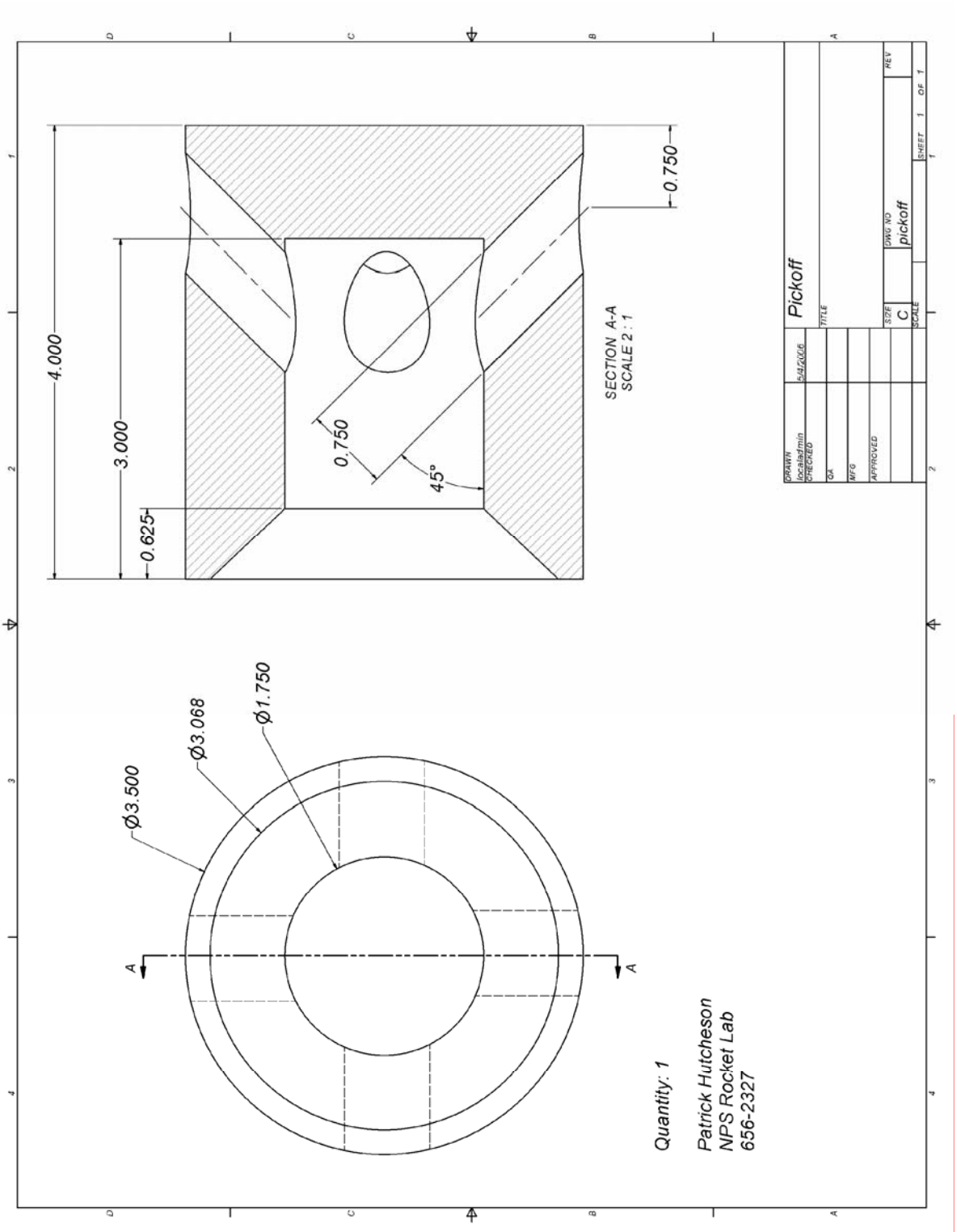

Figure 60. Pickoff

Figure 61. TPI Holder Extension Flange

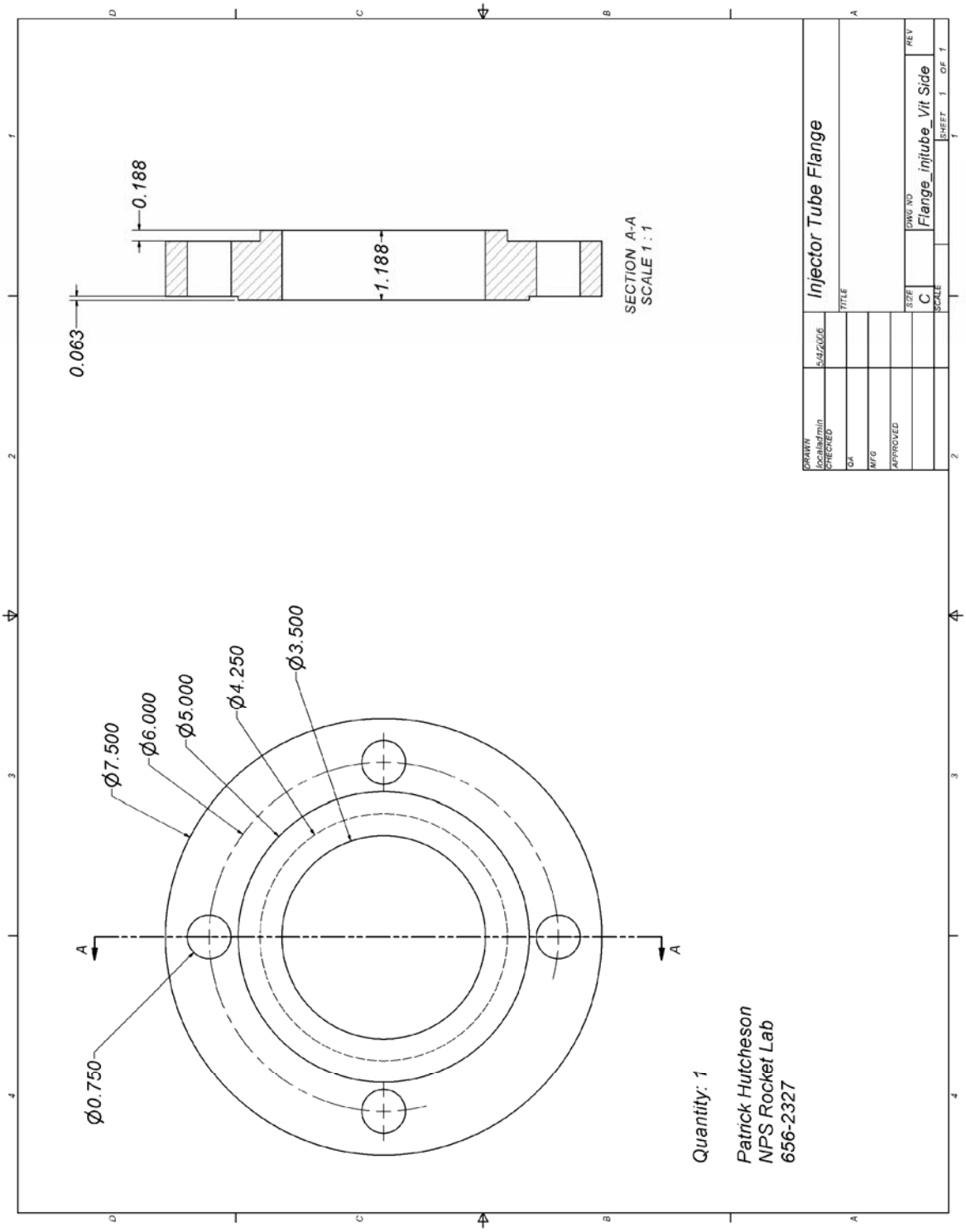

Figure 62. Pickoff Flange

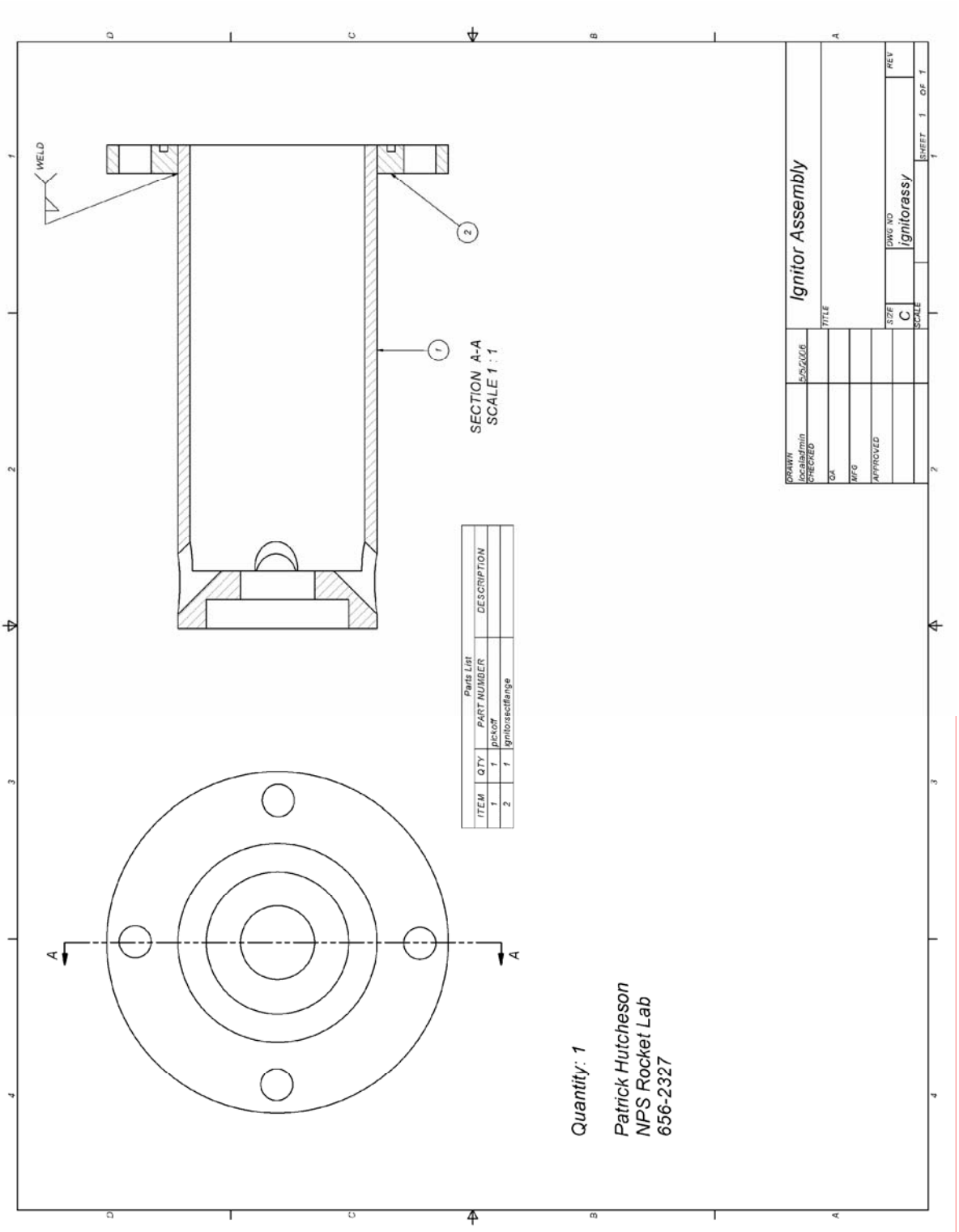

Figure 63. Igniter Assembly

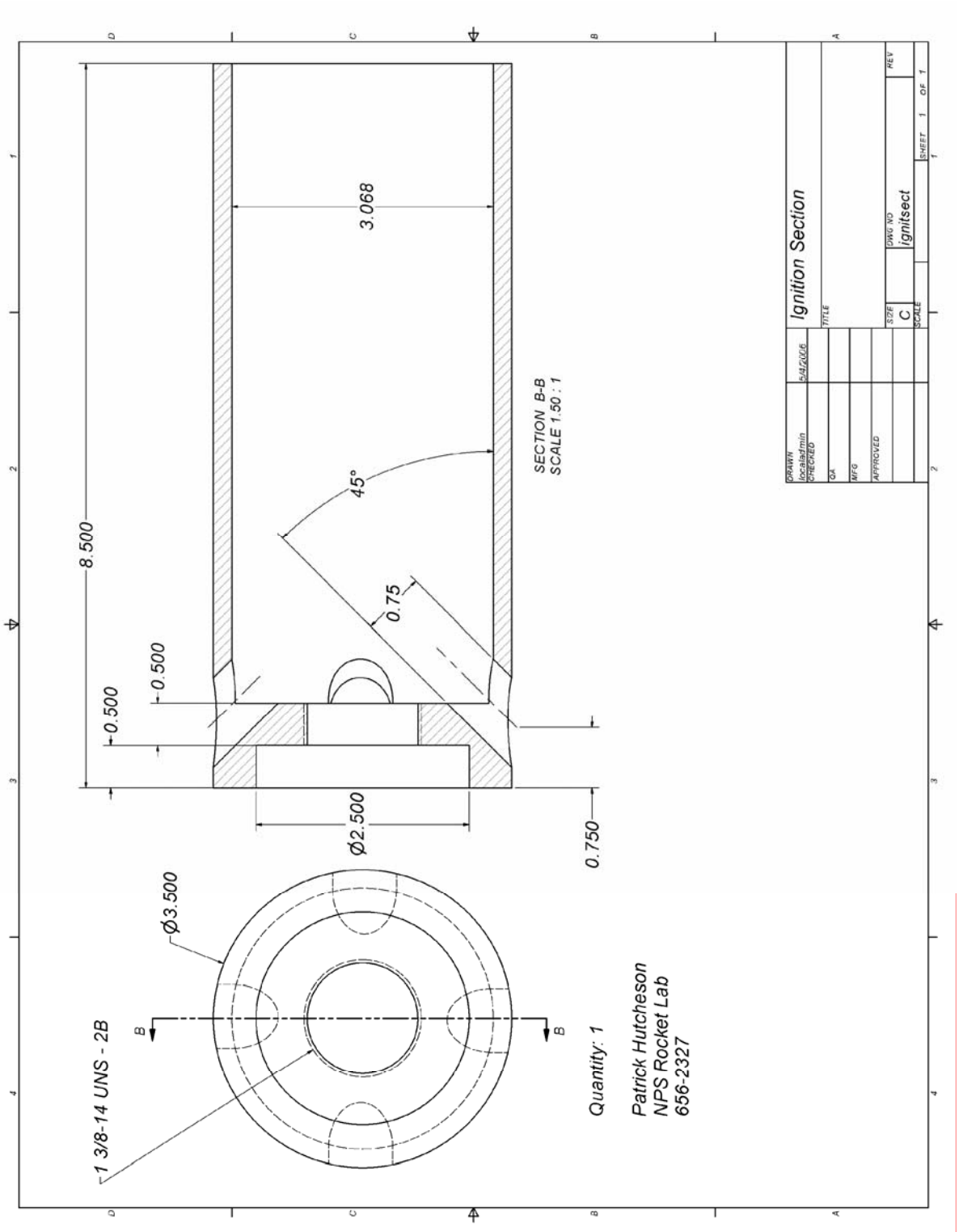

Figure 64. Igniter Section

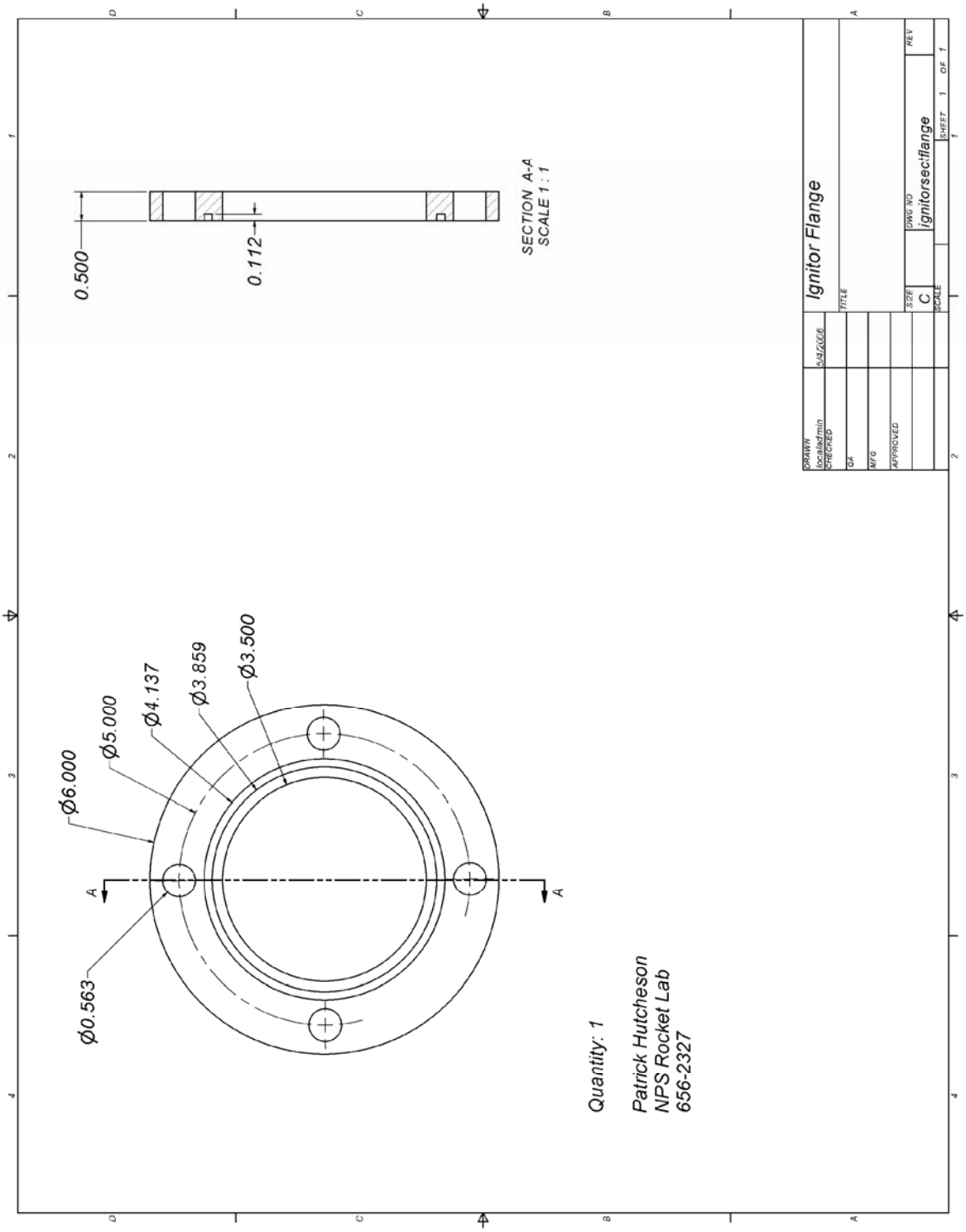

Figure 65. Igniter Section flange

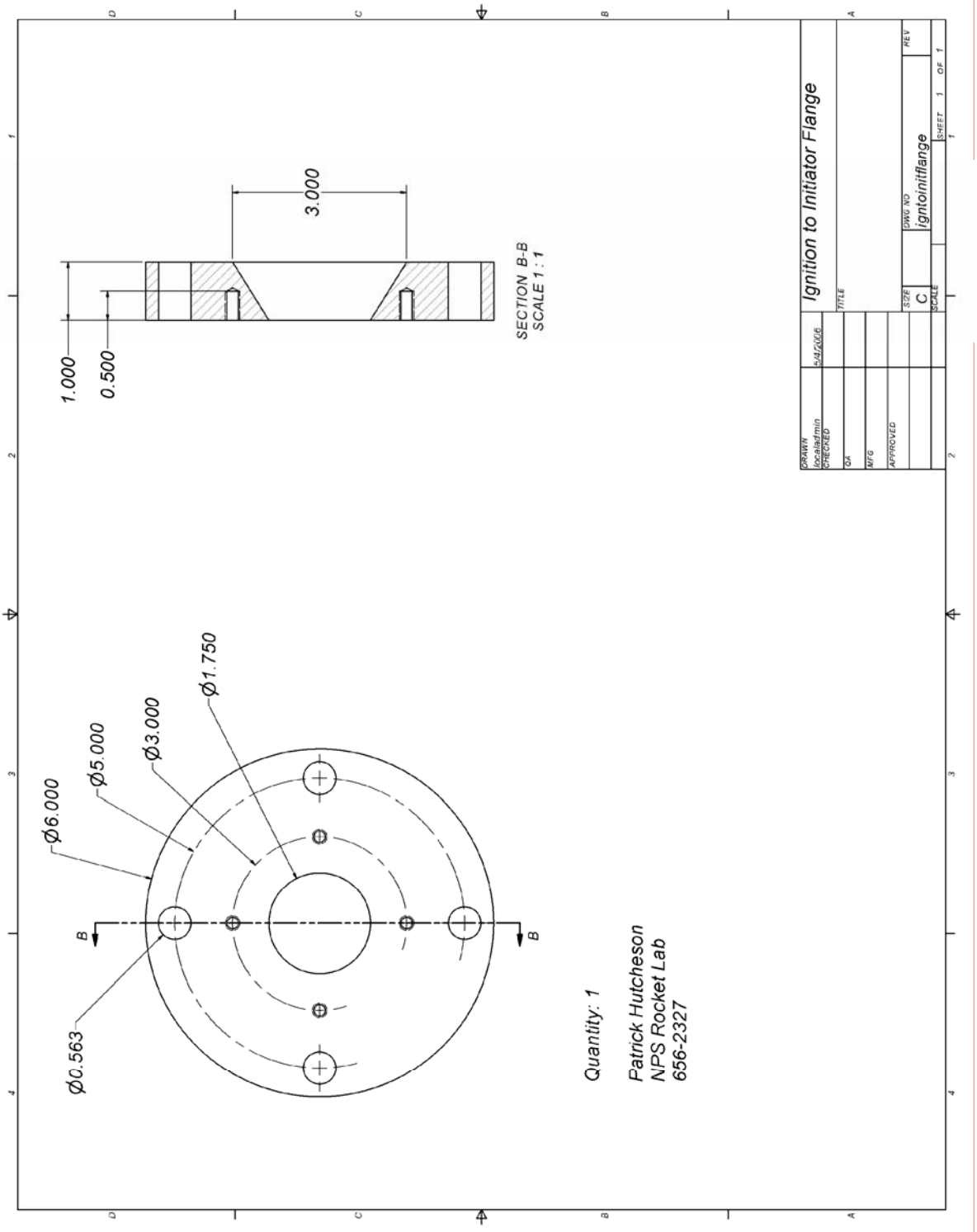

Figure 66. Igniter to Initiator Flange

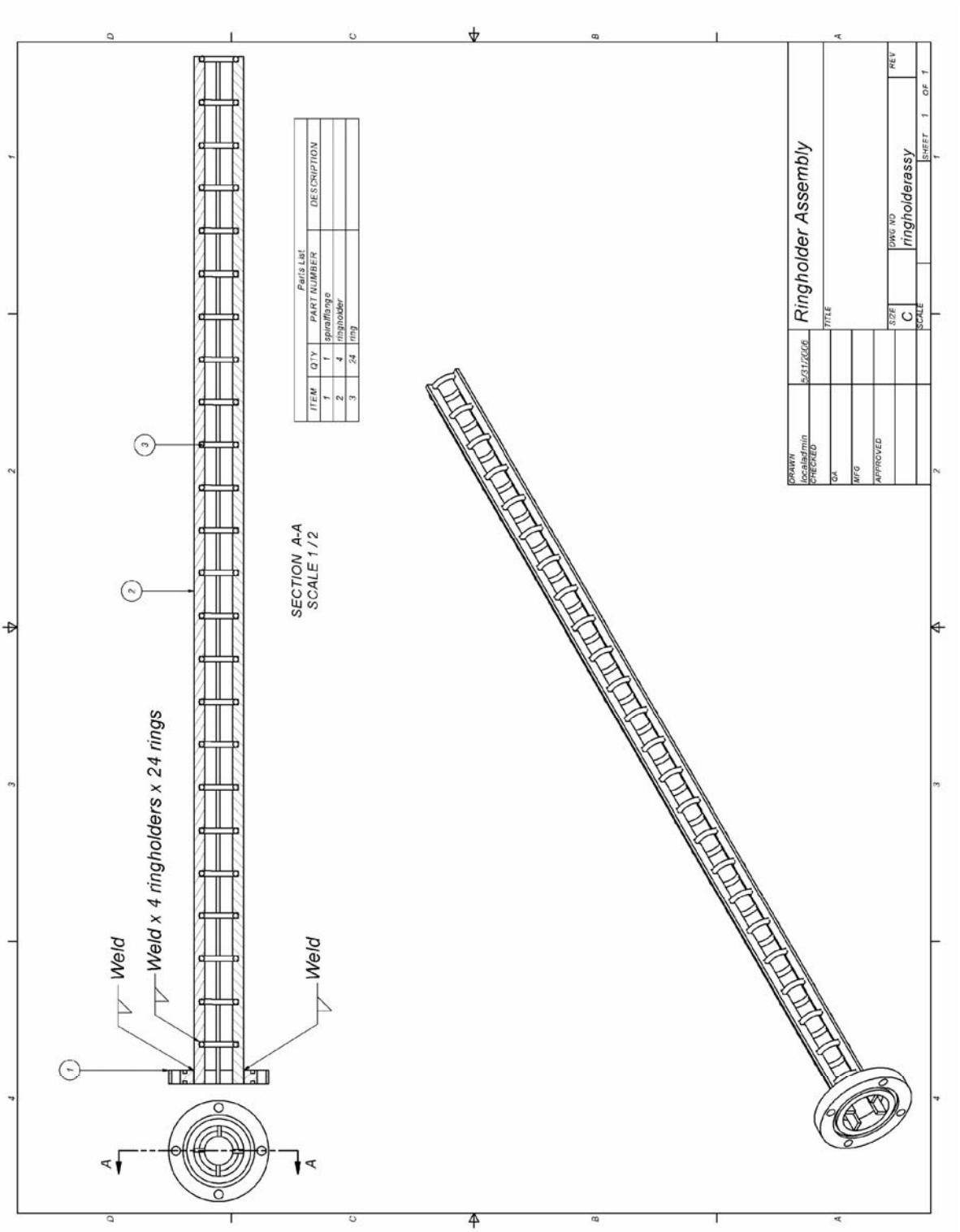

Figure 67. Ringholder Assembly

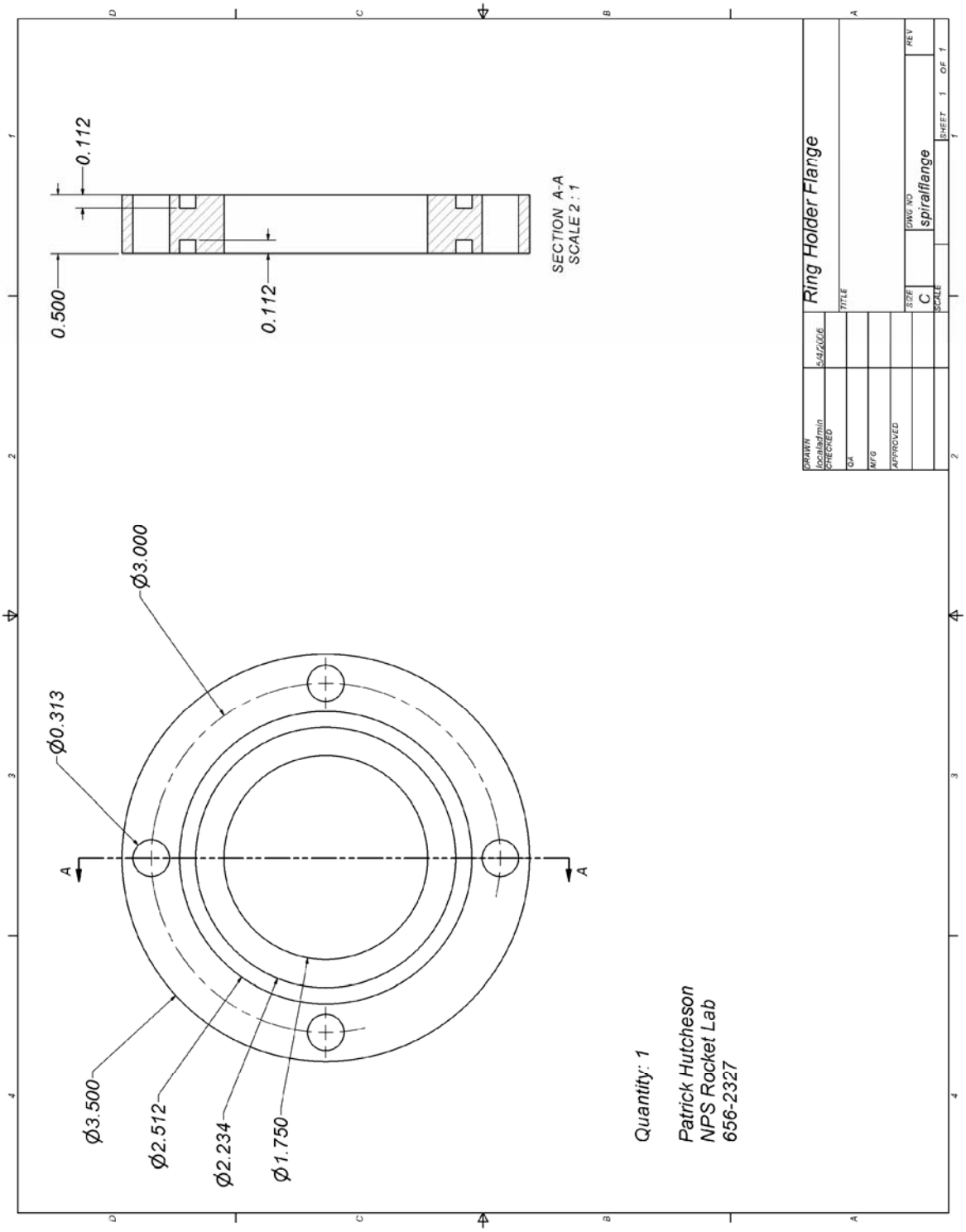

Figure 68. Ringholder Flange

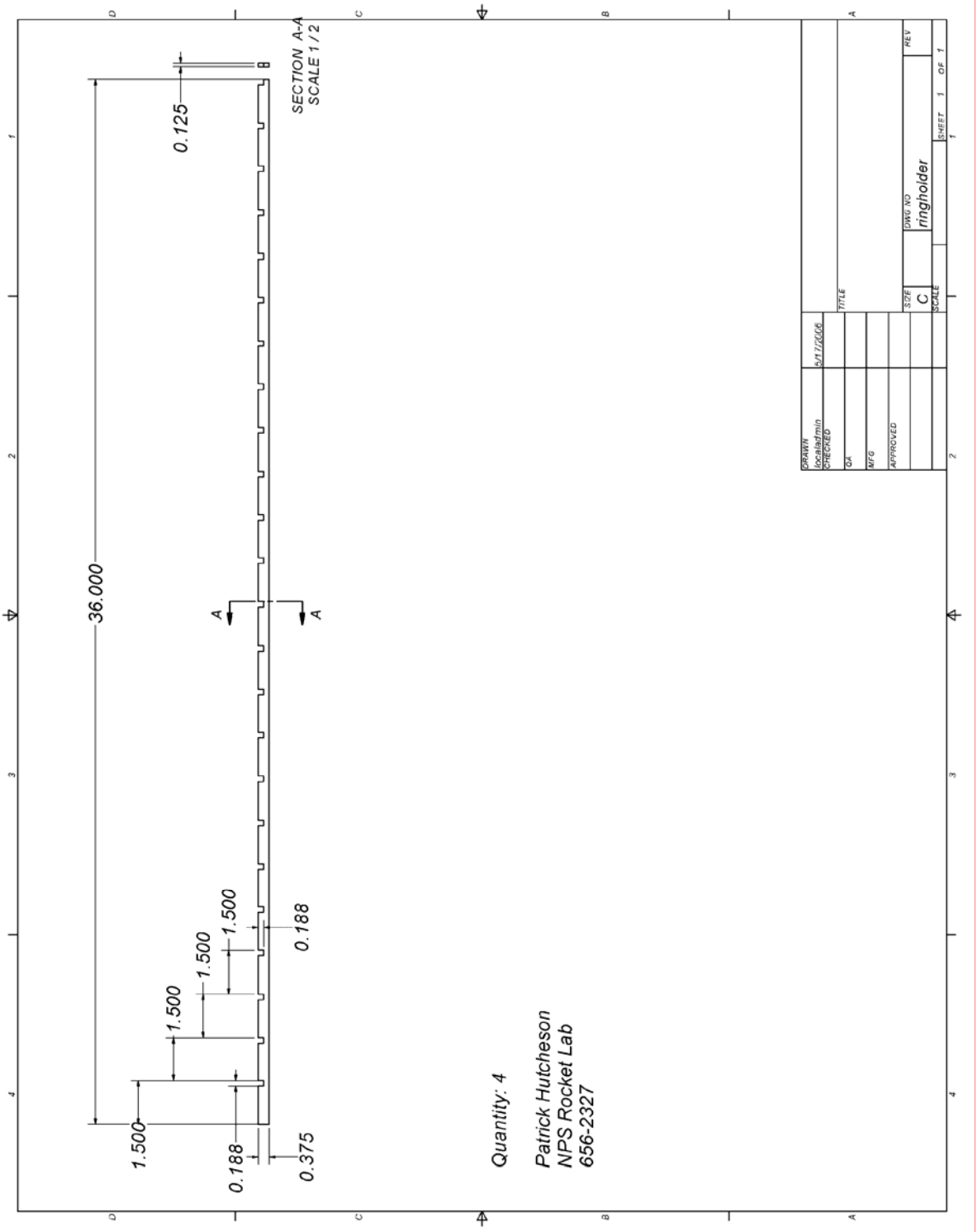

Figure 69. Ringholder

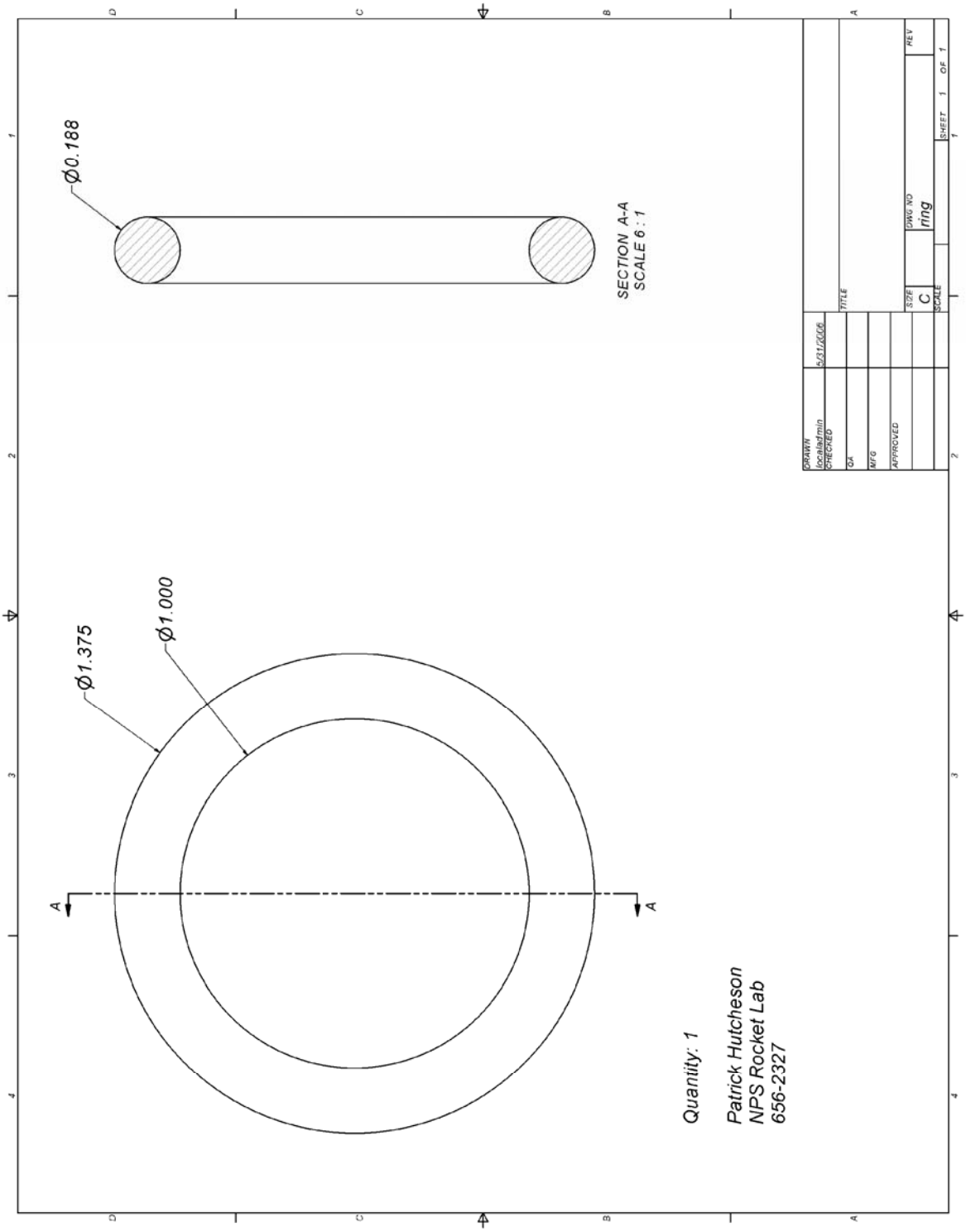

Figure 70. Ring

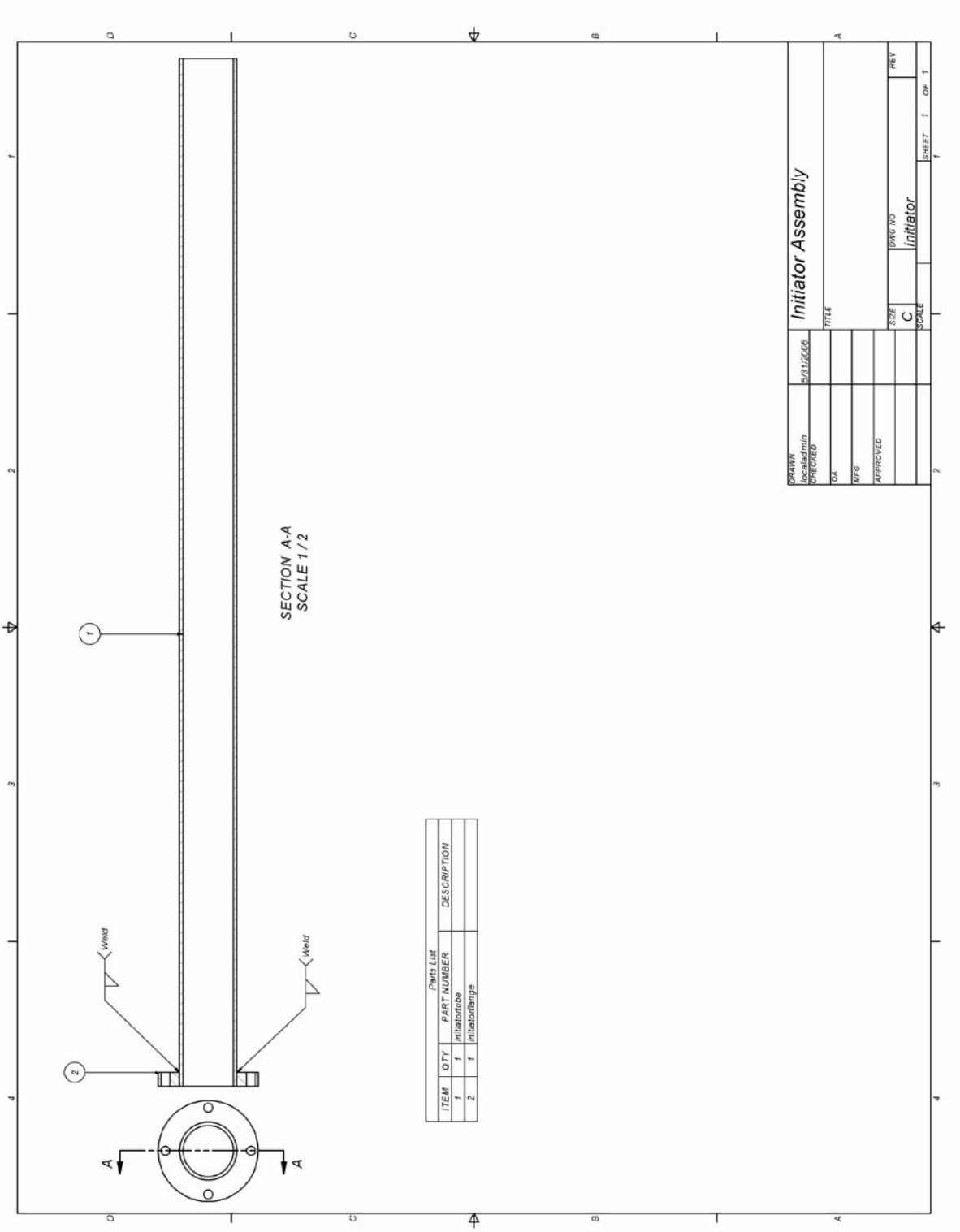

Figure 71. Initiator Assembly

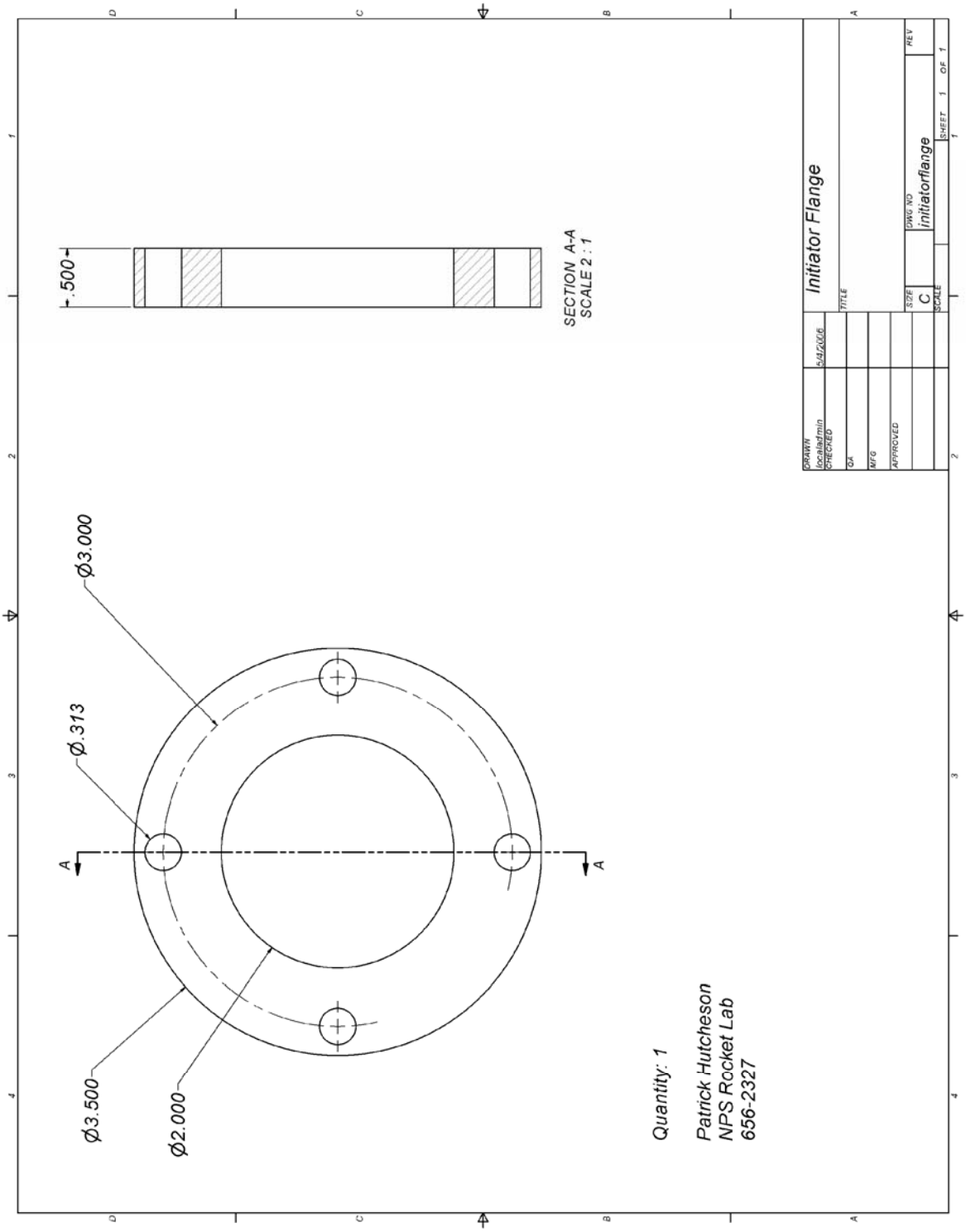

Figure 72. Initiator Flange

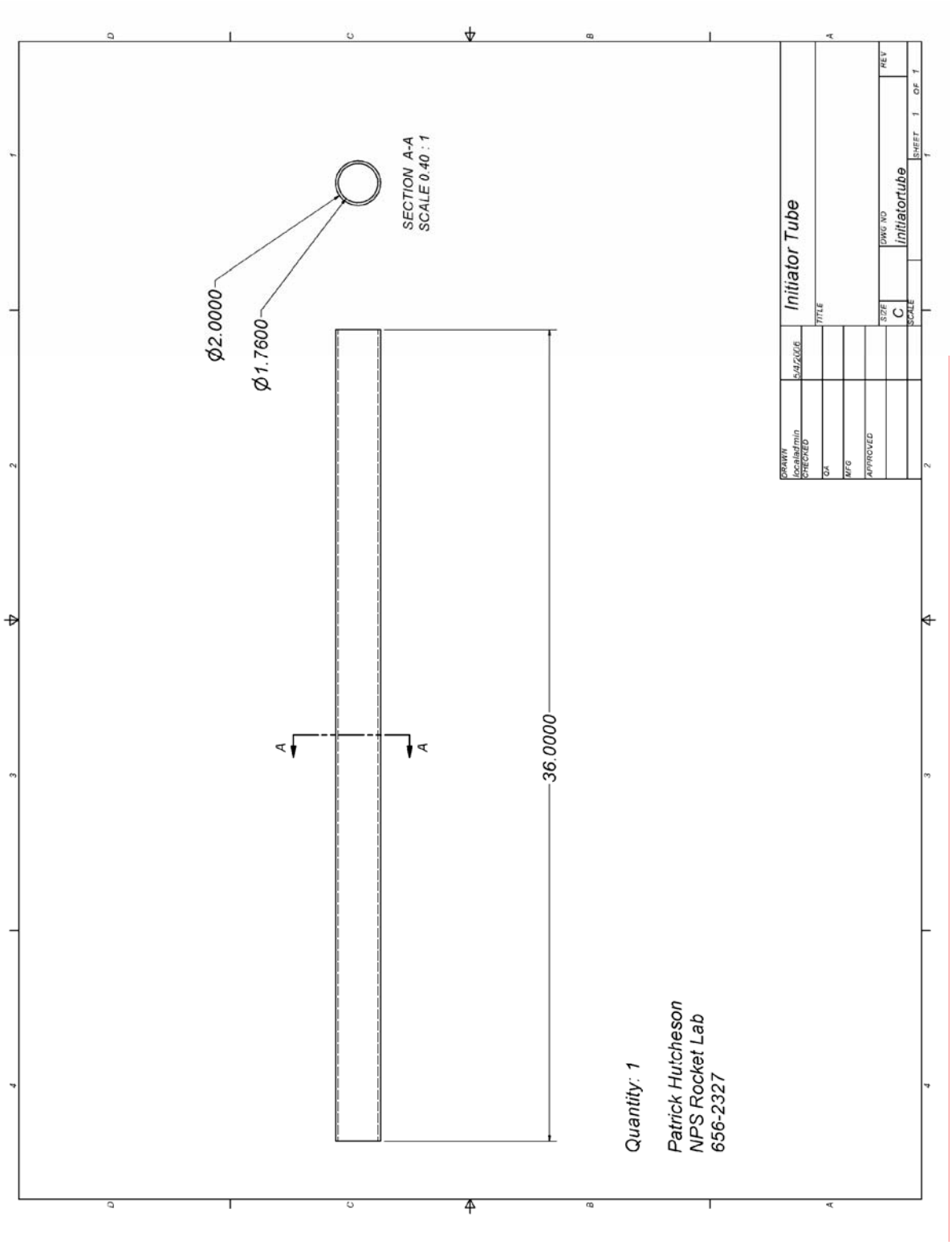

Figure 73. Initiator Tube

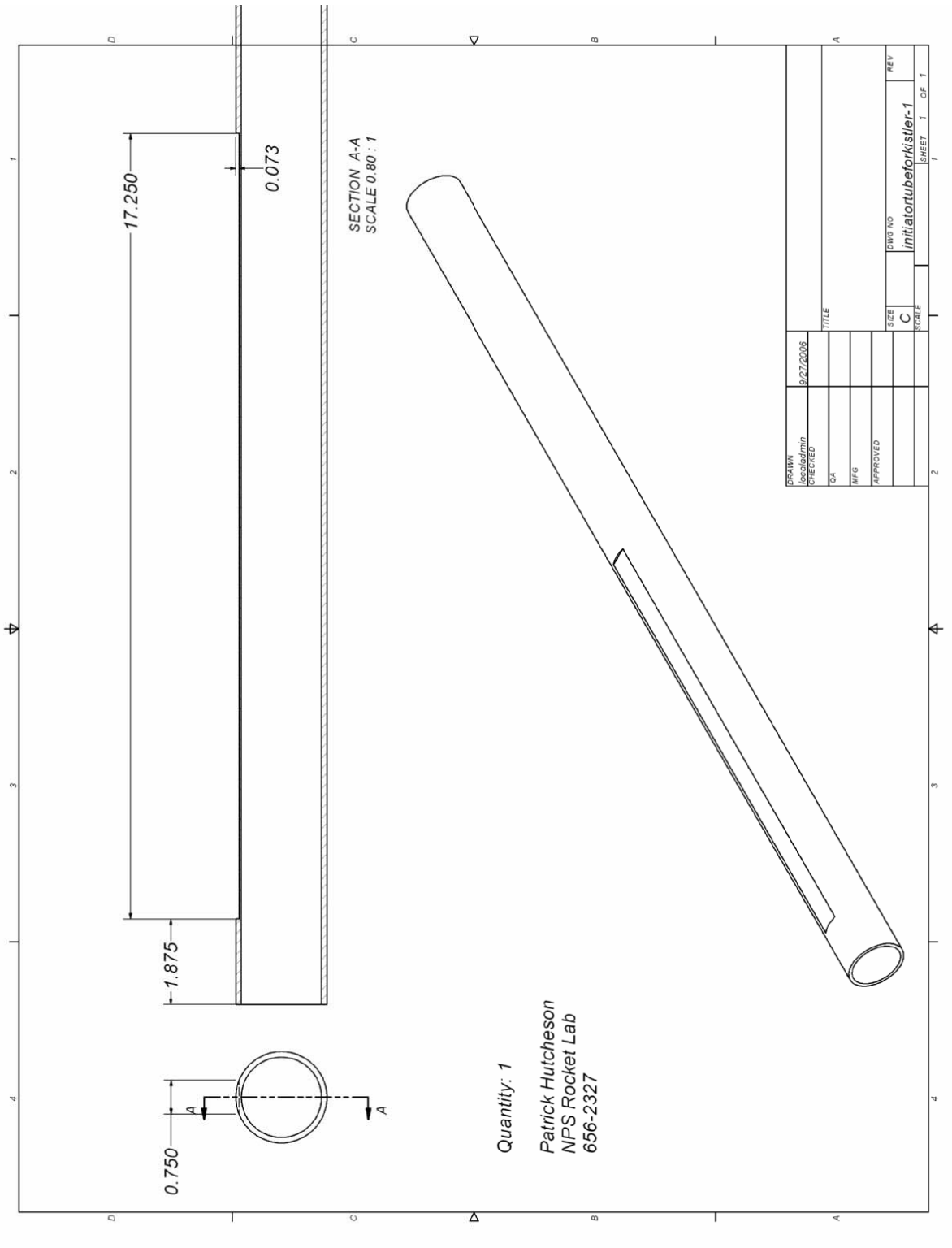

Figure 74. Initiator Tube Version 2 for Pressure Transducers

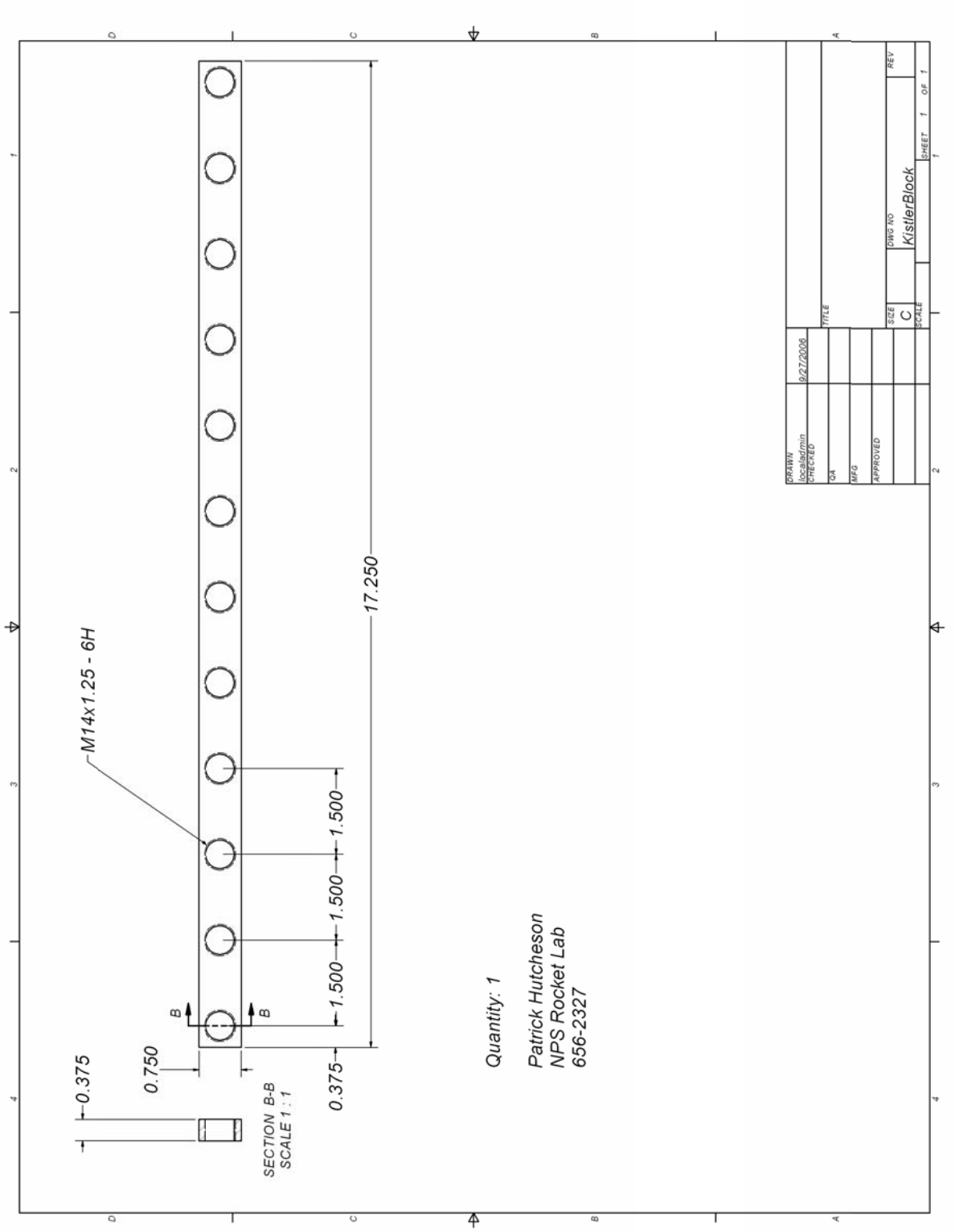

Figure 75. Pressure Transducer Mounting Block

THIS PAGE INTENTIONALLY LEFT BLANK

LIST OF REFERENCES

1. Hoffmann, H., "Reaction-Propulsion Produced by Intermittent Detonative Combustion," German Research Institute for Gliding, Report ATI-52365, August 1940.

2. Friedman, R., "American Rocket Society," Vol. 24, p.349, November 1953.

3. Ma F., Choi J., and Yang V. "Propulsive Performance of Airbreathing Pulse Detonation Engines" Journal of Propulsion and Power, Vol. 22, No. 6, November-December 2006.

4. Brophy C., Werner S. and Sinibaldi J., "Performance Characterization of a Valveless Pulse Detonation Engine" AIAA paper 2003-1344, *41st Aerospace Sciences Meeting and Exhibit*, Reno, Nevada, Jan. 6-9, 2003.

5. Brophy C.M., "Operation of a JP10/Air Pulse Detonation Engine" AIAA Paper 2000-3591, *Joint Propulsion Conference and Exhibit*, Huntsville, Alabama, 16-19 July 2000.

6. Kuo, K.K., *Principles of Combustion*, Second Edition, John Wiley and Sons, 2005.

7. Glassman, I., *Combustion*, Second Edition, Academic Press, Inc., 1987.

8. Cequel™ Chemical Equilibrium in Excel. Version 1.75, Carson City, Nevada, Software and Engineering Associates, Inc.

9. F. Wang, A. Kuthi, and M. Gundersen, "Technology for Transient Plasma Ignition" AIAA paper 2005-951, *43rd Aerospace Sciences Meeting and Exhibit*, Reno, Nevada, Jan. 10-13, 2005.

10. Sinibaldi, J.O., Rodriguez, J, Channell, B., Brophy, C., Wang, F., Cathey, C., and Gundersen, M.A., "Investigation of Transient Plasma Ignition for Pulse Detonation Engines", AIAA Paper 2005-3773, *Joint Propulsion Conference and Exhibit*, Tucson, Arizona, 11-13 July 2005.

11. Liu, J.B., Ronney, P., and Gundersen, M., "Corona Discharge Ignition of Premixed Flames", http://carambola.usc.edu/research/coronaignition/coronaignition.html, September 2005.

12. Hutcheson P.D., Brophy C.M., and Sinibaldi J.O. "Investigation of Flow Field Properties on Detonation Initiation" AIAA Paper 2006-5099, *Joint Propulsion Conference and Exhibit*, Sacramento, California, 9-12 July 2006.

13. Channell, B.T. “Evaluation and Selection of an Efficient Fuel/Air Initiation Strategy for Pulse Detonation Engines”, Master’s Thesis, Naval Postgraduate School, Monterey, California, September, 2005.

14. CFD-ACE Modules Manual. Version 2004, Huntsville, Alabama: ESI CFD, Inc.

15. CFD-FASTRAN Theory Manual. Version 2004, Huntsville, Alabama: ESI CFD, Inc.

INITIAL DISTRIBUTION LIST

1. DMCARM-7
   Department of National Defence
   Ottawa, Ontario, Canada

2. Dudley Knox Library
   Naval Postgraduate School
   Monterey, California

3. Dr. Gabriel Roy
   Office of Naval Research
   Arlington, VA

4. Professor Christopher Brophy
   Department of Mechanical and Astronautical Engineering
   Naval Postgraduate School
   Monterey, CA

5. Professor Garth Hobson
   Department of Mechanical and Astronautical Engineering
   Naval Postgraduate School
   Monterey, CA

6. Professor Jose O. Sinibaldi
   Department of Mechanical and Astronautical Engineering
   Naval Postgraduate School
   Monterey, CA

7. Dr. Martin Gundersen
   University of Southern California
   Los Angeles, CA

8. Capt Patrick Hutcheson
   Naval Postgraduate School
   Monterey, CA